博士論文

Improvement of Malaria Transmission Model by Calibration of Surface Water Formation Parameter and Future Projection over Africa

(地表水面形成パラメータの較正によるマラリア伝染モデルの改良及びアフリカにおける将来予測)

インナ シャファリナ

37-167205

INNA SYAFARINA

Abstract

Malaria has been a major public health and endemic disease in some countries over the world. There were estimated 429,000 malaria deaths globally and mostly in African region. Due to its burden, World Health Organization (WHO) designates malaria as one of Sustainable Development Goals' No.3 target 3.3 which states that "By 2030, end the epidemics of AIDS, tuberculosis, malaria and neglected tropical disease. Several attempts have been conducted to reduce malaria cases, such as using some treatments and protections. However, these efforts still could not eradicate malaria disease. Some researchers have conducted observation field studies by mosquito catchment, examination of sporozoite rate and human bite rate to derive Entomological Inoculation Rate (EIR) which represent probability of a person got infected from malaria disease. Unfortunately, these EIR numbers are limited in some observation sites and sparse. Therefore, malaria transmission model is utilized to describe malaria transmission risk.

Parasite, mosquito, and human are three main factors driver on malaria. Climatic factors affect development of mosquito and parasite. Availability of water is diagnosed become one of factor influencing the spread of malaria. The representation of surface water formation parameter in current malaria model assume constant and not realistic due to the availability of observation dataset. This study aims to determine highly influential climatic factor on malaria disease, determine an optimize pond growth rate optimized parameter and analyze the impact of climate change in the future projection.

Vector borne infectious disease model (VECTRI) developed by International Center for Theoretical Physics (ICTP) is used in this study. We implement VECTRI on Africa region with latitude -38^0 S – 38^0 N and longitude -20^0 W – 55^0 E due to high risk of malaria disease in this tropical region from year to year. This model is used as the basis for validation in historical period, parameterization of surface water formation parameter and projection simulation in future period. We select this model due to its dynamic, incorporation with climatic (precipitation and temperature) and non-climatic (population density) factor. Chapter 2 describe definition of malaria disease, malaria model development, climatic and non-climatic factors drivers on malaria and the detail of VECTRI model mechanism.

In Chapter 3, we explained the methodology, forcing datasets, and simulation scenario used in this study. We conducted three experiments on historical period and one experiment on projection period under three RCPs emission scenarios. Three experiments on historical period is used for validation of model result on historical period and calibration of water fraction against pond growth rate to optimize surface water formation parameter. Existing available observation data (EIR) is explained in this chapter. This study uses EIR annual number which is located in 12 countries in Africa, i.e. Senegal, Republic of Congo, Burundi, Gambia, Democratic Republic of Congo, Gabon, Cameroon, Eritrea, Uganda, Zambia, Tanzania and Kenya.

Validation of simulation results and parameterization of surface water on historical period are discussed in Chapter 4. Parameterization of pond growth rate (K_w) is conducted within two steps. First, by adjusting K_w parameter against EIR observation (K_{we}) on historical period (1983 - 2006) until EIR simulation is closest to EIR observation site studies. The results show that EIR overestimate or underestimate in existing EIR observation sites. Therefore, we do tuning this parameter by increasing (decreasing) K_w, to decrease (increase) EIR model result until the results improve and close to EIR observation result. The results reveal that K_{we} parameter is not constant in existing observation sites. Second, by tuning K_w parameter against water fraction. We utilize satellite observation water fraction, GSMaWS (Global Satellite Mapping of Wet Surface) for calibration of water fraction for period 2014 – 2018. Spatial distribution of pond growth rate against water fraction (K_{wg}) is derived by minimization of Root Mean Square Deviation (RMSD) between water fraction observation and water fraction from model calculation. From K_{we} and K_{wg}, a topographical parameter and a scaling factor is needed to refine the parameter. Then, by multiplication of scaling factor, pond growth rate optimized (by adjusting K_w from K_{we} and K_{wg}) and topography, we interpolate a scaling factor using simple inverse distance weighting. After multiplication of scaling factor, topography and optimized of K_w from HIST-1 and HIST-2&3, we derive a spatial distribution of optimized K_w to be used in projection simulation. K_w gives impact to the formation of water fraction changes. Water fraction give impact to the availability of surface water for malaria breeding places which will influence to the number of survival larva. The survival larva will affect to the number of larva which will hatch into adult mosquito. Then, the number of mosquito will determine percentage of parasite inside mosquito's body (Circumsporozoite Protein Rate or CSPR). If CSPR is multiplied with human bite rate (hbr), we derive EIR number. Therefore, K_w can control EIR number.

Climate change can alter the distribution of vector borne disease, increasing flood and drought, risk of disasters and malnutrition effects (Haines *et al*., 2006). It takes more effort and challenge to predict distribution of malaria in future period compare to historical period due to uncertainties, limited data, climate data variability and the complex physical, social and economic interactions (Semakula *et al.*, 2017). Malaria is sensitive to climate change in vector spreading and parasite development that cause malaria disease (Ngarakana-Gwasira *et al.*, 2016), the impact of climate change on future projection is still being examined. Impact of climate change on projection simulation period is discussed in chapter 5. We utilized CMIP6 (Coupled Model Intercomparison Project Phase 6) under three Representative Concentration Pathways (RCPs) scenarios (RCP 2.6, RCP 7.0 and RCP 8.5) for precipitation and temperature from MIROC model as climate forcing. We use SEDAC (Socioeconomic Data and Applications Center) for population density forcing datasets under three Shared Socioeconomic Pathways (SSPs) scenarios. Comparing to observed historical datasets, output from climate models are mostly bias (Muerth *et al.*, 2013). A bias correction is implemented to correct precipitation and temperature datasets for projection period. A scaling factor is determined to calculate difference

between historical observation and projection observation dataset. Then, this scaling factor is multiplied with daily projection datasets to correct predicted datasets on future period (Lafon *et al.*, 2013). A spatial distribution of optimized pond growth rate from Chapter 4 is applied to improve surface water formation parameter. Precipitation will increase or decrease regarding the emission scenario and location in projection simulation. Meanwhile, temperature is increasing in projection period. For projection simulation, west, central and southeast part of Africa are more favorable conditions for malaria transmission under three RCPs scenario. Inter annual variability of EIR annual projection is determined by calculating coefficient variation of EIR annual number. Coefficient variation is determined from standard deviation of EIR annual mean divided by average of EIR annual. Coefficient variation average for EIR annual projection under RCP 2.6 is 0.079, under RCP 7.0 is 0.087, and under RCP 8.5 is 0.087. From this number it shows that EIR annual projection under RCP 8.5 has higher variability compare to other two RCPs scenario.

Precipitation and temperature give impact to EIR number. In projection simulation, we divided the analysis of each scenario into two regions i.e. west part of Africa (latitude: $0^0 – 25^0$ N, longitude: -20^0W $– 12^0$ E) and central-south part of Africa (latitude: $25^0 – 38^0$ S, longitude: 12^0E – 55^0 E). In west part of Africa, the risk of malaria in projection period compare to historical period are -23.14% under RCP 2.6, -39.51% under RCP 7.0, and -19.22% under RCP 8.5. Therefore, the worst scenario is RCP 8.5 and the better scenario is RCP 7.0 for west part of Africa. In central-south part of Africa, the risk of malaria in projection period compare to historical period are 40.48% under RCP 2.6, 45.23% under RCP 7.0, and 100.78% under RCP 8.5. For central-south part of Africa, the worst scenario is RCP 8.5 and the better scenario is RCP 2.6.

Population density gives proportional impact to control EIR. Precipitation characteristic (monthly average precipitation, standard deviation of monthly average precipitation, and Consecutive Wet Days (CWD)) affect EIR changes from projection period compare to historical period. Monthly average of precipitation and standard deviation of monthly average precipitation have relative contribution to EIR in west part of Africa, meanwhile CWD give more impact to EIR in central and southeast part of Africa. Correlation coefficient of precipitation and standard deviation is higher in western, central and eastern part of Africa, CWD's correlation coefficient is higher near equator line from west to eastern part of Africa and temperature's correlation coefficient from central part to southern part of Africa.

Due to uncertainties on projection period, we add ensemble members of each RCPs scenario. We conducted simulations for three ensemble member of each RCPs scenario. By considering each value of correlation coefficient of each variable divided by value of total correlation coefficient of all variables, contribution of each variable related EIR changes from projection period compared to historical period for spatial mean of African region in west part of Africa is 21.68% for precipitation, 35.32% for standard deviation of precipitation, -6.71% for CWD and 49.72% for temperature. Meanwhile, in central – south

part of Africa, the contribution of each variable is 0.85% for precipitation, 41.01% for standard deviation of precipitation, -18.95% for CWD and 77.09% for temperature.

Chapter 6 conclude and discussed recommendation for further study improvement. This study utilizes Entomological Inoculation Rate (EIR) annual number for validation of model simulation in historical period. The result shows that by tuning pond growth rate parameter against EIR, the model result can be improved to EIR observation. Further, utilizing other validation datasets such as number of malaria cases in each observation site in Africa could improve the model result. Besides that, this study utilizes highly resolution of water fraction observation dataset around 0.1 degree resolution (~11 km). Higher resolution surface water with pond scale (< 10 m) daily datasets are needed to improve the model performance and make the model more realistic. An economic growth for projection simulation and other social factors need to be implemented to make the simulation more realistic.

Table of Contents

List of Tables

List of Figure

CHAPTER 1

Introduction

Abstract:

Malaria is a major public health problem which caused by transmission of parasite from mosquito into human. The highest malaria cases and death are mostly in African region, with 92% and 88%, respectively. Some attempts which had been conducted to control and eliminate malaria disease still could not eradicate the spreading of malaria. The lack of expert, health tools and infrastructures, political instability, health system and government policies also contributed to the unsuccessful of the program. Sparse of observation data, coast and time consuming encourage researchers to utilize mathematical models. The impact of environmental factors and socio-economic factors make improvement of the model from compartment (statistical) model into dynamical model create to be more realistic. Precipitation and temperature give a significant impact of malaria transmission. Availability of surface water is highly effected on development phase of vector and disease. Uncertainty of long-term precipitation and high temperature can reduce malaria in the future due to mosquito's habitat are not optimal to live in. This uncertainty and the impact of climate change make researcher to investigate more detail on malaria transmission projection. In future, malaria transmission is more likely to transmit in highland area compared to lowland.

1.1 Background

Malaria is a burden major public health problem which caused by transmission of parasite from mosquito into human. The disease has become endemic in some countries over the world. In 2015, there were an estimated 429,000 malaria deaths globally and mostly in African region, where an estimated about 92% of all deaths occurred (WHO, 2015)

Malaria has been designated as one of Sustainable Development Goals' No.3 target 3.3 which stated that "By 2030, end the epidemic of AIDS, tuberculosis, malaria and neglected tropical disease". Several approach have been conducted to control and eliminate malaria, such as using chloroquine and dichlorodiphenyltrichloroethane (DDT), Global Malaria Eradication Programme (GMEP) in Africa, personal protection (using insecticide-treated bed nets (ITNs), propagating of fast-acting artemisinin-based combination therapy (ACT)), African Initiative for Malaria Control (AIM), Roll Back Malaria (RBM) and Global Malaria Action Plan (GMAP) (Robert *et al*., 2012, Tambo *et al*., 2012). However, all these efforts have not been able to eradicate malaria. The lack of some experts incorporated in the programs, poverty, health infrastructure and equipment, political instability, health system and government policies also contributed to the unsuccessful of the program (Tambo *et al.,* 2012)

About 88% of malaria cases are spread in Africa (Tambo *et al.*, 2012). The highest fraction of malaria cases globally is Nigeria with 27%, followed by Democratic Republic of Congo with 10%, India with 6% and Mozambique with 4%. Sub Saharan Africa is the most endemic region in Africa. The impact of malaria is classified into three categories, such as health, social and economic (Orem *et al*., 2012). Malaria is one of inhibitors of a country's economic growth (The Economic Burden of Malaria by Gallup JL, Sachs JD). Malaria inhibit economic growth in Africa up to 1.3% each year.

The possibility of infected mosquito being influenced by various factors, such as host, parasite and mosquito which can be described by the experiments of feeding mosquito (Churcher *et al*., 2014). Measurement of malaria epidemic field studies has been conducted in several countries in Africa. Jones, (1964a, 1964b) examined the degree of control to reduce mosquito population's vectorial capacity. Elliot *et al*., (1972) investigated the influence of vector behavior on malaria transmission. Smith *et al*., (1995) conducted parasitological surveys in two villages of Kilombero district in Tanzania and revealed that a high risk of malaria of *Plasmodium falciparum* along the year and unstable risk of *Plasmosium malariae*. Four years entomological surveys (1993-1996) to analyze seasonal malaria in the village of Ndiop, Senegal and the mechanism of protective immunity is conducted by (Fontenille *et al*., 1997). Lemasson *et al*., (1997) studied ecology, population dynamics and malaria vector efficiency of *Anopheles gambiae* and *Anopheles arabiensis* for two years in a Sahelian village of Senegal. Aniedu *et al*., (1997) evaluated malaria-metric and conducted entomological survey near two permanent breeding sites in Baringo district, Kenya to investigate the prevalence and seasonality of malaria and the effect of two local mosquitoes as a vector. Shililu *et al.,* (2003) investigated spatial distribution of anopheline mosquito spesies from October – December during 1999 – 2001 in highlands and western lowlands and from February – April for the coastal region in Eritrea. Antonio *et al.,* (2012) conducted 12 months entomological survey in a highly populated district of Doala, Cameroon using human landing catch (HLC) and Centers for Disease Control and Prevention (CDC) light traps method. Facing all these observation datasets have not been able to represent malaria transmission throughout Africa due to the sparsity of observation site studies, high risk of mosquito catchment, cost and time consuming and some cases of malaria were not reported in the cause of lack of awareness of the local community.

Some researchers utilize mathematical model to overcome this issues. (Ross, 1915) developed a simple model to elucidate the relationship between number of mosquitoes and incidence of malaria in humans. Due to its simplicity, some models extension of Ross's model has been developed by researchers by considering additional factors, such as age structure (Anderson and May., 1991), host immunity response and parasite's ability to evades its host immune response (Koela and Boete., 2003), parasite replication and its regulation by innate and adaptive immunity (Gurarie et al., 2012).

To improve understanding the relationship between host, vector and parasite, it is necessity to model mosquito populations and take into account for environmental parameters and socio-economic

factors (Mandal *et al.*, 2011). Parham and Michael., (2009) investigated the effect of rainfall and temperature on mosquito population dynamics and implemented to estimate changes in basic reproduction number of malaria in Tanzania. Yang and Ferreira., (2000) assessed the impact of global temperature changes and socio-economic factor on malaria transmission based on compartmental model. These statistical models are influenced by the availability of data records.

Stochastic approaches describe the dynamics of malaria transmission and represent a more realistic malaria model. Gemperli *et al., (*2005) used Garki model to map spatial distribution of malaria in Mali. Ermert *et al.,* (2011) developed a Liverpool Malaria Model (LMM) to understand the mechanism of malaria transmission, examine the map distribution of climate change impact assessment (Tompkin and Ermet., 2013) The shortcoming of this model is they do not consider explicitly interplay between host and vector. Yamana and Eltahir, (2010) constructed Hydrology, Entomology and Malaria Transmission Simulator (HYDREMATS) to forecast mosquito populations and vectorial capacity in Banizoumbou village in western Niger in the year of 2005-2007. HYDREMATS is limited to village scale, does not appropriate for regional scale. In 2012, Tompkins and Ermert, (2013) developed a dynamical malaria transmission model that account for the impact of temperature, rainfall variability on development of malaria vector in its larval, adult stage and parasite. This model accounts for interaction between host and vector and more appropriate for regional simulation.

Malaria transmission is affected by climatic factor and non-climatic factors. Climatic factors such as precipitation and temperature give a high impact to mosquito phase development. Precipitation provide a mosquito breeding places. Availability of surface water is a critical factor for mosquito breeding places. Larvae habitat needs a warmer daytime temperature of water (Minakawa et al., 2004) and stagnant water body (Sattler et al., 2005) to develop. Fuzzy distribution model is used to represent mosquito breeding places (Ermert, et al., 2011). VECTRI model use simple water balance equation to represent surface water in the beginning of model development (Tompkins and Ermert, 2013). Further development of surface water calculation is conducted by (Asare *et al.*, 2016). They revise pond scheme by including parameterization of surface runoff and evaluate water fraction from VECTRI model with HYDREMATS model output as calibration surface water data. In 2008, They assume that HYDREMATS surface water output are reliable and assumed as validation datasets. Bomblies *et al.*, (2008) simulate pool formation by distributing flow routing in HYDREMATS model. They use Manning's equation with distributed roughness parameter to describe flow velocity. Kibret *et al*., (2019) investigated effect of large dams of malaria in Africa. They utilize Europian Comission's Joint Research Center (JRC) global surface water datasets to extract reservoir periometers. They find that topography near dam site (slope) is the most important factor affecting malaria incidence because the shallow puddles for mosquito breeding are more likely to build in the steeper slope. Nmor *et al*., (2013) predict mosquito breeding sites from topographical information (Digital Elevation Models (DEMs)). They use Shuttle Radar Topography Mission 3 (SRTM3, with 90 m resolution) and the Advanced Spaceborne

Thermal Emission (ASTER, with 30 m resolution) from DEMs using GIS technique to apply in western Kenya. They find that SRTM and ASTER models had similar predictive potentials. From all these efforts, formation of surface water with high resolution and daily dataset are lacking. Since, stagnant and small surface water body (ponds, puddle, or hoof prints) which is needed by mosquito for placing their eggs are formed approximately ten days (Shaman and Day, 2007).

The major factors which determine seasonality and variability of annual malaria transmission are climate and weather. Long term drought periods and precipitation can decrease malaria due to unsuitable conditions for vector and disease development. Variability of temperature alteration takes into account in vector mechanism, reproduction and survival rate (Patz, *et al*., 2005). Cold district and increasing precipitation delayed increase in malaria cases (Tkelehimanot *et al*., 2004, Guo et al., 2015). The uncertainty of the climate in the future encourage researchers to investigate malaria transmission in projection period.

Climate change is a significantly changing of climate pattern over a period of time as an effect of human activities: fossil fuel burning and greenhouse gasses accumulation (Haines *et al*., 2006). Climate change affects health by several approaches, such as alteration on distribution of vector borne disease, increasing flood and drought, risk of disasters and malnutrition effects (Haines *et al*., 2006). It takes more effort and challenge to predict distribution of malaria in future period compare to historical period, due to uncertainties, limited data, climate data variability and the complex physical, social and economic interactions (Semakula *et al.*, 2017). A better prediction scheme of malaria transmission in the future can decrease the incidence, determine a good way and control malaria risk (Hundessa *et al.*, 2018, Tanser *et al*., 2003, Yamana and Eltahir, 2013). Several attempts to predict malaria transmission projection in future period have been conducted, such as (Caminade *et al*., 2014; Béguin *et al*., 2011, Van Lieshout *et al.*, 2004; Rogers and Randolph., 2000) for global malaria transmission, (Semakula *et al.*, 2017; Hundessa et al., 2018; Ngarakana-Gwasira *et al.*, 2016, Ryan *et al.*, 2015, Ermert et al., 2011, Dalrymple *et al*., 2015) for regional malaria transmission.

For global malaria prediction, five statistical and dynamical malaria impact models for three projection period (2030s, 2050s, and 2080s) using five global malaria models have been conducted (Caminade *et al*., 2014). Their results show that there is a significant increase in number of people at risk annually under RCP 2.6 into RCP 8.5 scenario from 2050s to 2080s. They also mention that there are significantly differences on malaria distribution outcome from the model choice. Béguin *et al*., (2011) contributed to incorporate effect of climate change and socio-economic development to past, present and future malaria distribution. They utilize logistic regression model and combine precipitation, temperature and gross domestic product per capita (GDPpc) to describe global malaria distribution. They find that GDPpc and population consistent with IPCC A1B scenario using projection climate and in 2050, projected population account for 5.2 billion, 1.74, 1.95 billion and 1.74 billion considering

climate, GDP, and both effect, respectively. Van Lieshout *et al*., (2004) explain a new method to represent vulnerability to the potential impacts of climate change using MIASMA v2.2 model under four SRES emission scenario (A1F1, A2, B1, and B2). They find that the greatest impact of population growth in risk area in Eurasia and Africa under B2 scenario and climate change does not give influence to malaria transmission in the poorest countries due to this region is already more vulnerable for malaria transmission. Rogers and Randolph, (2000) analyze the effect of temperature on global malaria distribution in present and future period using statistical approach. They predict the future distribution of habitat are similar to present *Plasmodium falciparum* distribution. They also predicted that malaria will survive in southern United States and into Turkey, Turkmenistan, and Uzbekistan, southward in Brazil, and westward in China, and malaria will be diminished in other area.

For regional domain, Ermert *et al.,* (2011) studies that in future projection, malaria is predicted increase in southern part of Sahel and intensity of malaria transmission increase in most of East Africa. They conclude that malaria risk will increase in highland region and will decrease in lower-altitude of East Africa high-lands. Semakula *et al.,* (2017) utilize GIS-BBN (Geographical Information System and Bayesian belief networks to forecast malaria hotspots in 2030, 2050, and 2100 using Representative Concentration Pathways (RCPs) 4.5 and 8.5 in Sub Saharan Africa (SSA). They reveal that majority area of SSA will have medium malaria prevalence in 2030 under RCP 4.5. Meanwhile, only in highlands area will have malaria under RCP 8.5, remaining part have no malaria. Ngarakana-Gwasira *et al.*, (2016) examine climate change impact of malaria in Africa using mathematical model combined with GIS. They find that malaria is more likely to increase in tropics, highland, East Africa and along northern limit of falciparum malaria. They reveal that *P.falciparum* is likely not survived in the southern part of Africa by 2040. The model does not take into account for human migration and socioeconomic factors in malaria transmission dynamics. Hundessa *et al.,* (2018) investigated the distribution of two species of malaria disease (*Pasmodium vivax* and *Plasmodium falciparum*) in China using Generalized Additive Model (GAM) under RCP 4.5 and 8.5 scenario. They found that *Plasmodium falciparum* are predicted to enhance more than *Plasmodium vivax.* The number of increasing is higher under RCP 8.5 scenario than RCP 4.5 scenario. Ryan *et al.,* (2015) conclude that high temperature region all year round in Africa are higher risk of malaria and spread from coastal West Africa to Albertine Rift between Democratic Congo and Uganda. Meanwhile, region with seasonal suitable transmission are located in sub-Saharan coastal area. A better forecasting scheme of malaria transmission in the future can predict in proper place, decrease the incidence, determine a good way and control malaria risk (Hundessa *et al.*, 2018, Tanser *et al*., 2003, Yamana and Eltahir, 2013). Therefore, it is important to understand the impact of climate change on malaria transmission in the future.

1.2 Objectives and limitations of this study

The purposes of this studies are:

1. To determine the highly influential climatic factor on malaria transmission
2. To determine pond growth rate optimized parameter to be utilizing in projection period
3. To analyze the impact of climate change on malaria transmission projection under Representative Concentration Pathway (RCP) scenario

There are some limitations of conducted in this study:

1. Lack of observational datasets to measure malaria risk
2. Surface water observation datasets for calibration K_w parameter with higher resolution on daily time are limited

These limitations can be overcome by utilizing existing EIR observation datasets from existing annual dataset and assumed that all existing observation datasets are valid and applied to 11 x 11 km spatial grid. For surface water observation datasets, we utilize Global Satellite Mapping of Wet Surface (GSMAWS) with 0.1 x 0.1 degree spatial resolution from 2014 – 2018 daily datasets.

1.3 Dissertation outline

Chapter 1 describes background of the study, objectives and limitations of this study, and dissertation outline.

Chapter 2 explains a brief definition of malaria disease, climatic (e.g. precipitation, temperature, relative humidity, wind speed, and topography) and non-climatic factor (e.g. population density, access to health facilities, migration, and poverty) driver on malaria transmission. In addition, the development of malaria transmission model and malaria indicator number also provided.

Chapter 3 describes methodology used in this study, experimental design, forcing datasets used, some simulation scenario, and observation sites for historical period for validation simulation result. This study utilized precipitation, temperature, population density and topography as forcing datasets.

Chapter 4 investigate malaria transmission on historical period. This chapter analyze parameterization of pond growth rate compare with EIR observation in the past. Optimization of pond growth rate parameter in some observation sites in Burkina Faso, Cote D' Ivoire and other countries are derived.

Chapter 5 investigate the impact of climate change on malaria projection. This chapter begins with linear bias correction method used for precipitation and temperature.

Chapter 6 summaries the findings of this study regarding optimized surface water parameter and impact of climate change in future period.

CHAPTER 2

Malaria Disease, Transmission Model and Indicator Number

Abstract:

Malaria is an infectious disease which spread all over the world. The number of patient is increasing annually. It is important to understand the climatic and non-climatic factor which affect to malaria transmission. Climatic factor will give effect to vector and parasite development. Some climatic factors impact to malaria, such as precipitation, temperature, humidity, wind speed, topography, land use change/cover and irrigation density are explained. Sparse of the observation data, time and cost limitation encourage researchers to use malaria transmission model. Meanwhile, some non-climatic factors which driver on malaria (population density, health facilities, migration, and poverty) are also described. Some malaria transmission models are developed around the world. Malaria model development start with compartment model which consider three compartment: susceptible (S) – infected (I) – recover (R). From this simple malaria model, some researchers develop into dynamical model due to malaria accounts stochastic process in its development. Malaria dynamical model is developed by incorporating climatic or non – climatic factor driver on malaria. Malaria indicator number is used to measure the risk of malaria transmission in one area. Some malaria indicator number such as: human bite rate (HBR) and CircumSporozoite Protein Rate (CSPR) are used in calculation of entomological inoculation rate (EIR) observation datasets.

2.1 Definition of malaria disease

Malaria is a mosquito-borne infectious disease caused by parasitic protozoans of the genus *Plasmodium (vivax, malariae, ovale, knowlesi* and *falciparum)* and is transmitted by female mosquito vectors of the *Anopheles* species (Caminade e*t al.,* 2014). Mosquito which is influenced in this disease only accounted for female mosquito due to male mosquito only consume nectar (flower essence), only female mosquito which need blood for their eggs development. Mosquito development starts from egg, larvae, pupa, and adult. In larva, it has 4 development stages. Mosquito life cycle describes in Fig. 2. 1.

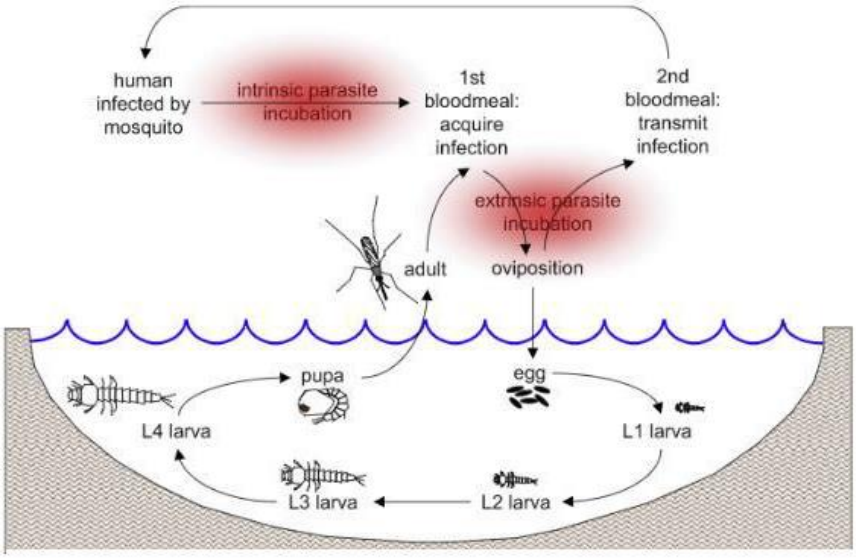

Fig. 2.1 Mosquito life cycle (Bomblies *et al.*, 2008)

Malaria disease is spread by an infected female mosquito (which carry parasite) bite human and leave the parasite on blood stream. Infant, children under five years old, pregnant women and HIV/AIDS patients are more vulnerable to malaria disease (WHO). Pregnant woman which carry malaria parasite can directly inherit malaria into the baby from placenta and bloodstream (Eijk et al., 2015). The symptoms of malaria disease, such as headache, fever, chills and vomiting, if these symptoms do not have any treatment within 24 hours, *Plasmodium falciparum* parasite can develop into a more severe disease, even to death (WHO, 2014).

Inside human body, there are some process of parasite development (Fig. 2.2). The parasite life cycle begins when a mosquito takes a blood meal, an infected mosquito will leave a sporozoite in human body. Sporozoite will move to liver and infected liver cell and change to be schizont. Ruptured schozont will be transferred into human blood stages and change to be immature tropozoite. Tropozoite will transform into mature tropozoite and form schizont. Ruptured schizont will released merozoites. After that, some parasite will be distinguished into sexual erythrocytic stage (microgametocytes: male and macrogamtocytes: female gametocytes). These gametocytes will be swallowed by a mosquito during blood meal. Then, parasite's do multiplication inside mosquito (called as sporogonic cycle).

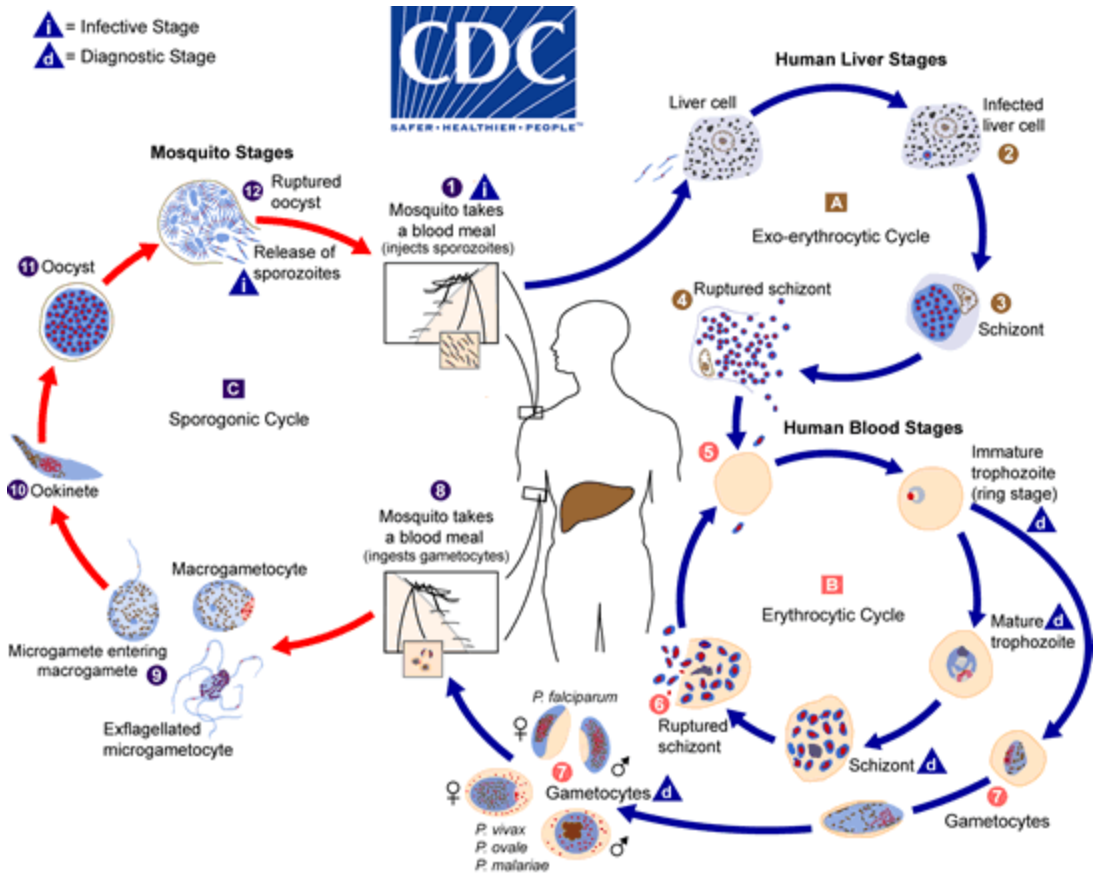

Fig 2.2 Parasite life cycle in human body

Anopheles gambiae complex (include *Anopheles gambiae, Anopheles arabiensis, Anopheles merus* and *Anopheles melas*) is more dominant species found in Africa region as a vector of malaria disease (Sinka et al., 2010). *Anopheles funestus, Anopheles moucheti and Anopheles nili* become highly anthropophilic after *Anopheles gambiae complex* (Sinka et al., 2010). *Anopheles gambiae and Anopheles arabiensis* spread in some localities in arid savannah zones and forest (Onyabe and conn., 2001). *Anopheles gambiae sensu lato* is found in a temporal and sunlit breeding habitat, such as a hoof prints, rice puddles, and ground water depression created during rainy season (Gillies and Meillon., 1968, Minakawa et al., 2004). *Anopheles sp* prefer to stay in permanent and temporal habitat about 60% and 34%, respectively (Mattah et al., 2017). Meanwhile, *Anopheles funestus* choose semi-permanent and permanent breeding habitats, for example swamps and large ponds (Gillies and Meillon., 1968).

There are some climatic factors drivers on malaria, such as precipitation (provides breeding sites for larvae), temperature (larvae growth, vector survival, egg development in vector, parasite development in vector), relative humidity (desiccation of vector), and wind (advection of vector, strong winds reduce CO_2 tracking) (Tompkins and Ermert, 2012). Other factors which can alter disease range, such as land use changes (drainage or wetland cultivation), interventions (bed net, spraying, treatment), socio-economics factors (access to health facilities, population density, migration, and poverty), and

vector predators, competition and dispersion limits. Each climatic impacts will be explained in the following subsection.

2.1.1 Climatic factor on malaria

Climatic factors give impact to mosquito parasite development and disease spreading. Some climatic factors, such as precipitation, temperature, humidity and topography driver on malaria transmission. The detail explanation of each factors are described as followed.

2.1.1.1 Precipitation

Water becomes a crucial factor for egg and larvae stage of mosquito. Adult mosquito needs water to place their eggs and larvae needs water to develop all four stages. Aquatic stages determine abundances, dynamics and fitness of mosquito adults and can effect malaria transmission (Paaijmans., 2008). Precipitation is the source that determine mosquito breeding places. High precipitation can flush aquatic habitat of larval mosquito and kill them (Paaijmans *et al.*, 2007). Therefore, there is an optimum surface water for mosquito to breed and develop. Some effects of changes in precipitation on vector (WHO, 2015):

- Increased rain may increase larval habitat and vector population size by creating new habitat
- Excess rain or snowpack can eliminate habitat by flooding, decreasing vector population
- Low rainfall can create habitat by causing rivers to dry into pools (dry season malaria)
- Decreased rain can cause synchronize vector host-seeking and virus transmission
- Increased humidity increases vector survival, decreased humidity decreases vector survival

2.1.1.2 Temperature

Temperature give effect to the development of egg (gonotrophic cycle) and parasite (sporogonic cycle) inside mosquito's body. Development and survival rates of both Anopheles mosquito and Plasmodium parasites also are determined by temperature (Beck-Johnson et al., 2013). Several effect of changes in temperature on vectors (WHO, 2015):

- Survival rate can decrease or increase depends on species
- Some vectors have higher survival at higher latitude and altitude with higher temperature
- Changes in the susceptibility of vectors to some pathogen (microorganism) e.g. higher temperature reduce size of some vectors but reduce activity of others
- Changes in rate of vector population growth
- Changes in the rate of vector population growth
- Changes in feeding rate and host contact (may alter survival rate)
- Changes in seasonality of populations

2.1.1.3 Humidity

Increasing of 1% of relative humidity could increase 3.99% of number of malaria cases in Guangzhou, China (Li et al., 2013). Decreasing of relative humidity effect to the uncomfortable levels of mosquitoes in the end of rainy season (Yamana and Eltahir., 2013). Optimized of relative humidity for malaria transmission is above 60% (Kumar *et al*., 2014). Increasing relative humidity could increase mosquito longevity (Gillies, 1988).

2.1.1.4 Wind speed

Increasing of wind speed about 1 m/s could increase about 164% and 171% in the monthly of malaria cases in savanna and humid forest (Omonijo *et al*., 2011). The relationship of behavior mosquitoes and wind effect (attraction of adult mosquito dispersion of CO_2, advection of adult mosquitoes, and aquatic-stage mortality due to wind-induce surface waves) have been investigated (Endo and Eltahir., 2018). They revealed that wind has a significant effect near reservoir due to the waves give a huge impact to aquatic-stage of mosquito development at large water bodies. The depth and fetch of reservoir is increased by the height of wave, therefore wave prefers to influence *Anopheles* mosquitoes' breeding at reservoir than a small water bodies (Endo and Eltahir., 2018).

2.1.1.5 Topography

Atieli *et al.*, (2011) examined influence of some topographical parameters (elevation, slope, aspect and ruggedness) in the highland areas in western Kenya. They revealed that aquatic-stage presence and productivity of mosquito is affected by these parameters. They also found that in lower gradient topography has a stable and higher malaria risk compare to steep gradient topography. They conclude that topographic parameters have significant effect to identify higher risk of malaria.

Githeko *et al*., (2006) investigated topography effect to spatial vector and parasite distribution. They found that malaria transmission is stable at valley bottom, unstable at the hilltop and intermediate state in the mid-hill village in western Kenya highland.

Balls *et al*., (2003) analyzed the effect of malaria risk infection and topography in the Usambara Mountains, Tanzania. Altitude influenced in malaria transmission because of its effect on temperature Balls *et al.*, (2003). High altitude with low temperature decrease the survival and development of aquatic stage of Anopheline mosquito and the development of vector which can reduce probability of malaria transmission (Lindsay and Birley, 1996).

2.1.1.6 Land use change/cover

Muturi *et al.*, (2006) conducted entomological survey to describe mosquito diversity and distribution in land use area in Mwea rice field, Kenya. They find that Anopheles arabiensis, Cx quinquefasciatus and Anopheles pharoensis were more abundant in rice agroecosystems than in non-irrigated agroecosystem. Meanwhile, Anopheles funestus was more abundant in non-irrigated agroecosystem.

2.1.1.7 Irrigation density

An area with proper irrigated and sunlit pools are highly favourable place for mosquito breeding sites (Carnevale *et al.*, 1999).

From all climatic parameter, this study account for precipitation and temperature as forcing dataset due to the main climatic effect are precipitation will give impact to aquatic (larvae) life cycle and temperature will give effect to mosquito and parasite development in the model setting.

2.1.2 Non-climatic factors on malaria

Besides climatic factors, there are some non-climatic factors affect malaria transmission.

2.1.2.1 Population density

Population density was an important predictor of malaria risk (Kabaria *et al*., 2017). Migration of people are contributed to the spread of disease (Prothero., 1977). Increasing of malaria incidence in sub-ruban area than in rural area are found during low transmission season in highland region in East Africa (Siraj *et al*., 2015).

Previous studies found that high population density in urban areas have low Entomological Inoculation Rate (EIR) due to a chance of probability of one people got infected decrease among many people (Oyewole and Awoloa., 2006, Smith *et al*., 2007).

2.1.2.2 Health facilities

Malaria data which drive from hospital or clinic can be misleading to overestimate or underestimate of malaria cases. This inaccuracy due to misdiagnosis in patients or lack of equipped and trained nurse and clinician (Afrane et al., 2013). Access to health facilities also another issues of malaria cases. From the existence of health care, availability of medicine or vaccine, service quality and affordability also give impact to the health interventions (O'meara et al., 2009).

2.1.2.3 Migration

Migration affect malaria transmission on infection spreading, transmit to non-immune people from the risk of infection and make the malaria spreading more difficult to be controlled (Prothero ., 2001). In developing countries, irregular and rapid urbanization caused enhancement in malaria transmission due improverished house and sanitation, drainage surface water deficiency, and utilize of exposed water reservoir which enhance interaction between host-vector and mosquito breeding places (Martens and Hall., 2000).

2.1.2.4 Poverty

Poverty is identical with the cause of malaria cases. The relationship between malaria and poverty is also complex. Poverty made malaria flourish, inhibit economic growth and keep people still in poverty (Sachs and Malaney., 2002). Houses with low income could not provide some treatment to malaria (buy

insecticide-treated bednet (ITNs)), awareness to check the health facilities, food insecurity, undernourished children, less knowledge about malaria prevention, symptoms and early warning of malaria infection (Teklehaimanot and Mejia., 2008)

2.2 Malaria transmission model

Due to sparsity of the observation dataset, time and cost limitation, malaria transmission model are developed to assist researchers to predict and examine malaria transmission trend in historical period.

2.2.1 Compartment model

Malaria transmission model is firstly developed by Sir Ronald Ross. (Ross., 1911) developed a first deterministic compartment model and classify human population into two compartments, i.e. susceptible (S) and infected (I) and assumed the infected people will return to susceptible again or known as SIS structure (Mandal et al., 2011). Due to it's simplicity, this model ignored latency period of the parasite inside mosquitoes and their survival rate. Then, Ross model is developed by other researchers, such as (Macdonald., 1957) add a new compartment exposed (E) on mosquito after susceptible state, (Anderson and May., 1991) add exposed (E) state on human state after susceptible state. Other factors, such as human age (Aaron and May., 1982), human age and immunity function (Filipe et al., 2007), human migration or visitation (Torres-Sorando and Rodriguez., 1997), vary population size (Ngwa and Shu., 2000, Chitnis et al., 2006), environment on mosquito (Parham and Michael., 2010), socio-economic factors on human and environment on mosquito (Yang., 2000).

Table 2.2.1 Compartment Model Development

Author	Model name	Climate/nonclimate/mechanism or improvement
(Ross., 1911)	SIR (Ross model)	Compartment model : SIR Susceptible – Infectious – Recovered)
(Macdonald., 1957)	Susceptible – Infectious – Susceptible – Exposed (on mosquito)	Adding latency period and introduced in exposed class in the mosquito part (E_m)
(Anderson and May., 1991)	Susceptible – Infectious – Susceptible – Exposed (on human state)	Latency of infection in humans is added by making additional exposed class in humans (E_h)

(Aaron and May., 1982)	Susceptible – Infectious – Recovered – Susceptible (on human state)	Adding recovered class after infected before return to susceptible on human state
(Filipe *et al.*, 2007)	Susceptible – Exposed – Infectious – Susceptible (on human)	Human age and immunity function on human stage
(Torres-Sorando and Rodriguez., 1997)	Susceptible – Infectious – Susceptible (on human)	Human migration or visitation on human stage
(Ngwa and Shu., 2000; Chitnis *et al*., 2006)	Susceptible – Exposed – Infected – Recovered – Susceptible (on human stage)	Add recovered class on human stage (Ngwa and Shu) and consider constant immigration on beginning of susceptible class on human stage Vary population size o
(Parham and Michael., 2010)	Susceptible – Infected – Recovered – Susceptible (on human stage)	Add environment factor on mosquito stage
(Yang., 2000)	Susceptible – Exposed – Infected – Recovered – Susceptible (on human stage)	Add socio-economic factors on human and environment on mosquito
Laneri *et al*., (2010)	VSEIRS	Rainfall together with malaria data
White *et al*., (2018)	Treated (T) – Prophylaxis (P) – Susceptible (S) – Infected (I) by three types (high-density parasites with fever,	Heterogeneity and seasonality exposure to mosquito bites, detailed mosquito bionomics and modelling of larval population densities, demographic age structure, exposure and age-dependent acquisition of immunity against blood-stage infection and clinical episodes,

	LM detectable parasites and PCR detectable parasites)	maternally-acquired immunity, and treatment of clinical cases and drug prophylaxis
Addawe *et al.*, (2016)	Susceptible humans (S_H) – Infectious humans (I_H) – Recovered humans (R_H)	Subdivided into two human classes : pre-school shildren ($\leq$ 5 years old) and the rest of the humans (>5 years old)
Orwa *et al*., (2018)	Sporozoite (S) – Susceptible hepatocytes (H) – infected hepatocytes (H_X) – susceptible red blood cells (RBCs) – infected red blood cells (IBRCs) R_X – morozoites (M) and macrophages (Z)	Dynamics of *Plasmodium falciparum* parasite during hepatocytic and erythrocytic stages and their interactions with the host's red blood celss, liver hepatocytes and the macrophages in host malaria model

These models do not consider the dynamic of malaria disease which lead to stochastic event. Therefore, some researchers develop a dynamic malaria model to describe the distribution more realistic.

2.2.2 Dynamical model

There are three factors which is caused malaria disease: parasite, human, and vector (mosquito). Due to difficulties to calculate the abundance of mosquito, one approach is by utilizing malaria transmission model. Besides that, the availability of the dataset is also sparse, takes time, costly and more risks to do the sampling observation site. There are some dynamic malaria transmission models over the world (Fig. 2.1).

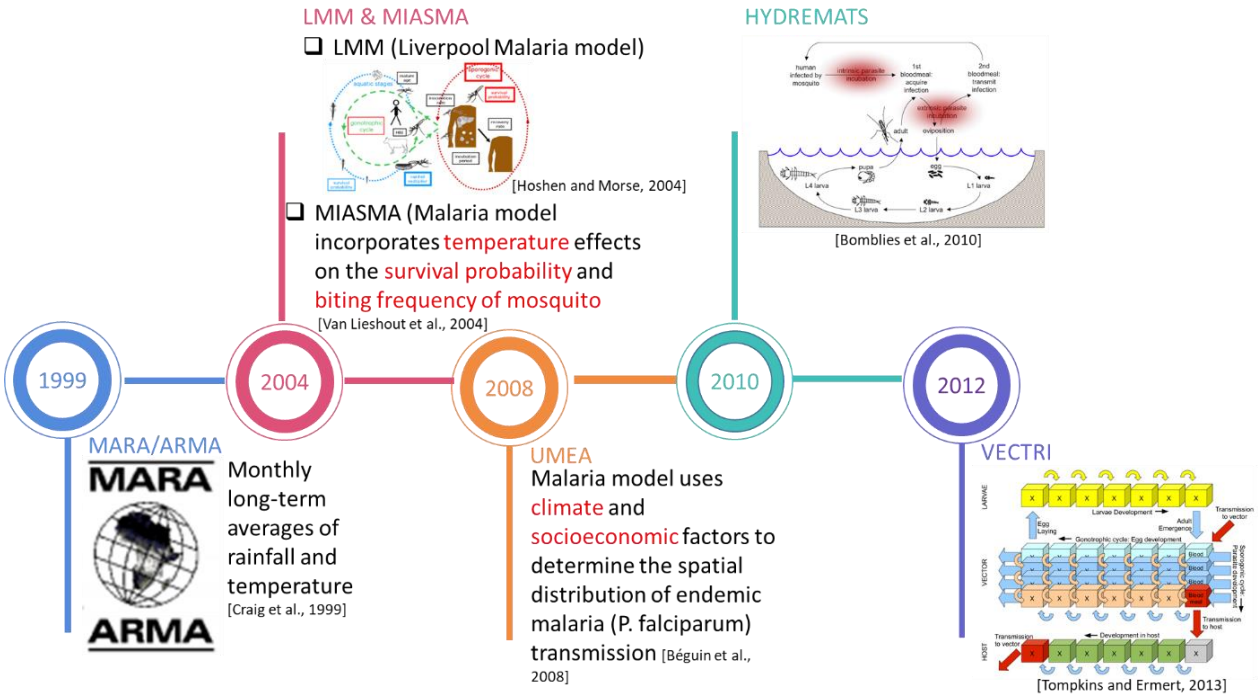

Fig. 2.2 Malaria transmission model timeline

In 1999, MARA (Malaria Risk in Africa) is developed. This model incorporates malaria transmission season for locations in Africa based on monthly long-term averages of rainfall and temperature (Craig et al., 1999). In 2004, Liverpool Malaria Model (LMM) and MIASMA are developed. LMM is a mathematical-biological model of the parasite dynamics, comprising both the weather-dependent within-vector stages and the weather-independent within-host stages (Hoshen and Morse, 2004). In 2008, UMEA model is developed. This model uses climate and socioeconomic factors to determine the spatial distribution of endemic malaria (*P. falciparum*) transmission (Belguin et al., 2008). In 2010, Hydrology, Entomology and Malaria Transmission Simulator (HYDREMATS) is developed to simulate the mechanism between environmental variables (spatially distributed, satellite-derived vegetation and soil parameters) and malaria transmission with high temporal and spatial resolution (Bomblies et al., 2010). HYDREMATS is limited to local scale with 10 m resolution. In 2012, Vector-borne infectious disease is developed by International Center for Theoretical Physics, Trieste, Italy (VECTRI). VECTRI is a mathematical model for malaria transmission that account for the impact of temperature and precipitation variability on development cycle of malaria vector in its larval, adult stage and parasite development (Tompkins and Ermert, 2013). This study utilized VECTRI because this model could simulate at regional scale and incorporate climate, population density, and surface hydrology. VECTRI incorporate precipitation, temperature and population density as forcing datasets.

Table 2.2.2 Dynamical Model Development

Author	Model	Climate/nonclimate/mechanism
Craig *et al*., (1999)	MARA (Malaria Risk in Africa)	Monthly long-term average of precipitation temperature

Hoshen and Morse., (2004)	LMM (Liverpool Malaria Model)	weather-dependent within-vector stages and the weather-independent within-host stages
Van Lieshout *et al*., (2004)	MIASMA (Modelling framework for the heal Impact ASsesment of Man-induced Atmospheric changes)	Temperature effect on the survival probability and biting frequency of mosquito
Belguin *et al*., (2008)	UMEA	Climate and socio-economic factors to determine the spatial distribution of endemic malaria (*P. falciparum*) transmission
(Bomblies *et al*., 2010).	HYDREMATS (Hydrology Entomology and Malaria Transmission Simulator)	limited to local scale with 10 m resolution

2.3 VECTRI model scheme

VECTRI is a first spatially explicit malaria model that can simulate at high resolutions by incorporating climate, population density and surface hydrology on malaria transmission. VECTRI mimics from mosquito life cycle and the mechanism of VECTRI model is described in Fig 2.3.

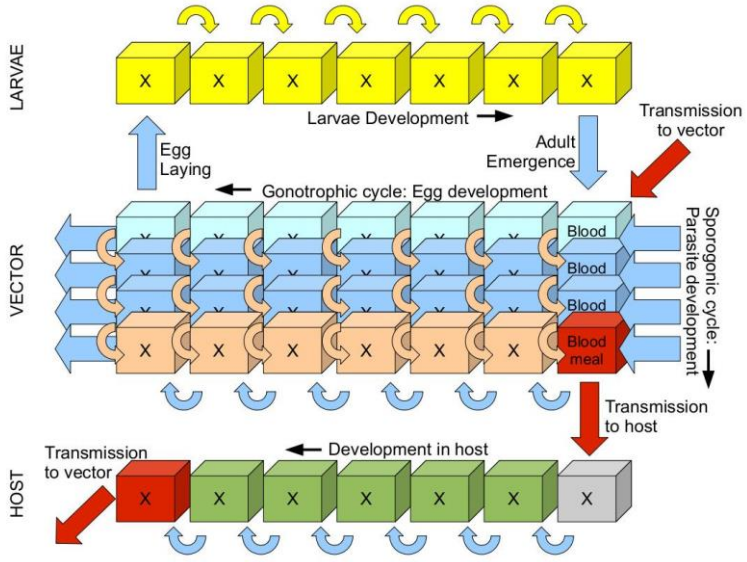

Fig. 2.3 VECTRI model scheme (Tompkins and Ermert, 2013)

Mosquito life cycle start from egg, then its growth into larva. In larva there are four stages of development. In this model, larva stage development is described in some yellow boxes. Each x symbol in yellow boxes is described larva density with specific fractional growth stage. Mature larva will hatch into adult mosquito. In adult stage there are two phase of development, i.e. egg development and parasite development. When a parasite inside mosquito's body in mature stage, it will transmit to host. The development of parasite inside host's body is represented in lower boxes. Like in mosquito's body, when a parasite has enough age, it will transmit to host if a new fertile mosquito bites an infected host and spread to a non-infected host. Red arrows represent parasite distribution between host and mosquito. direction of development stage of larvae, vectors and host conditions are arranged by curved arrows.

2.3.1 Larvae stage development

2.3.1.1 Larvae cycle

Degree day is a way of measuring insect growth development in response to daily temperature introduced by (Detinova, T.S. et al., 1962).. This concept is implemented on larvae growth rate:

$$RL = \frac{T_{wat} - T_{L,min}}{K_L} \tag{1}$$

Where $R_L$is larvae growth rate, T_{wat} is temperature of pools fix offset to the air temperature, $T_{L,min}$ is minimum pool temperature for larvae development and K_L is larvae growth degree days. In this study, $T_{wat}$is 2^0 K (Paaijmans et al., 2008), T_{Lmin} is 16^0 K (Bayoh and Lindsay, 2003), and K_L was following (Jepson et al., 1947) estimated to be 90.9 degree days. Meanwhile, (Bayoh and Lindsay, 2003) approximated K_w was 200 degree days.

2.3.1.2 Larvae mortality

Survival rate of larva is calculated as :

$$P_{L,surv} = \left(\frac{1 - M_L}{w\, M_{L,max}}\right) K_{flush}\, P_{L,surv0} \tag{2}$$

Where $M_L$represents total larvae biomass per unit surface area, w is fraction of water coverage of a grid for potential mosquito breeding sites, $M_{L,max}$ is a maximum carrying capacity, $P_{L,surv0}$ represents daily larva survival base, which is set to be 0.825 (Ermert et al., 2011), and K_{flush} is larvae flushing rate, which will be determined from equation (3). Total larvae biomass follows (Bomblies et al., 2008) which is assumed to increase linearly for a stage 4 larva, with average mass 0.45 mg. Maximum carrying capacity used in this model is 300 mg/m^2 (Depinay et al, 2004). If there is no water fraction of water coverage (w=0), larva could not survive $(P_{L,surv} = 0)$.

$$K_{flush} = L_f + (1 - L_f)\left((1 - K_{flush,\infty})e^{\frac{-R_d}{\tau_{flush}}} + (K_{flush,\infty})\right) \quad (3)$$

Where L_f represents larvae fractional growth state, $K_{flush,\infty}$ larvae flushing factor for infinite rain rate, R_d is precipitation rate in (mm/day), τ_{flush} is the rate of flushing effect as a function of precipitation. In this study, $K_{flush,\infty} = 0.4$ and $\tau_{flush} = 50$ mm/day.

2.3.2 Vector (Adult) stage development

On adult stage, there are two stages of mosquito development. First, related to egg development known as gonotrophic cycle and second, related to parasite development inside mosquito's body known as sporogonic cycle.

2.3.3 Gonotrophic cycle

Gonotrophic cycle is time needed from first day of blood searching until adult female put their first egg. Gonotrophic cycle describes development of mosquito's egg. VECTRI model assumed that mosquito found a blood meal in the first night of searching. Therefore, after blood meal taken, egg development, which follows degree day concept, is calculated as:

$$R_{gono} = \frac{T_{2m} - T_{gono,min}}{K_{gono}} \quad (4)$$

where T_{2m} is 2 meter air temperature, $T_{gono,min}$ is minimum T_{2m} for egg development, and K_{gono} is gonotrophic cycle degree days. In this study, $T_{gono,min} = 7.7^0$C and $K_{gono} = 37.1$ K day.

2.3.4 Sporogonic cycle

Sporogonic cycle describes parasite development inside mosquito's body. During blood searching meal, there is a probability to transmit parasite between vector and human or vice versa. The transmission probability from an infected host to the vector is assumed to be constant $P_{hv} = 0.2$ based on (Ermert et al., 2011) Then, transmission probability is calculated by:

$$P_{h \to v} = \frac{H_{inf}}{H} P_{hv} \quad (5)$$

Where H_{inf} is infected host population density and H is total host population density. The ratio of vector got infected and parasite development inside vector's (sporogonic cycle) following degree day concept:

$$R_{sporo} = \frac{T_{2m} - T_{sporo,min}}{K_{sporo}} \quad (6)$$

Where $T_{sporo,min}$ is minimum T_{2m} for sporogonic cycle $(T_{sporo} = 16^0 C)$ and K_{sporo} is sporogonic cycle degree days $(K_{sporo} = 111 \text{ K day})$.

2.3.5 Vector survival

Non-linear relation between vector mortality and air temperature is described as a quadratic equation in Marten I and II scheme. The higher air temperature increases the higher vector mortality. Vector survival probability following scheme:

Marten I scheme :

$$P_{V,surv1} = 0.45 + 0.054\, T_{2m} - 0.0016\, T_{2m}^2 \quad (7)$$

Marten II scheme :

$$P_{V,surv2} = \exp\left(-\frac{1.0}{-4.4 + 1.31\, T_{2m} - 0.03\, T_{2m}^2}\right) \quad (8)$$

This study used the Marten II scheme (revised version of Marten I) since in Marten I scheme vector survival probability starts earlier air temperature, in 20^0 C (Asare, 2015)

2.3.6 Host and vector transmission

Since in VECTRI incorporate population density, the average number of bites per human is estimated as follow:

$$hbr = \left(1 - e^{\frac{-H}{\tau_{zoo}}}\right) \frac{\sum_{j=1}^{N_{sporo}} V\,(1,j)}{H} \quad (9)$$

where $\left(1 - e^{\frac{-H}{\tau_{zoo}}}\right)$ is the level of vector zoophily and $\frac{\sum_{j=1}^{N_{sporo}} V\,(1,j)}{H}$ is the proportion of biting vectors to hosts. Population density zoophilic factor (τ_{zoo}) used in this study is $50/km^2$.

The daily transmission probability from a person can be calculated as:

$$P_{v\to h} = \sum_{n=1}^{\infty} G_{\overline{EIR_d}}(n)\,(1 - (1 - P_{vh})^n) \quad (10)$$

Where $G_{\overline{EIR_d}}(n)$ is the Poisson distribution for mean $\overline{EIR_d}$ and $(1-(1-P_{vh})^n)$ is the transmission probability of n infective bites per person. $\overline{EIR_d}$ is daily average of infectious bites per person per day. This number is calculated from hbr multiply by circumsporozoite protein rate (CSPR: percentage of parasite on vector's body).

P_{vh} is transmission probability from vector to host per bites per infective vector and assumed constant $(P_{vh} = 0.3)$ (Ermert et al., 2011).

2.3.7 Surface hydrology/small surface water

Fractional surface water coverage of each grid for mosquito breeding places is defined as w. This fraction is determined by permanent water bodies (w_{perm}) add with temporary ponds (w_{pond}) as in equation (11):

$$w = w_{pond} + w_{perm} \tag{11}$$

In this model, permanent water body is constant and set to be zero. This is because larvae need a stagnant surface water body to develop (Sattler et al., 2005).

Coverage is simply linearly to pond coverage and calculated from equation (12):

$$\frac{dw_{pond}}{dt} = K_w\left(P\left(w_{max} - w_{pond}\right) - w_{pond}(E+I)\right) \tag{12}$$

Where K_w is pond growth rate parameter, P is precipitation, w_{max} is maximum waterfraction, E is evaporation rate, and I is infiltration rate. VECTRI default K_w, E, and I to bet constant, with $K_w = 0.001$, $E = 5$ mm/day, and $I = 245$ mm/day.

2.4 Malaria Indicator Number

To describe malaria risk number, researchers set some malaria indicator numbers from observation site study, such as Human Bite Rate (HBR), Circumsporozoite Protein Rate (CSPR), Entomological Inoculation Rate (EIR), malaria incidence rate, *Plasmodium falciparum* Parasite Rate (*PF*PR), and Basic Reproduction Number (R_0).

2.4.1 Human Bite Rate (HBR)

HBR was calculated by dividing the number of *An. funestus* and *An. gambiae s.s.* vectors from CDC LTs by the number of people sleeping in the household the night of the collection. The challenges to collect mosquito using CDC LTs is mosquito traps to catch mosquito outdoors which is expensive and need to charge the battery to utilized (Kilama et al., 2014). One of method to determine this number is called Human Landing Catch (HLC). Mosquito collector catch and collect mosquito which come into their exposed hand. Human Bite Rate (HBR) is average number of bites per person per night. This number calculated by examining the number of mosquito bite human per human in a period then divided

by the number of days. The equipment to catch mosquito is called aspirator or pooter pipe as described in Fig 2.4.1 (a).

Fig. 2.4.1 (a) Aspirator or pooter

Aspirator or pooter consist of a glass or plastic pipe and a rubber. This rubber is installed at one end of the pipe and a filter is installed to obstruct mosquito enter into the tube. The collectors catch mosquito which come into them as describe in Fig 2.4.1 (b). This figure represents mosquito catchment methodology called Human Landing Catch (HLC).

Fig 2.4.1 (b) Human Landing Catch (HLC) process

Mosquito collector was sitting inside or outside house overnight without cover their arms and legs.

2.4.2 Circumsporozoite Protein Rate (CSPR)

Circumsporozoite Protein Rate (CSPR) is the percentage of parasite of malaria disease inside mosquito body. CSPR is calculated by CSP-ELISA method to separate thorax, abdomen, and salivary gland test. CSPR method is described in Fig. 2.4.2.

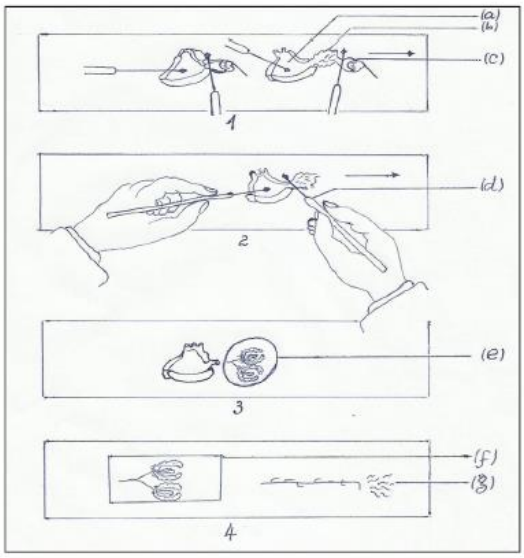

Fig 2.4.2 Dissection of salivary glands on *Anopheles* (Saotoing P. *et al.*, 2013)

Figure 2.4.2 illustrate various stages of dissection of the salivary glands of adult female *Anopheles.* Step 1 -4 describe stages of dissection and (a) – (g) describe each part of the process. Start with (a) thorax of *Anopheles*, (b) salivary gland of *Anopheles*, (c) head of *Anopheles* (d) needle attached, (e) saline and salivary glands, (f) salivary gland covered with leaf, and (g) sporozoites.

2.4.3 Entomological Inoculation Rate (EIR)

Entomological Inoculation Rate (EIR) is the average number of infections caused by the bite of an infected mosquito in the population of the area (infected bites/person/per unit time). EIR is calculated by multiplication of HBR and CSPR. There are some uncertainties of EIR from observation site, such as: different time period to collect mosquito, different number of sampling area or household and different species in observation site.

2.4.4 Malaria Incidence Rate

Malaria incidence rate was estimated as the number of malaria cases per 1000 population at risk (de Oliveira Padilha *et al.*, 2019).

2.4.5 *Plasmodium falciparum* Parasite Rate

Plasmodium falciparum parasite rate (*Pf*PR) is an index to represent malaria transmission intensity. *Pf*PR is related to EIR number at the steady state (Smith *et al.*, 2007). *Pf*PR increase during early

childhood due to related to age and transmission intensity (Gupta *et al.*, 1999) and decrease in teenage and adult due to increasing immunity of malaria (Baird *et al.*, 1991)

2.4.6 Basic Reproduction Number (R_0)

Basic reproduction number (R_0) define as an index of transmission intensity and threshold criteria of the transmission. (Smith *et al.*, 2007). If R_0 uis higher than one, the number of people get infected by the parasite increase. If R_0 is less than one, the number of people get infected decrease.

CHAPTER 3

Material and Methods

Abstract:

This chapter explain the methodology used in this study. Starting from running malaria model on historical period, collecting existing observation datasets in historical period, validating simulation on historical period, calibrating and optimizing pond growth rate, running malaria model on projection period and analyze simulation results on historical and projection period to examine malaria trend and impact of climate change. Three experiments on historical period (one experiment for validation of EIR from 1983-2006, and two experiments for calibration water fraction from 2014-2018) and one experiment for future period under three SSP scenario from 2020-2100 are conducted in this study. Availability of observation datasets also explain and available in some countries, i.e. Senegal, Republic of Congo, Burundi, Gambia, Democratic Republic of Congo, Gabon, Cameroon, Eritrea, Uganda, Zambia, Tanzania, and Kenya.

3.1 Methodology

The methodology used in this study described in Fig. 3.1.

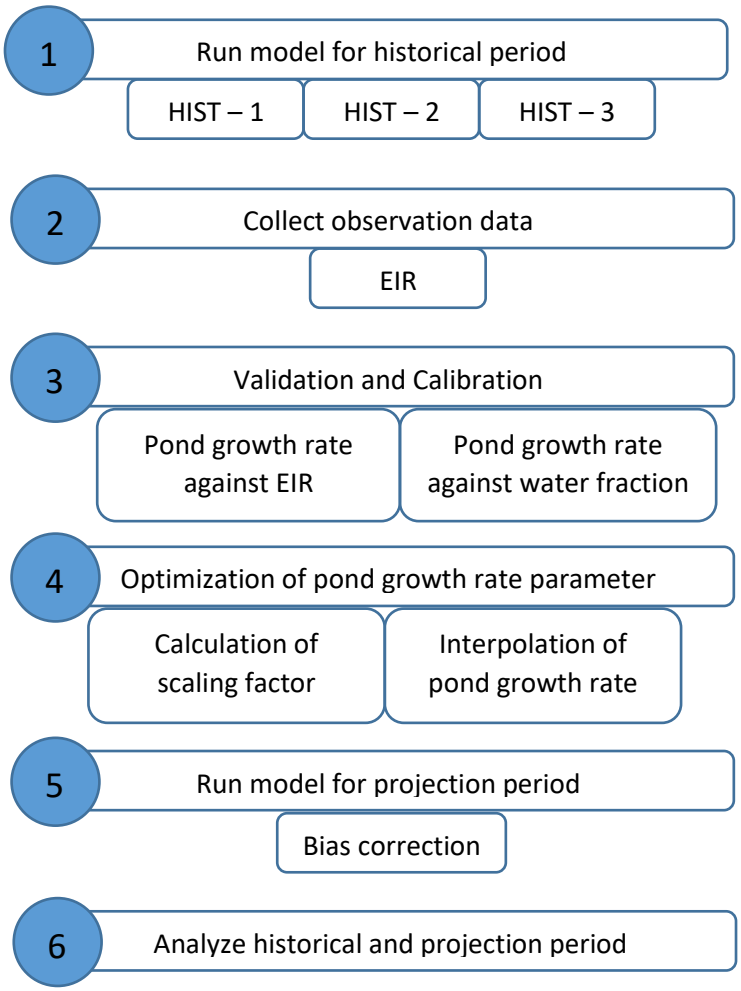

Fig. 3.1 Methodology

Methodology used in this study starts with run malaria transmission model, collect observation dataset, validate simulation on historical result to all observation site studies, optimize pond growth rate parameter, run simulation of projection period, and analyze simulation on historical and projection period. Firstly, running VECTRI model on three historical periods is conducted. Optimization of pond growth rate parameter is divided into two steps. First step, calibration of pond growth rate parameter against Entomological Inoculation Rate on first historical period. Second step, calibration of pond growth rate parameter against observation surface water on second and third historical period. To optimize pond growth rate from both step, a scaling factor is needed by implementing topography factor. After scaling factor is derived, an interpolation is needed to predict unknown value of an optimized pond growth rate parameter in spatial domain of Africa. An optimized pond growth rate parameter will be used to simulate malaria transmission on projection period. Finally, analyzing historical simulation and projection simulation to investigate the change or trend of malaria transmission.

This study starts from running VECTRI model for historical period with forcing datasets. The next step is collecting observation dataset to be used for validation the model result. After collection Entomological Inoculation Rate (EIR) for validation, the comparison between EIR model result and EIR observation is conducted. After that, simulate malaria transmission for projection period. Finally, analyze historical and future period to examine the changing of malaria transmission in the past and future period.

3.2 Experimental design

To run the model, some forcing datasets is needed as input data.

3.2.1 Forcing datasets used in VECTRI model

To do the simulation, several forcing datasets used in this study:

1. Precipitation:
    a. CPC/Africa Rainfall Climatology 2 with 0.1x0.1 degree resolution
    b. Tropical Rainfall Measuring Mission (TRMM) with 0.1 x 0.1 degree resolution)
2. Temperature: ERA-interim with 0.1x0.1 degree resolution
3. Topography: USGS EROS Archive – Digital Elevation – Global 30 Arc-Second Elevation (GTOPO30)
4. Population density: Socioeconomic Data and Application Center (SEDAC) with 30 arc degree resolution
5. Water fraction: Global Satellite Mapping of Wet Surface (GSMaWS) with 0.1 x 0.1 degree resolution
6. Projection:

a. Precipitation: CMIP6 with 0.1x0.1 degree resolution for RCP scenario 2.6, 7.0 and 8.5
b. Temperature: CMIP6 with 0.1x0.1 degree resolution using SSP scenario 2.6, 7.0 and 8.5
c. Population density: SEDAC with 0.1x0.1 degree resolution using SSP scenario 1, 3 and 5

3.2.2 Simulation Domain

This study analyses malaria transmission in African region.

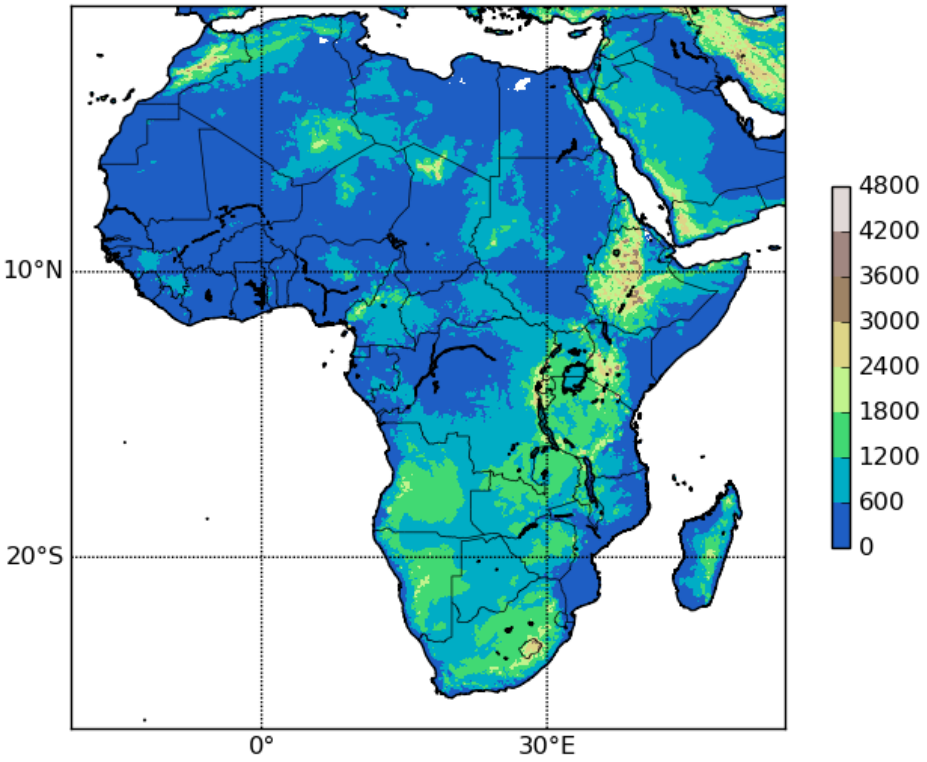

Fig. 3.2 Topography map of Africa (meter)

With latitude 38^0N and -38^0S, longitude -20^0W and 55^0E.

3.2.3 Simulation scenario used in this study:

This study conducted 3 scenario of simulation. Two scenario for historical period and one scenario for future period. All scenario listed Table 3.2

Table 3.2 Simulation scenario for historical and future period

Experiment Name	Simulation Period	Precipitation	Temperature	Population density	Water fraction

HIST-1	Historical period (1983-2006)	CPC/Africa Rainfall Climatology 2	ERAIN	SEDAC	Calculated in the model
HIST-2	Historical period (2013-2018)	TRMM	ERAIN	SEDAC	Calculated in the model
HIST-3	Historical period (2013-2018)	TRMM	ERAIN	SEDAC	GSMaWS
PROJECT-1	Projection period (2020 – 2100)	CMIP6	CMIP6	SEDAC	Calculated in the model

Due to availability of EIR observation is limited (from 1983 – 2006), we used CPC/Africa Rainfall Climatology 2 for precipitation in HIST – 1 experiment. From HIST – 1 experiments, pond growth rate (K_w) parameter is tuned against EIR to derived EIR simulation value is close to EIR observation.

For recent simulation period, we used TRMM for precipitation in HIST – 2 and HIST – 3 experiment. HIST – 2 and HIST – 3 experiment is used to derived optimized of pond growth rate parameter by minimizing the root mean square deviation of water fraction simulation and observation.

Optimized pond growth rate parameter against EIR from HIST – 1 and against water fraction from HIST – 2 and HIST – 3 are obtained. By optimizing this two optimized pond growth rate parameter, an optimized pond growth rate parameter is derived. Then, this optimized pond growth rate parameter will be used to conduct simulation in future period.

3.3 EIR observation sites for historical period

EIR observation from literature studies 1983 – 2006 :

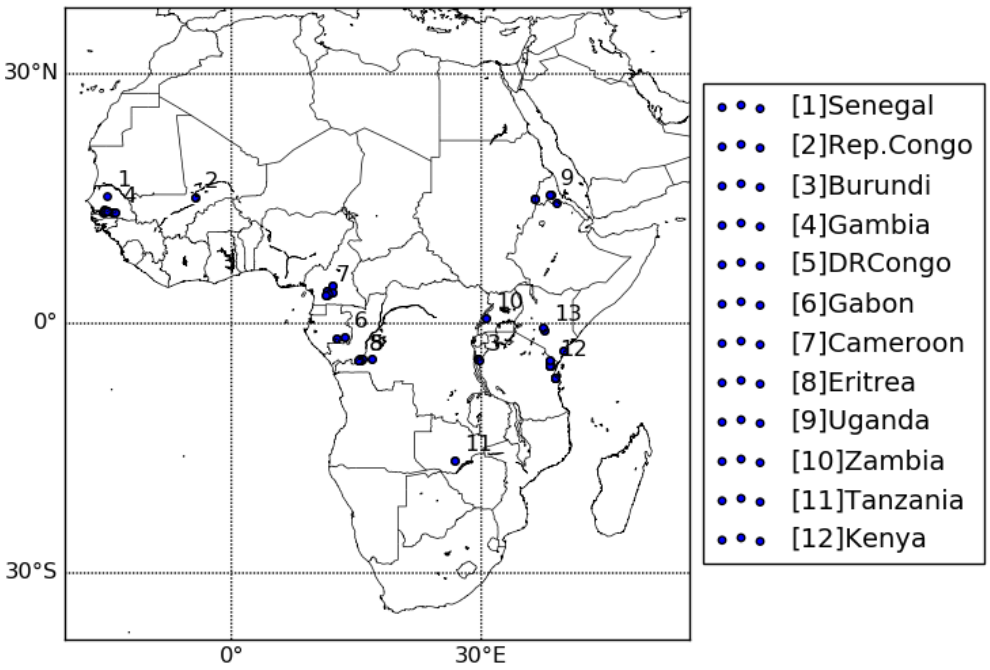

Fig. 3.3.a. EIR observation site in Africa

Fig. 3.3.a represents EIR observation in some sites in Africa from 1983 – 2006. Blue dots represent location of EIR annual datasets. The detail of EIR observation sites are explained in Appendix 1.

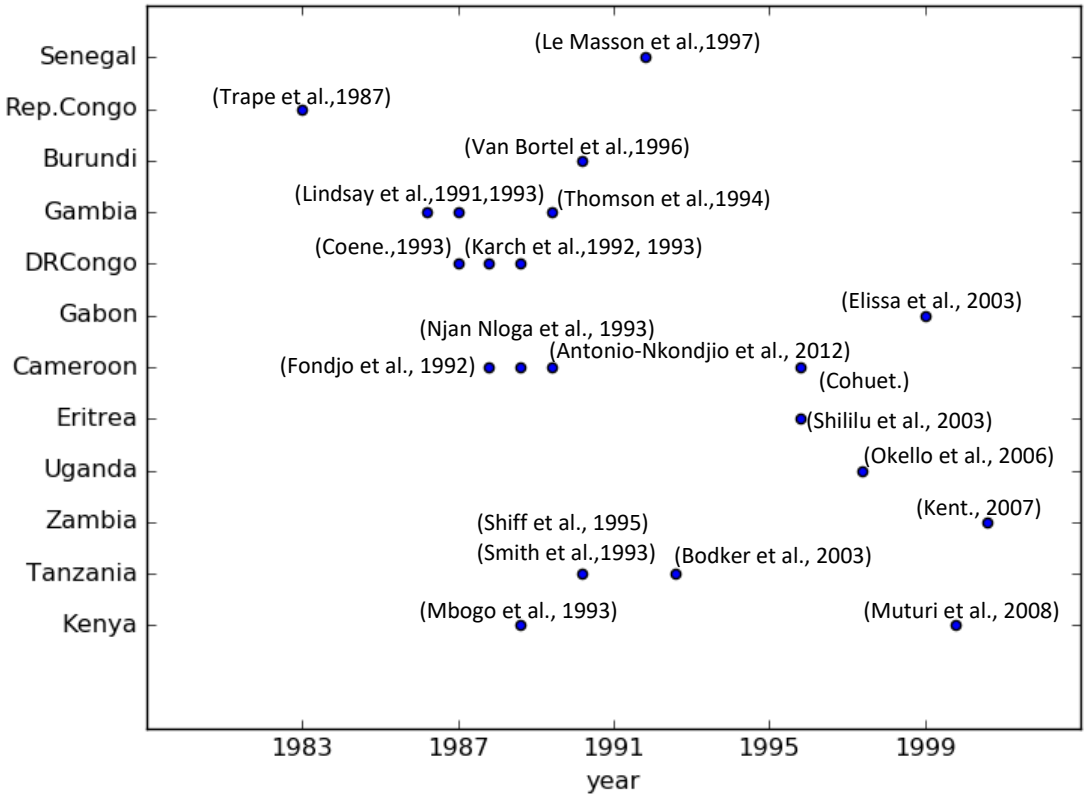

Fig 3.3.b Distribution of annual EIR in some observation sites in Africa

Fig 3.3.b describe distribution of EIR annual and monthly EIR in some observation sites in Africa. Blue circle represent location of annual EIR observation in Africa. EIR annual observation were located in 12 country, as : Senegal, Republic of Congo (Rep.Congo), Burundi, Gambia, Democratic Republic of Congo (DRCongo), Gabon, Cameroon, Eritrea, Uganda, Zambia, Tanzania, and Kenya.

CHAPTER 4

Malaria Transmission on Historical Period

Abstract:

Availability of surface water is a critical for mosquito breeding places (Emidi et al., 2017). Mosquitoes needs a stagnant water for laying their eggs. Representation of small surface water is not realistic enough in malaria transmission model. Surface water formation parameter is assumed constant in VECTRI model setting. By doing sensitivity analysis of this parameter could increase validation of EIR. Surface water satellite dataset is used to calibrate EIR on historical period. By calibrating surface water parameter against EIR and surface water calculated from model setting, an optimized number of surface water formation parameter could be estimated. Surface water optimized from tuning against EIR and surface water optimized from calibrating against water fraction will be used to determine an optimized pond growth rate parameter (K_w). This K_w will be used to predict malaria transmission in the future.

4.1 Seasonal climate over Africa

In Africa, based on peak precipitation is divided into three categories: unimodal, bimodal, and trimodal. Unimodal is a region where only have one precipitation peak. Bimodal is a region which has two precipitation peak. Trimodal is a region which has three precipitation peak.

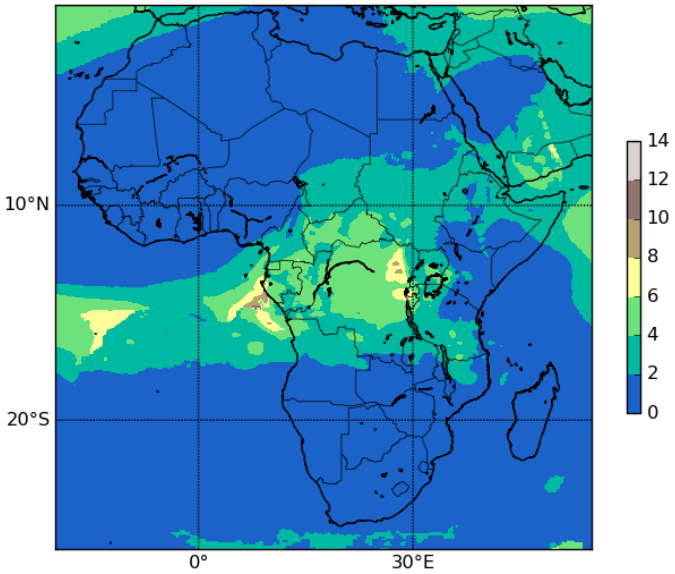

Fig. 4.1 Spatial distribution daily mean precipitation (mm/day) 1983-2006

In West Africa and Horn of Africa, it has only one precipitation peak or unimodal. Monthly mean precipitation of Senegal and Gambia in West Africa and Eritrea in Horn of Africa is described in Fig.4.1.1

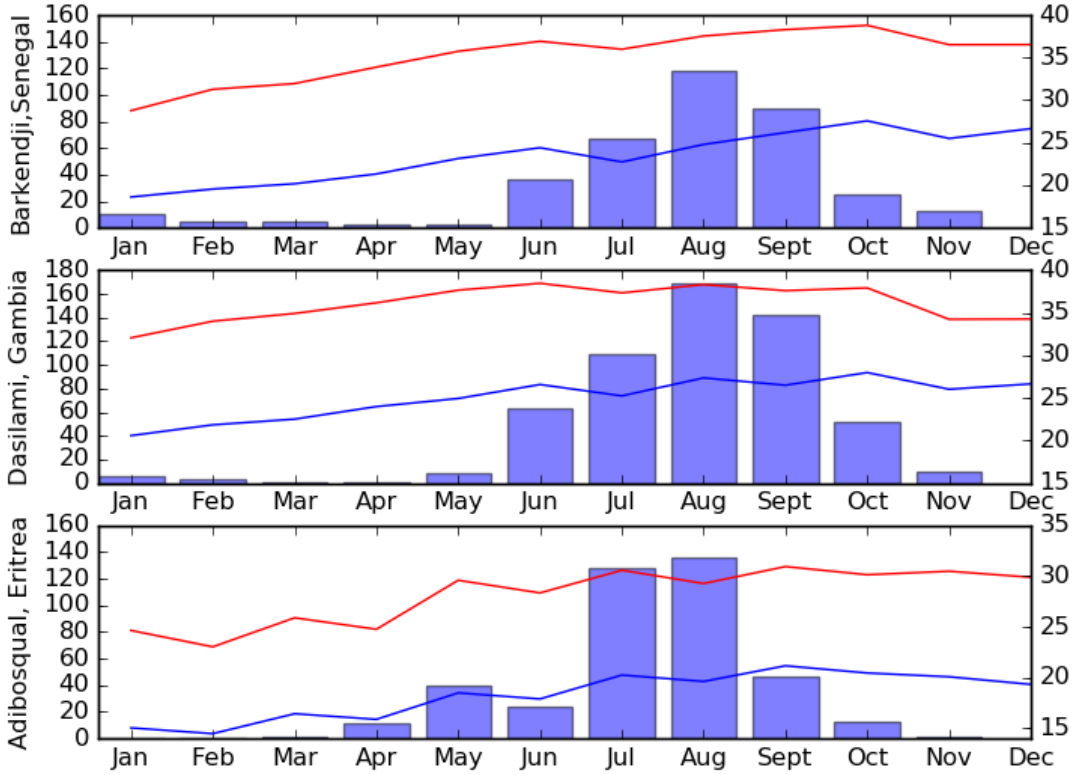

Fig. 4.1.1 Monthly mean precipitation, maximum and minimum temperature in Barkendji (Senegal), Dasilami(Gambia) and Adibosqual (Eritrea) from 1983-2006 (bar: monthly precipitation, red line: maximum temperature, blue line: minimum temperature)

In Barkendji (Senegal) and Dasilami (Gambia), precipitation peak is from July – September with the highest amount is mm and mm, respectively. Meanwhile in Adibosqual (Eritrea), precipitation peak is from July – August., with mm. Maximum and minimum temperature in Barkendji (Senegal) is in range 15 – 40 ^{0}C, with the peak of maximum temperature is on October with x^{0}C and peak of minimum temperature is on January with ^{0}C.

In Central Africa, South-Central Africa, and West-Central Africa, have two precipitation peaks or bimodal. Monthly mean precipitation of Democratic Republic of Congo, Cameroon in Central Africa, Tanzania in South-Central Africa and Gabon West Central Africa is described in Fig.4.1.2

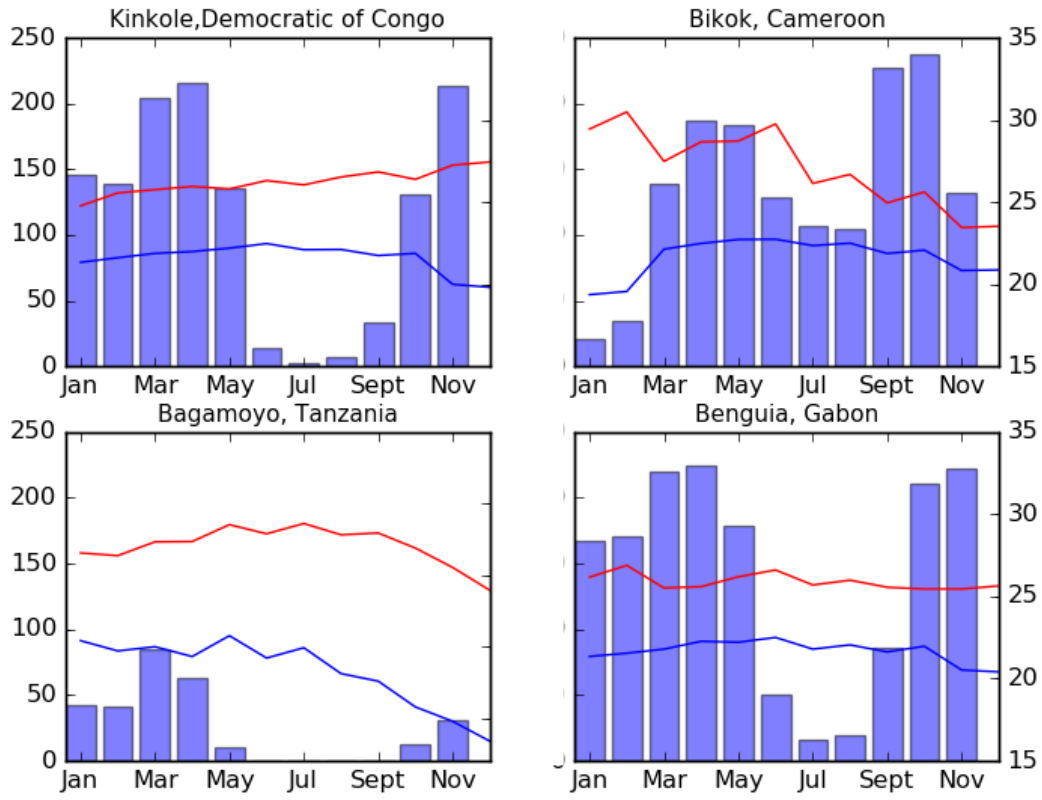

Fig. 4.1.2 Monthly mean precipitation, maximum and minimum temperature in Kinkole (Democratic Republic of Congo), Bikok (Cameroon), Bagamoyo (Tanzania), and Benguia (Gabon) from 1983-2006 (bar: monthly precipitation, red line: maximum temperature, blue line: minimum temperature)

In Kinkole (Democratic Republic of Congo), Bagamoyo (Tanzania), Benguia (Gabon), first precipitation peak is from March – April and second peak is from October – November. Meanwhile, in Bikok (Cameroon), first precipitation peak is from April – May and second peak is from September – October. Precipitation in Bagamoyo (Tanzania) is the lowest compared to other three sites and has no precipitation on June – September (dry season). In Bikok (Cameroon), the lowest precipitation peak is January. Meanwhile in Benguia (Gabon) and Kinkole (Democratic Republic of Congo), the lowest precipitation peak is July. Maximum and minimum temperature in Kinkole (Democratic Republic of Congo) and Benguia (Gabon) is in range 20 – 30 ^{0}C. Temperature in Bagamoyo (Tanzania) is decreasing from July into December.

4.2 Parameterization of pond growth rate on historical period

Small surface water is a critical place for mosquito breeding places (Emidi et al., 2017). But, surface water is not currently realistic represented in malaria transmission model (Tompkins,

and Ermert, 2013). Therefore, a satellite observation of water fraction is used to represented a more realistic model. Calculation of water fraction is highly determined by pond growth rate (K_w) parameter (as in equation (12)). To achieve optimized EIR simulation fit well to EIR observation, experiment from HIST-1 and HIST-2 are conducted.

From experiment HIST-1, precipitation, temperature, topography and population density are used as a forcing data to tune K_w parameter against EIR. Meanwhile, from experiment HIST-2, precipitation, temperature, topography, population density, and water fraction observation are utilized to tune K_w parameter against water fraction. From this two experiments, the optimized K_w parameter could be derived.

4.2.a EIR annual by tuning pond growth rate (K_w) in Benguia, Gabon, West-Central Africa from experiment HIST-1

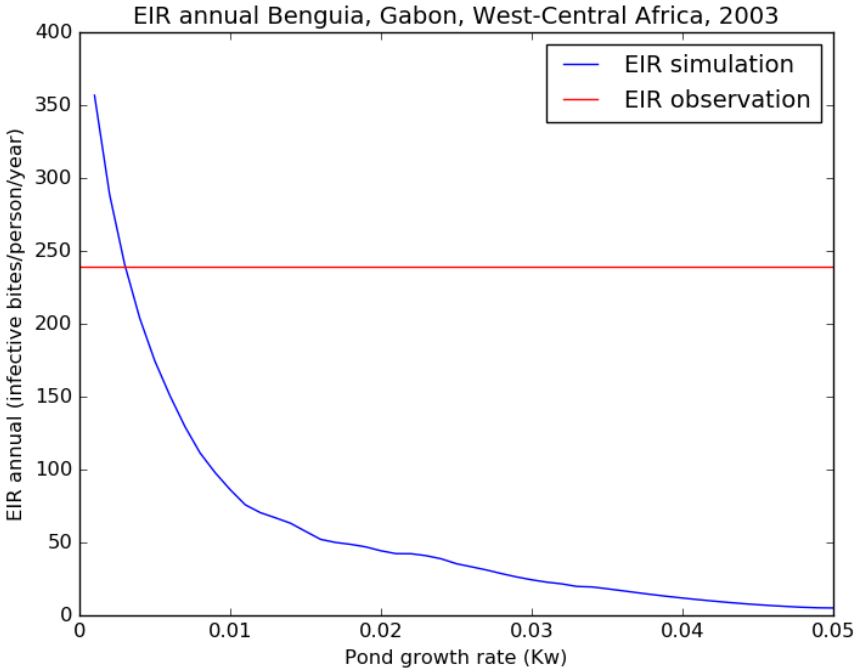

Fig. 4.2(a) EIR annual in Benguia, Gabon, West-Central Africa, 2003 with tuning pond growth rate (K_w) parameter

Fig 4.2(a) describes relation between K_w and EIR observation and simulation in Benguia, Gabon. EIR annual observation in Gabon is 239.1054. By using default setting of $K_w = 0.001$ EIR annual simulation with default setting (CTRL) is 356.7138. If K_w parameter is increased into 2x from default setting ($K_w = 0.002$), EIR annual simulation decrease into 288.672. Then, if K_w is increased into 3x, 4x, and 5x from default setting, EIR annual model will be 240.744, 203.818, and 174.49 respectively. EIR annual optimized will be achieved when K_w is 3.04x default setting ($K_w = 0.00304$). The higher K_w , the lower EIR number. Physically, if the small surface number fill in by the pond growth rate, the

surface water will be filled by water quickly and mosquito could not stay longer on that surface water because mosquito needs a stagnant place to growth (the surface water would be filled by precipitation).

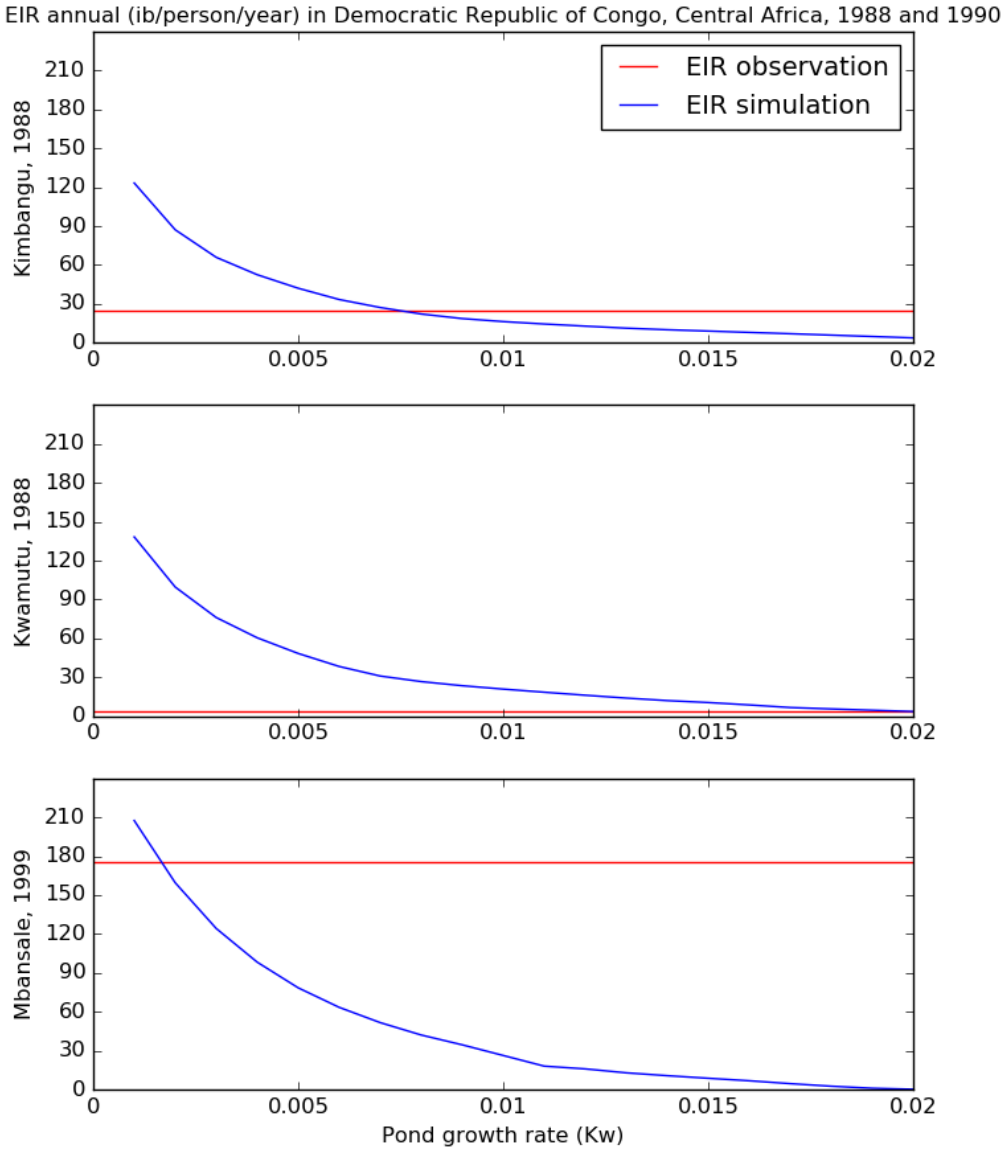

Fig 4.2(b) EIR annual with tuning K_w in three observation sites in Democratic Republic of Congo, Central Africa

Fig 4.2(b) describes EIR simulation in three observation sites in Democratic Republic of Congo, Central Africa. EIR observations in Kimbangu and Kwamutu are 24.322 and 3.989, respectively for 1988. EIR observations in Mbansale is 175.2 for 1990. By using default setting $K_w = 0.001$, EIR simulation overestimates in Kimbangu and Kwamutu in the year of 1988 and in Mbansale in the year of 1990. EIR annual default setting (CTRL) in Kimbangu, Kwamutu and Mbansale are 123.261, 138.268, and 207.452 respectively. If we do sensitivity of parameter K_w by increasing into 5x, 10x, 15x and 20x from the default setting, EIR simulation will be decreased until EIR with K_w optimized number is achieved. In Kimbangu and Kwamutu, EIR simulation with K_w optimized is derived with $K_w =$

0.00752 and $K_w = 0.01959$, respectively in 1988. Meanwhile, in Mbansale, EIR simulation with optimized K_w is derived with $K_w = 0.00164$ in 1990. From Fig. 4.1(b), EIR simulation with optimized K_w parameter are achieved with various number (K_w is not constant) in each site observations.

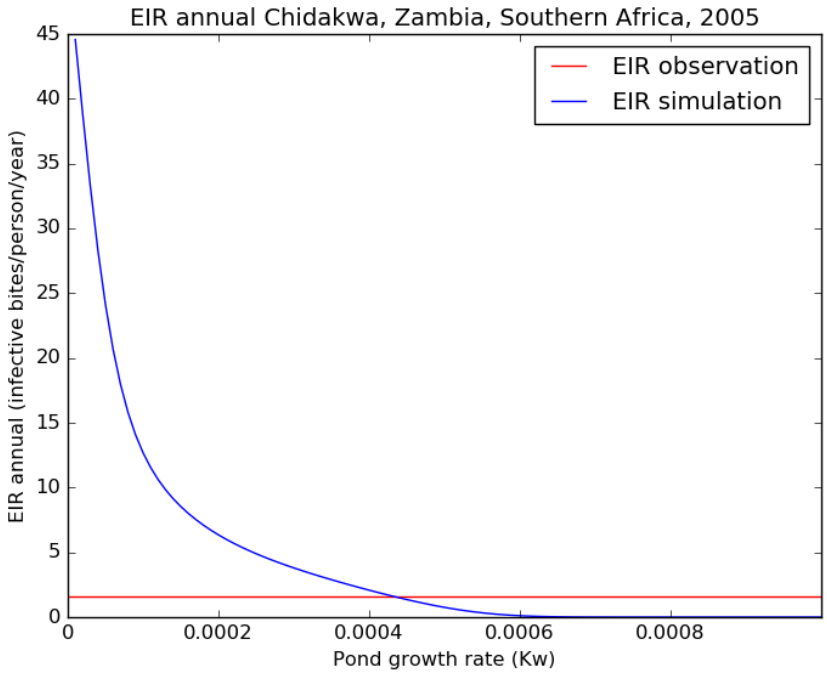

Fig 4.2(c) EIR annual with tuning K_w in Chidakwa, Zambia, Southern Africa

Fig 4.2(c) describes EIR observation in Chidakwa, Zambia, Southern Africa in 2005. From Fig. 4.1(c), EIR observations are 1.608 in Chidakwa, Zambia. EIR simulation with default setting (CTRL) in an observation site in Zambia overestimate, i.e. 4.01E-07. If sensitivity analysis is conducted for K_w by decreasing into 0.1x, 0.5x, 0.01x and 0.05x, EIR simulation will be increased. EIR simulation in Chidakwa is optimized when K_w is 0.52x from EIR default setting ($K_w = 0.00052$). Fig. 4.2(a) - Fig. 4.2(c) explain that optimized pond growth rate parameter is not constant in all sites.

Plot spatial trend relation in all Africa grid between EIR observations vs Kw pond growth rate optimized

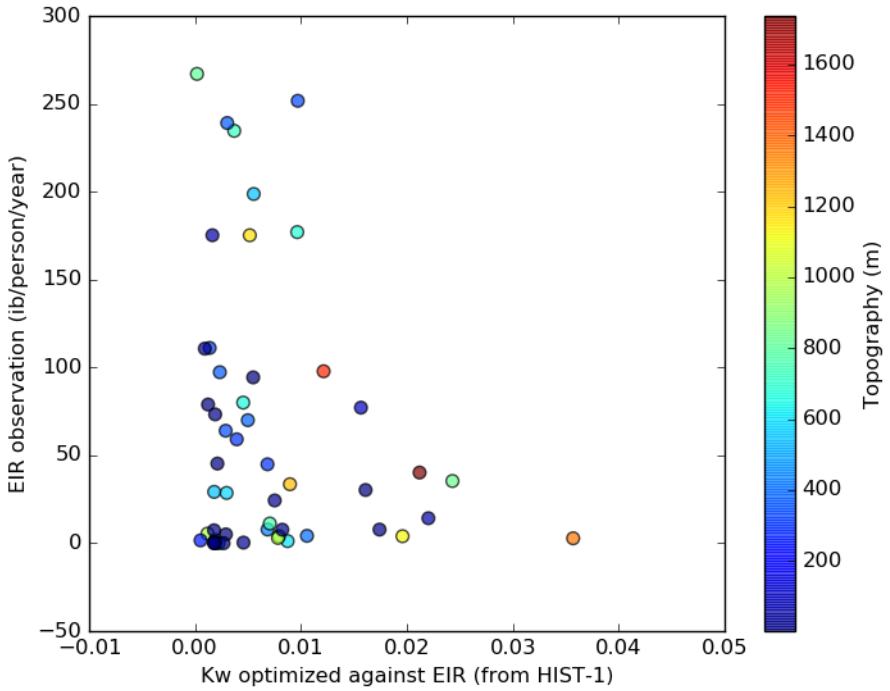

Fig 4.2(d) EIR simulation vs EIR with optimized K_w parameter in all observation sites with colorbar represents topography

Fig. 4.2(d) describes optimized K_w parameter (by tuning K_w against EIR from experiments HIST – 1) compare with EIR simulation in all observation sites in Africa. From this scatter plot, there is not clear relationship between K_w parameter and EIR observation. If we see from the distribution of K_w and EIR observation, if K_w parameter,

This figure represents the higher pond growth rate (K_w), the lower EIR simulation from the model.

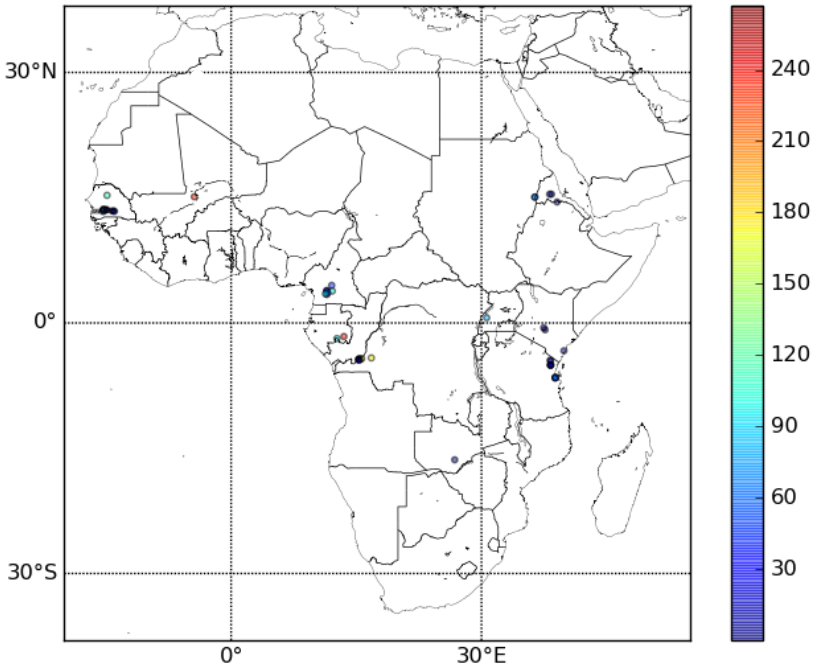

Fig 4.2(e) EIR observation distribution over Africa

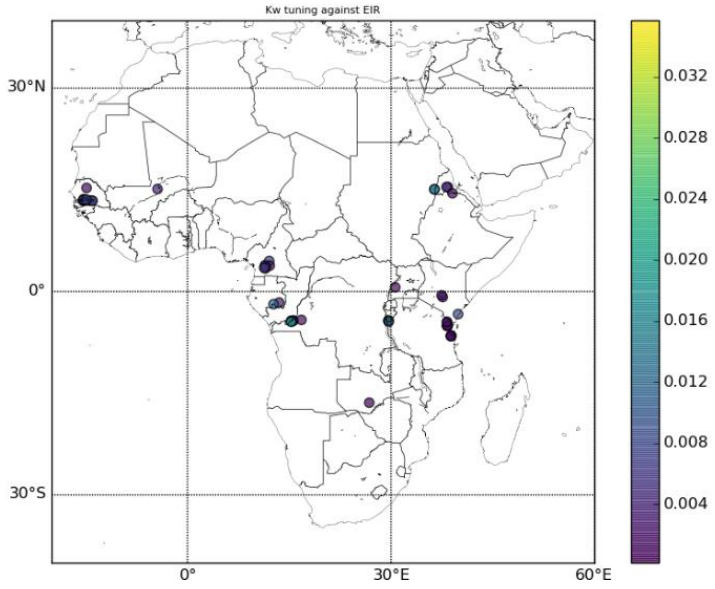

Fig 4.2(e) K_w optimized distribution over Africa

From Fig 4.2(d) and Fig 4.2(e), EIR observation and Kw optimized is various in each sites, not related each other.

4.3 Water fraction observation and model calculation

An optimized parameter of pond growth rate (K_w) from HIST – 2 and HIST – 3 is derived by minimizing root mean square deviation of water fraction from model calculation and water fraction from observation.

Correlation between water fraction observation and model calculation is described in Fig. 4.3

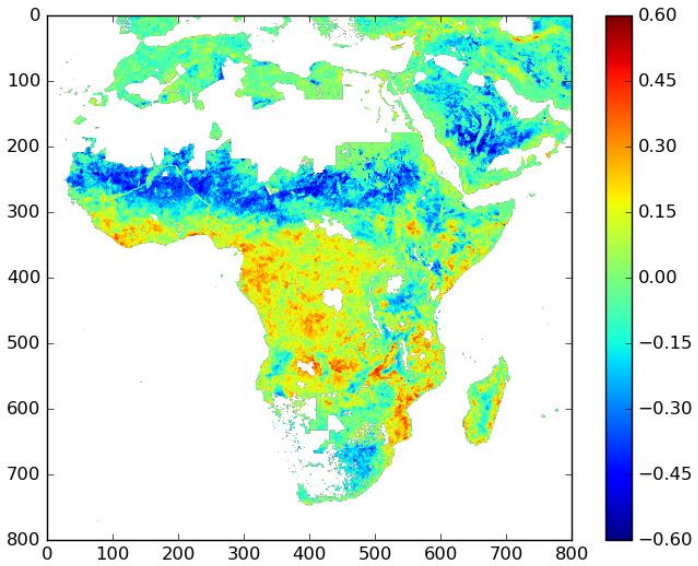

Fig 4.3 Spatial correlation between water fraction observation and model calculation

Correlation water fraction observation and water fraction calculated from the model near desert areas are neglected because in desert area malaria transmission could not transmit. An optimum temperature for malaria transmission is 29^0 C, with minimum and maximum temperature of 12^0 C and 38^0 C (Saphiro et al., 2007). Correlation between water fraction observation and water fraction simulation is 0.377. By examining this correlation distribution map, an optimized K_w parameter is estimated.

4.4 Scaling factor and interpolation of pond growth rate

After an optimized pond growth rate parameter (K_w) is derived from HIST – 1 to HIST – 3, by tuning K_w against EIR and water fraction, a scaling factor and an interpolation are needed to smooth the calculation of K_w which will be used for future period.

4.4.1 Scaling factor of pond growth rate

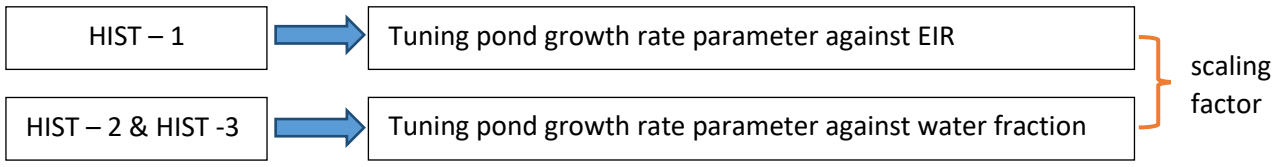

Fig 4.2.1 Methodology to optimized pond growth rate parameter

Fig.4.2.2 tuning pond growth rate parameter against EIR is conducted to derived a good model result using experiment HIST – 1, meanwhile tuning pond growth rate parameter against water fraction is conducted to minimized minimum root mean square deviation between water fraction observation and water fraction simulation.

$$K_{we}{}' = \alpha \times K_{wg} \times z \quad (13)$$

From equation (13):

$$\alpha = \frac{K_{we}{}'}{K_{wg} \times z}$$

Where Kwe', is pond growth rate optimized against EIR observation, Kwg is pond growth rate optimized against water fraction, z is topography, and α is a scaling factor. To derive malaria transmission projection more realistic, a scaling factor is calculated from pond growth rate optimized against EIR from HIST – 1 divided by multiplication of pond growth rate optimized against water fraction from HIST – 2 and HIST – 3 and topography. Topography give impact to the number of pond growth rate optimized. In some part of high elevation, K_w optimized is also high. In lower latitude, Kw optimized is also lower.

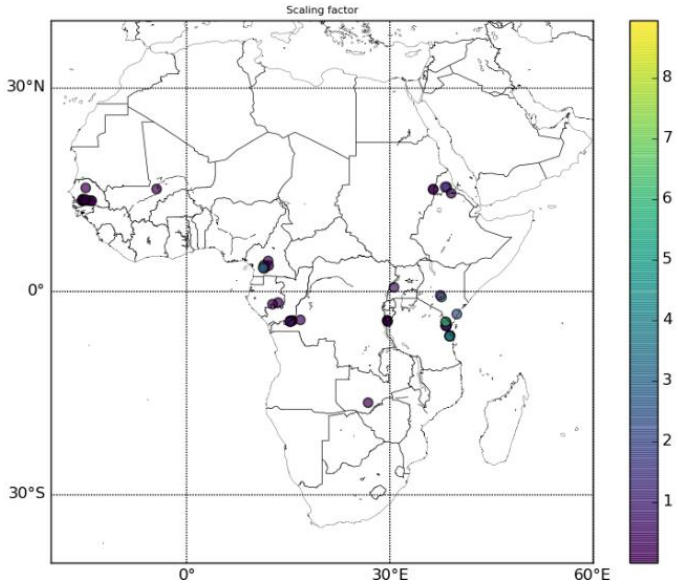

Fig. 4.4.1 Scaling factor in all EIR observation sites with colorbar represents range of scaling factor

From equation (13), a scaling factor is calculated. This scale is needed to refine K_w parameter. Due to EIR observations are limited to some observation sites, an interpolation is conducted to derive a spatial scaling factor to be multiplied with K_w optimized from calibration with water fraction.

4.4.2 Inverse distance weighting interpolation

Due to limited number of observation site, an interpolation method is used to interpolate unknown value of pond growth rate parameter to be more realistic. Inverse distance weighting method will be used to interpolate pond growth rate parameter. This interpolation has been applied in various spatial GIS problem, such as interpolate rainfall (Dirks et al., 1998), mesh deformation (Witteveen and Bijl., 2009), mapping soil properties (Robinson and Metternicht., 2006), and soil heavy metal pollution (Xie et al., 2011). This method assumes the characteristic of some points with nearby locations are similar, but

their similarity is vice versa with the distance between them (Lu and Wong., 2008). Calculation of unknown value could be formulated as in equation (14):

$$z_p = \frac{\sum_{i=1}^{n}\left(\frac{z_i}{d_i^p}\right)}{\sum_{i=1}^{n}\left(\frac{1}{d_i^p}\right)} \quad (14)$$

Where z_p is point that will be interpolated (unknown point), z_i is known point from point that will be interpolated, d_i^p is distance from point that will be interpolated and n is number of known point.

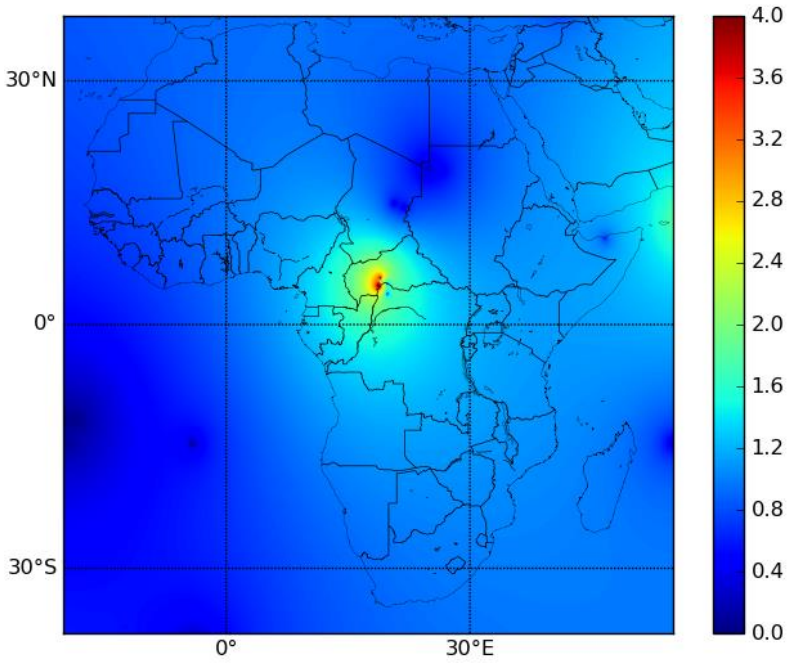

Fig. 4.4.2 Scaling factor after applying simple inverse distance weighting interpolation

From this interpolation, we derive spatial map for scaling factor to be multiply with $K_{we}{}'$. Then, K_w optimized is derived to be used in future period. Due to known points (EIR observations) are very limited, interpolation result is in close range.

4.5 Optimized pond growth rate parameter

Pond growth rate optimized parameter is derived from multiplication of scaling factor (α) with pond growth rate optimized from HIST – 1, HIST – 2 and HIST – 3 and topography, which is denoted in equation .

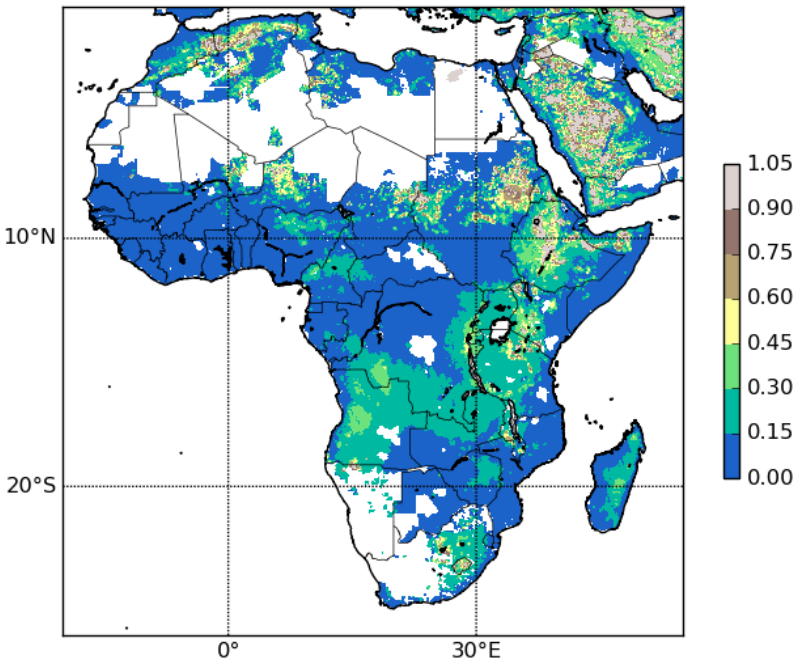

Fig. 4.5 Optimized pond growth rate parameter to be used in future simulation

4.6 Water fraction observation and precipitation observation

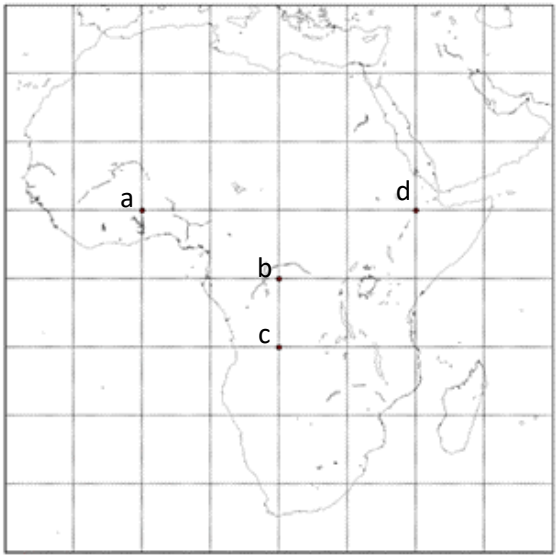

Fig 4.3 Precipitation and Observation site correlation

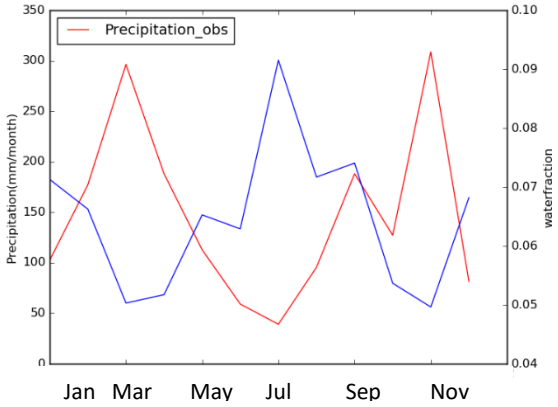

(a) Lon 20^0 E, Lat 20^0 N, corrcoef=-0.696

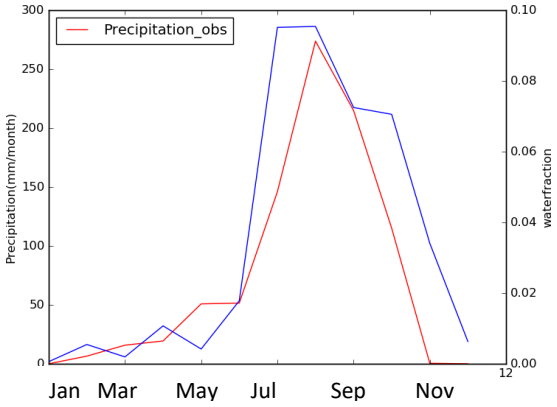

(b) Lon 0^0 E, Lat 10^0 N, corrcoef=0.885

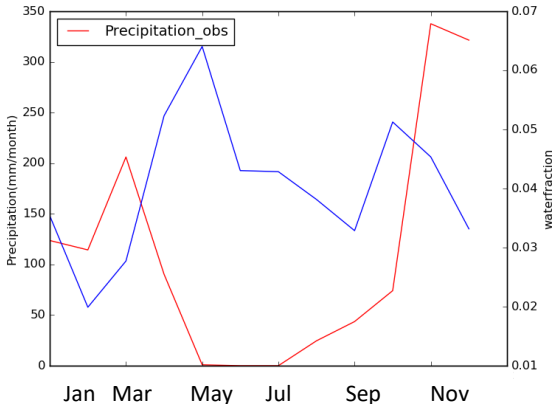

(c) Lon 20^0 E, Lat -10^0 S, corrcoef=-0.309

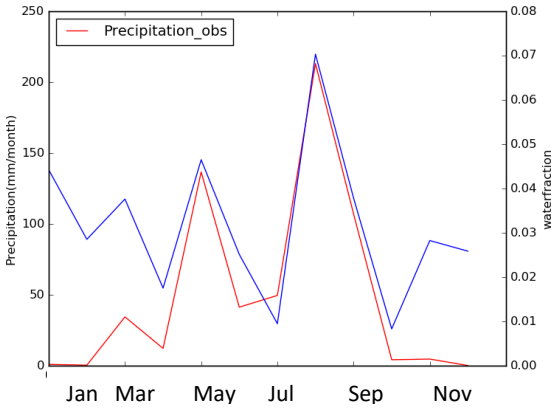

(d) Lon 20^0 E, Lat 10^0 N, corrcoef=0.737

Fig 4.3 (a)-(d) waterfraction observation and precipitation observation. In dry area, site (b) and (d), correlation between precipitation and observation is higher than in non-dry area (site (a) and (c). In site (c), there is no precipitation for May – July. Red line represents precipitation from observation and blue line represents water fraction observation.

4.7 Relationship between K_w parameter and EIR

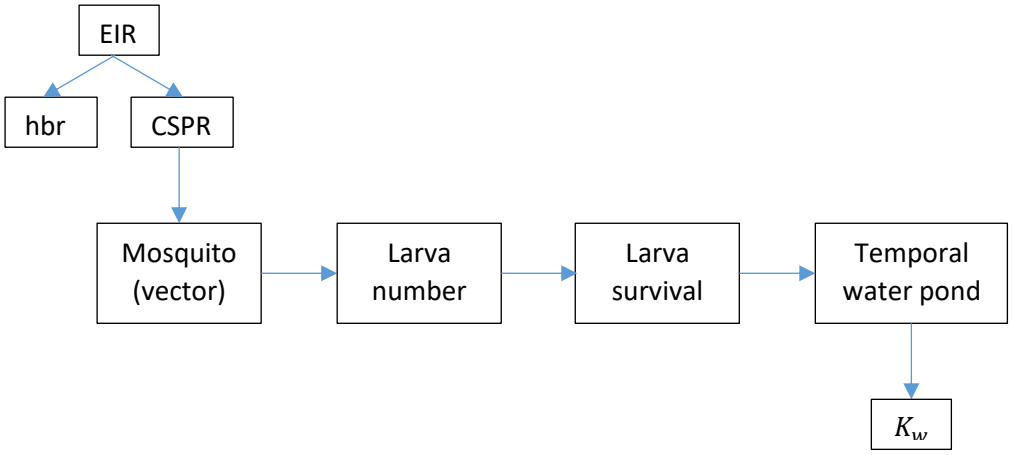

Fig 4.7 Scheme of Entomological Inoculation Rate (EIR) and pond growth rate (K_w) parameter relationship

Scheme of relationsip between Entomological Inoculation Rate (EIR) and pond growth rate parameter (K_w) is described in Fig. 4.7. From this study, we can increase or decrease value of EIR by tuning K_w parameter. EIR is multiplication of human bite rate (hbr) and Circumsporozoite Protein Rate (CSPR). As defined in chapter 2.3, hbr defines as average number of bites per person per night. It calculated from the level of zoophily vector multiply by proportion of biting vectors to host divided by population density of host. Meanwhile, CSPR is determined by the number of vector which contain parasite on sporogonic cycle. The number of vector is highly determined by the number of larva which can survive until mosquito stage. Larva survival rate is determined by the availability of temporal water pond. Larva survival rate is calculated from equation (2) :

$$P_{L,surv} = \left(\frac{1 - M_L}{w\ M_{L,max}}\right) K_{flush} P_{L,surv0}$$

Larva survival rate is determined by total larvae biomass per unit surface area (M_L), water fraction (w), maximum carrying capacity ($M_{L,max}$), daily larva survival base ($P_{L,surv0}$) and larvae flushing rate (K_{flush}). If there is no water fraction ($w = 0$), larva could not survive ($P_{L,surv} = 0$). Water fraction changes is determined by pond growth rate parameter (K_w), precipitation (P), maximum water fraction (w_{max}), infiltration (I) and evaporation (E) as mentioned in equation (12). From this scheme, we can see clearly the relationship between EIR and K_w parameter.

4.8 Conclusion

There are two precipitation categories which have similar location to EIR observation in Africa, i.e. unimodal (one precipitation peak) and bimodal (two precipitation peaks). Location which has unimodal include Senegal and Gambia (West Africa) and Eritrea (Horn of Africa), the precipitation ranges are 0 – 160 mm per month. Location which has bimodal include Democratic Republic of Congo, Cameroon, Tanzania and Gabon. Tanzania is drier compared to other region. In Democratic Republic of Congo, Cameroon and Gabon, precipitation is in range 0 – 250 mm per month, meanwhile in Tanzania precipitation is between 0 – 100 mm per month.

Parameterization of pond growth rate (K_w) against EIR number is various in each observation sites. But, there is not clear relationship between K_w parameter and EIR observation if we analyzed from all EIR observation sites in this study. Water fraction observation and model calculation has correlation 0.377. EIR optimized against water fraction is calculated by minimizing root mean square deviation between water fraction observation and model calculation.

By tuning pond growth rate parameter against EIR and water fraction from HIST – 1 to HIST – 3, a scaling factor is calculated to get a better pond growth rate parameter. After calculation of scaling factor, inverse distance weighting interpolation is applied to interpolate unknown pond growth rate optimized. Then, by multiplying pond growth rate tuned against water fraction and topography, pond growth rate optimized is obtained.

CHAPTER 5

Malaria Transmission on Projection Period

Abstract:

Complex relationship between climatic factor and malaria transmission encourage researchers to analyze impact of climate change in future period. This study utilized CMIP6 dataset for precipitation and temperature projection under RCP 2.6, RCP 7.0, and RCP 8,5 scenario and SEDAC for population density with SSP1, SSP3 and SSP5. To correct precipitation a bias correction method is applied by determining a scaling factor of precipitation from model output comparing to observation dataset. On projection period, temperature will increase in some locations. Meanwhile, precipitation will increase or decrease regarding the emission scenario and location. Change of temperature does not give significant impact to EIR calculation. Meanwhile, precipitation give significant impact EIR in future simulation, Population density give proportionally impact in increasing or decreasing malaria transmission in the future period. Precipitation characteristic, such as monthly average, standard deviation and consecutive wet days (CWD) drivers on EIR. On projection period, malaria transmission increasing in western part and central part of Africa in line with increasing emission scenario. Increasing malaria transmission under RCP 8.5 is higher compare to RCP 2.6 and RCP 7.0. Increasing EIR in western part is determined by monthly average precipitation, meanwhile increasing EIR in central and south east Africa is affected by CWD.

5.1 Data used and bias correction method

Data used in this study precipitation and temperature from CMIP6 using MIROC output for precipitation and temperature. This study used linear bias correction (Lafon *et al.*, 2013) scheme for malaria transmission. First, determine a scaling factor for this number.

$$a = \frac{\bar{O}}{\bar{P}} \tag{15}$$

Where a is scaling factor, $\bar{O}$ is observed CMIP6 monthly precipitation, and $\bar{P}$ is predicted monthly precipitation. Monthly scaling factor is applied to each uncorrected daily observation of the month, generating the corrected daily time series. Linear correction method is similar with delta change method (Hay *et al.*, 2000). From this scaling factor, a daily simulation precipitation for projection period will be corrected by:

$$P^* = a\,P \tag{16}$$

Where P^* is corrected daily precipitation and P is simulation daily precipitation.

5.2 Precipitation, temperature and population density in projection period

Representative Consentration Pathways (RCP) describe pathways of radiative forcing. RCP represents the range of greenhouse gas radiative forcing values from 2.6 to 8.5 W/m^2 (Nazarenko *et al.*, 2015). This study selects three RCP scenarios, which represent low, medium and high emission scenario, respectively. Before analyzing malaria projection in future period, precipitation, temperature and population density in future period is important to be examined to analyze the trend in projection. The climate trend under three scenarios are explained in the following subsection.

Shared Socioeconomic Pathways (SSPs) is a scenario to investigate future climate impact, vulnerabilities, adaptation and mitigation (Riahi *et al.*, 2017). SSPs based on five scenarios which represent alternative socio-economic developments, which take into account sustainable development, regional rivalry, inequality, fossil-fueled development, and middle-of-the-road development. This study utilize three SSPs scenario.

5.2.1 Precipitation, temperature and population density projection period in Barkendji, Senegal

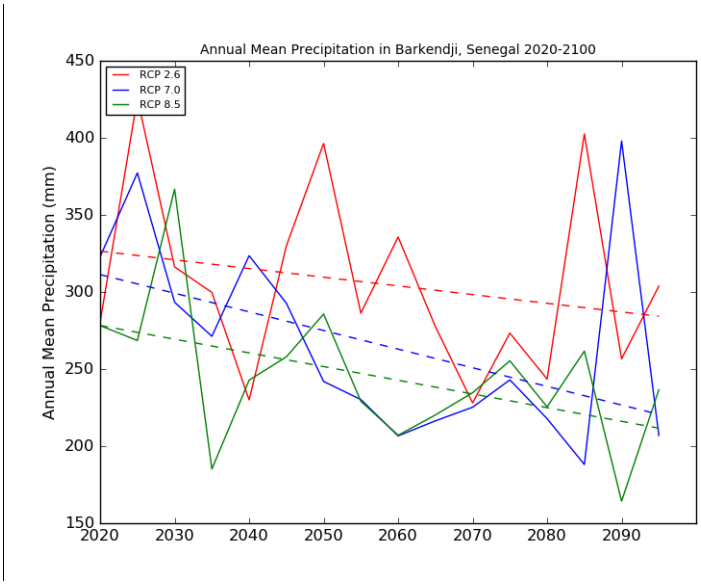

Fig 5.2.1(a) Annual precipitation trend in Barkendji, Senegal in 2020 – 2100 (red: RCP2.6, green: RCP 7.0, blue: RCP 8.5)

Figure 5.2.1(a) represents precipitation trend in Barkendji, Senegal from 2020 – 2100. The trend of precipitation decrease in all RCP scenarios from 2020 – 2100. Annual precipitation under RCP 2.6 is higher than RCP 7.0, and RCP 8.5.

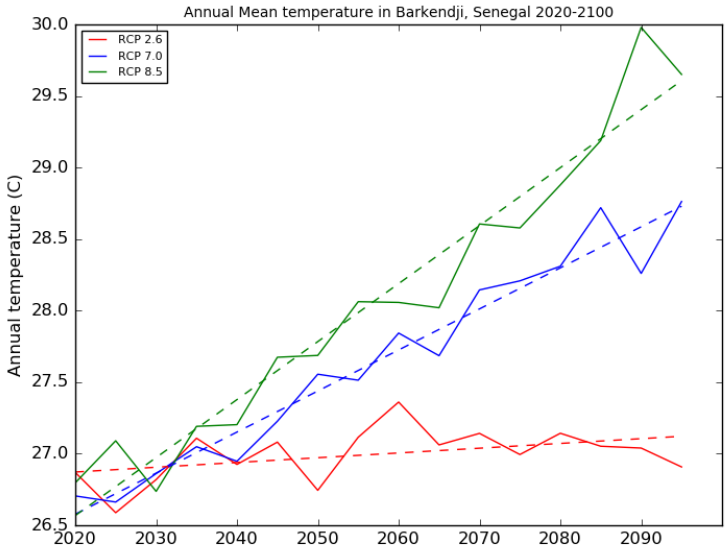

Fig 5.2.1(b) Annual mean temperature in Barkendji, Senegal in 2020 – 2100 (red: RCP 2.6, blue: RCP 7.0, green: RCP 8.5)

Figure 5.2.1(b) represents annual mean temperature in Barkendji, Senegal from 2020 – 2100 under three RCP scenario. Annual mean temperature tends to increase in future period under RCP 2.6, RCP 7.0 and RCP 8.5.

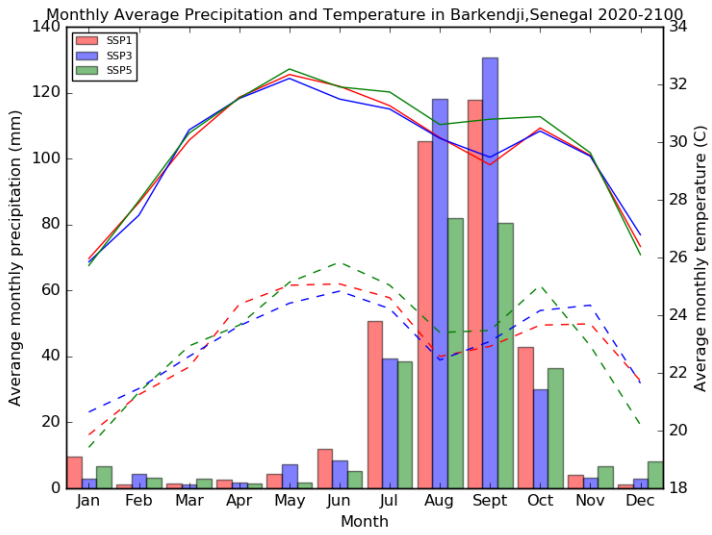

Fig 5.2.1(c) Monthly average precipitation and temperature in Barkendji, Senegal in 2020 – 2100 (bar chart for precipitation, solid line: maximum temperature, dash line: minimum temperature, with red: RCP 2.6, blue: RCP 7.0, green: RCP 8.5)

Figure 5.2.1(c) represents monthly average precipitation and temperature in Barkendji, Senegal from 2020 – 2100. Monthly average precipitation with RCP2.6 and RCP 7.0 climate data more than RCP 8.5.

The peak of monthly average precipitation is more than 1000 mm per month, from August – September. Maximum and minimum temperature is higher in March – April and October – November.

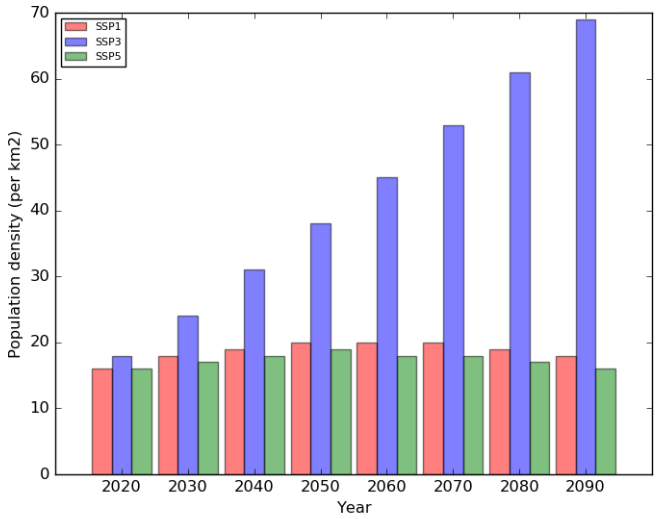

Fig 5.2.1(d) Population density in Barkendji, Senegal in 2020 – 2090 (red:SSP1, blue:SSP3, green:SSP5)

Population density in Barkendji, Senegal increase in every 10 years smoothly, with less than 5 people/km^2, except in 2040 (SSP1) with increment 15 people/km^2 from 2020. Population density from 2020 – 2090 with SSP3 scenario is much higher than SSP1 and SSP5 scenario. Population density under SSP3 is gradually increasing every 10 years in Barkendji, Senegal.

5.2.2 Precipitation, temperature and population density changes in Mbansale, Democratic Republic of Congo

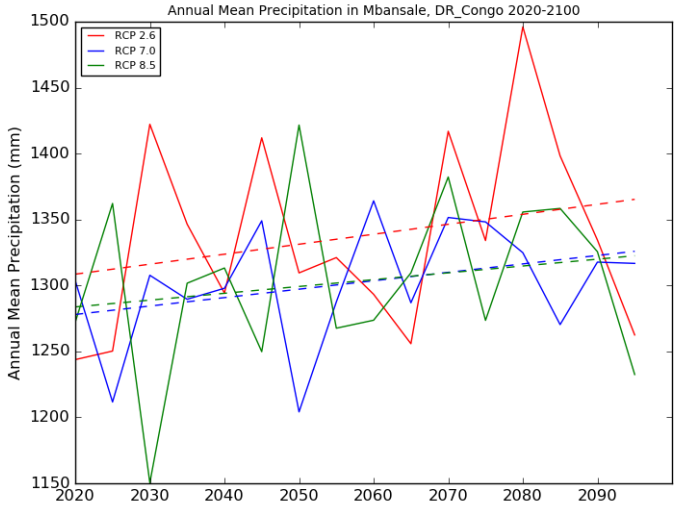

Fig 5.2.2(a) Annual precipitation trend in Mbansale, Democratic Republic of Congo in 2020 – 2100 (red: RCP 2.6, blue: RCP 7.0, green: RCP 8.5)

Figure 5.2.2(a) represents precipitation trend in Mbansale, Democratic Republic of Congo from 2020 – 2100. Precipitation trend under RCP 2.6 is higher than precipitation under RCP 7.0 and RCP 8.5 scenario for all projection year (2020 – 2100). Precipitation under RCP 7.0 has similar amount with precipitation under RCP 8.5.

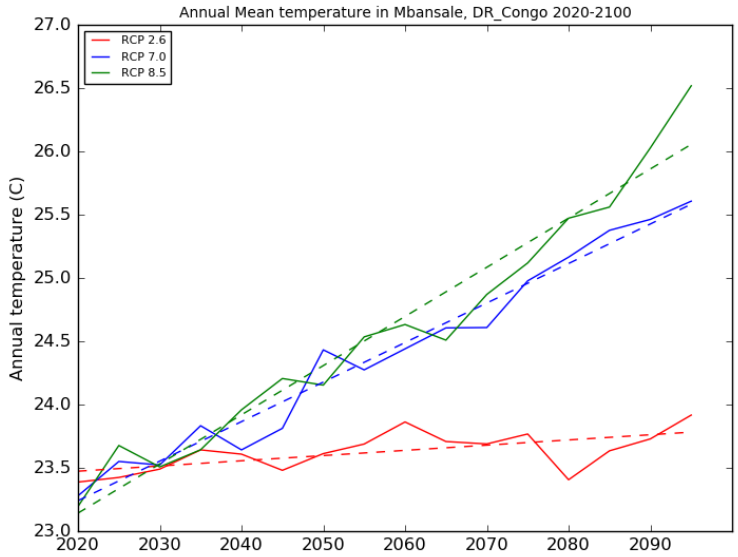

Fig 5.2.2(b) Annual mean temperature in Mbansale, Democratic Republic of Congo in 2020 – 2100 (red: RCP 2.6, blue: RCP 7.0, green: RCP 8.5)

Figure 5.2.2(b) represents annual mean temperature in Mbansale, Democratic Republic of Congo form 2020 – 2100 under three RCP scenario. Annual mean temperature tends to increase in future period under RCP 2.6, RCP 7.0 and RCP 8.5. As in precipitation, RCP 7.0 and RCP 8.5 have similar trend in Mbansale, Democratic Republic of Congo.

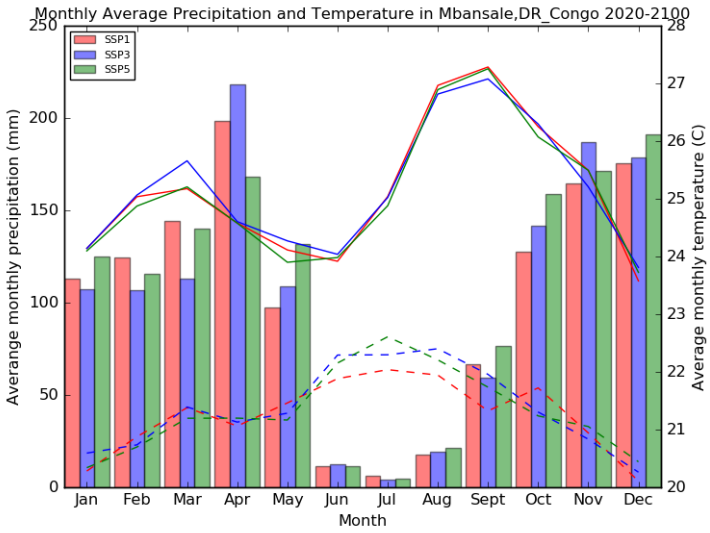

Fig 5.2.2(c) Monthly average precipitation and temperature in Mbansale, Democratic Republic of Congo in 2020 – 2100 (bar chart for precipitation, solid line: maximum temperature, dash line: minimum temperature, with red: RCP 2.6, blue: RCP 7.0, green: RCP 8.5)

Figure 5.2.2(c) represents monthly average and temperature in Mbansale, Democratic Republic of Congo. In this site, it has two precipitation peak, first peak is on April (under RCP2.6, RCP 7.0 and RCP 8.5). Second peak, is from October –December (under RCP 2.6, RCP 7.0 and RCP 8.5). The highest amount of precipitation is on April (RCP 2.6 and RCP 7.0) and December (RCP 8.5). Monthly average precipitation in Mbansale (Democratic Republic of Congo) is higher than monthly average precipitation in Barkendji (Senegal), precipitation. This means, Barkendji (Senegal) is drier than Mbansale (Democratic Republic of Congo).

Temperature in Mbansale, Democratic Republic of Congo has two peak, i.e. March and August – September. The highest peak is on September. Temperature in Mbansale, Democratic Republic of Congo tends to increase monthly.

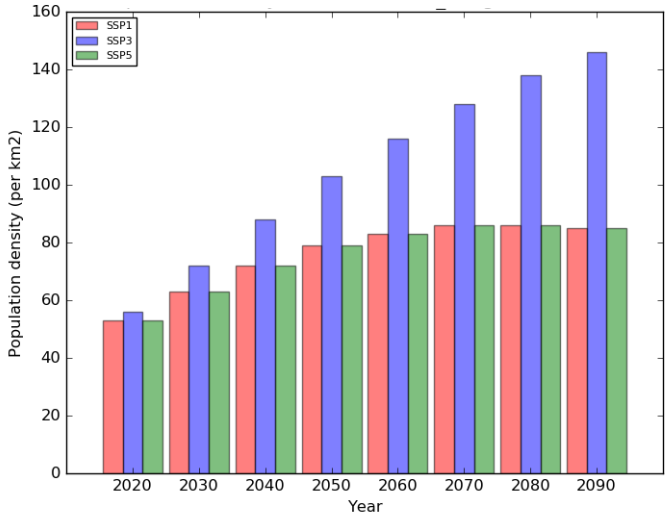

Fig 5.2.2(d) Population density in Mbansale, Democratic Republic of Congo in 2020 – 2090 (red:SSP1, blue:SSP3, green:SSP5)

Projection population density in Mbansale, Democratic Republic of Congo is increasing from 2020 – 2090 under SSP1, SSP3 and SSP5. As in Barkendji, Senegal, population density in Mbansale, Democratic Republic of Congo is gradually increasing under SSP3 scenario.

5.2.3 Precipitation, temperature and population density changes in Nsimalen Ekoko, Cameroon

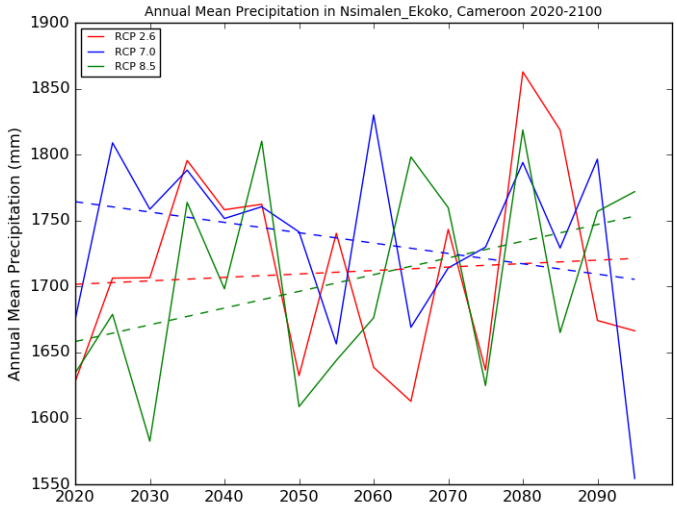

Fig 5.2.3(a) Annual mean precipitation in Nsimalen Ekoko, Cameroon in 2020 – 2100 (red: RCP 2.6, blue: RCP 7.0, green: RCP 8.5)

Figure 5.2.3(a) represents annual mean precipitation in Nsimalen Ekoko, Cameroon from 2020 – 2100. Precipitation trend under RCP 2.6 and RCP 7.0 increase in future period. Meanwhile, precipitation trend under RCP 8.5 decrease from 2020 – 2100.

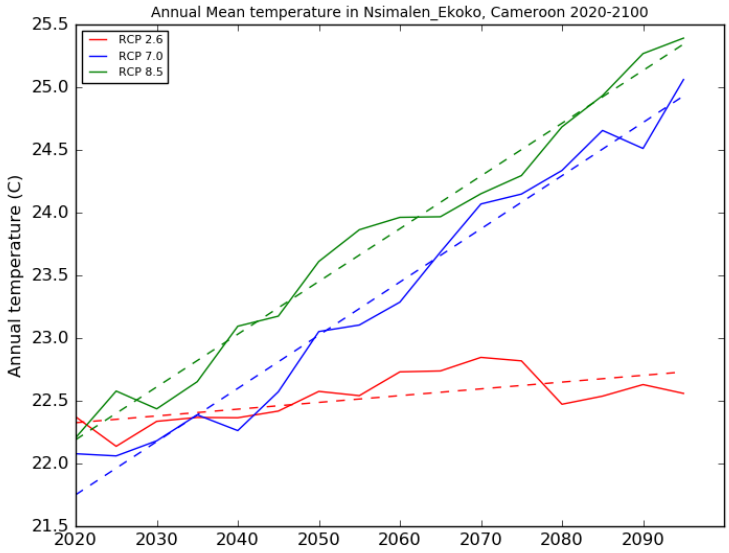

Fig 5.2.3(b) Annual mean temperature in Nsimalen Ekoko, Cameroon in 2020 – 2100 (red: RCP 2.6, blue: RCP 7.0, green: RCP 8.5)

Figure 5.2.3(b) represents annual mean temperature in Nsimalen Ekoko, Cameroon form 2020 – 2100 under three RCP scenario. Annual mean temperature tends to increase in future period under RCP 2.6, RCP 7.0 and RCP 8.5.

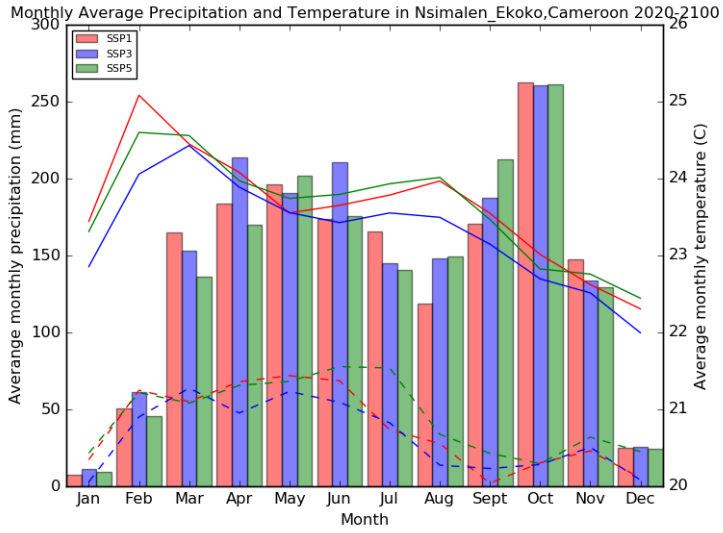

Fig 5.2.3(c) Monthly average precipitation and temperature in Nsimalen Ekoko, Cameroon in 2020 – 2100 (bar chart for precipitation, solid line: maximum temperature, dash line: minimum temperature, with red: RCP 2.6, blue: RCP 7.0, green: RCP 8.5)

Figure 5.2.3(c) represents monthly average and temperature in Nsimalen Ekoko, Cameroon. This site has two precipitation peak, first peak is from April – June (under RCP 2.6, RCP 7.0 and RCP 8.5).

Second peak, is from September – October (under RCP 2.6, RCP 7.0 and RCP 8.5). The highest amount of precipitation is on October (under RCP 2.6, RCP 7.0 and RCP 8.5).

There are two peak of high temperature, first peak is on March and second is on August. Temperature trend in Nsimalen Ekoko, Cameroon tends to decrease monthly from May – June is the transition temperature from low into high temperature, unlike in Barkendji (Senegal) and Mbansale (Democratic Republic of Congo).

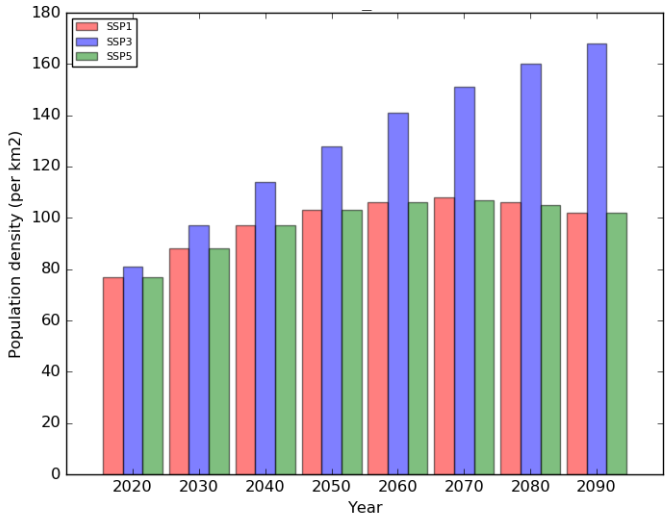

Fig 5.2.3(d) Population density in Nsimalen Ekoko, Cameroon in 2020 – 2090 (red:SSP1, blue:SSP3, green:SSP5)

Projection population density in Nsimalen Ekoko, Cameroon is increasing from 2020 – 2090. The number of people is same in each 10 different year using different SSP scenarios, except population density on 2040 (SSP1) is the highest increment, with more than 100 people/km^2. Nsimalen Ekoko (Cameroon) is more populated region compared to Barkendji (Senegal) and Mbansale (Democratic Republic of Congo).

5.3 Inter annual variation of EIR under scenario RCP 2.6, RCP 7.0 and RCP 8.5

5.3.1 Temporal variability of EIR projection simulation under RCP 2.6, RCP 7.0 and RCP 8.5

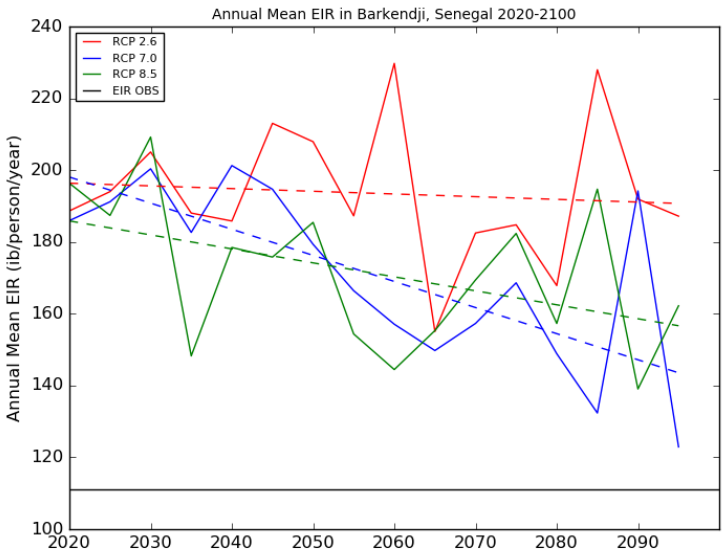

Fig 5.3.1(a) Entomological Inoculation Rate (EIR) annual in Barkendji, Senegal from 2020 – 2100 (red: RCP 2.6, green: RCP 7.0, blue: RCP 8.5, black: EIR observation in historical period)

EIR annual mean in Barkendji, Senegal is various from 2020 – 2100 projection simulation period with RCP 2.6, RCP 7.0 and RCP 8.5. EIR annual mean on projection period under three RCPs scenario overestimate EIR observation (black line, with EIR observation = 111.1 infective bites/person/year).

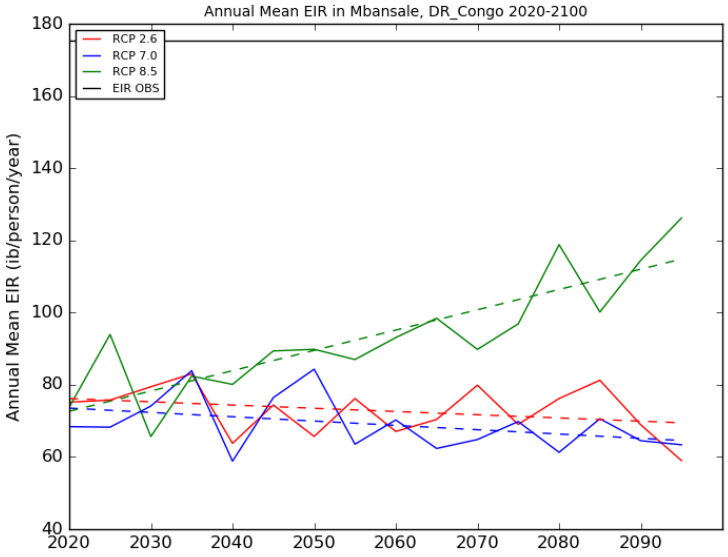

Fig 5.3.1(b) Entomological Inoculation Rate (EIR) annual in Mbansale, Democratic Republic of Congo from 2020 – 2100 (red: RCP 2.6, green: RCP 7.0, blue: RCP 8.5, black: EIR observation in historical period)

EIR annual mean in Mbansale, Democratic Republic of Congo in projection simulation from 2020 – 2100 under three RCPs scenario underestimate EIR observation (black line, with EIR observation = 175.2 infective bites/person/year).

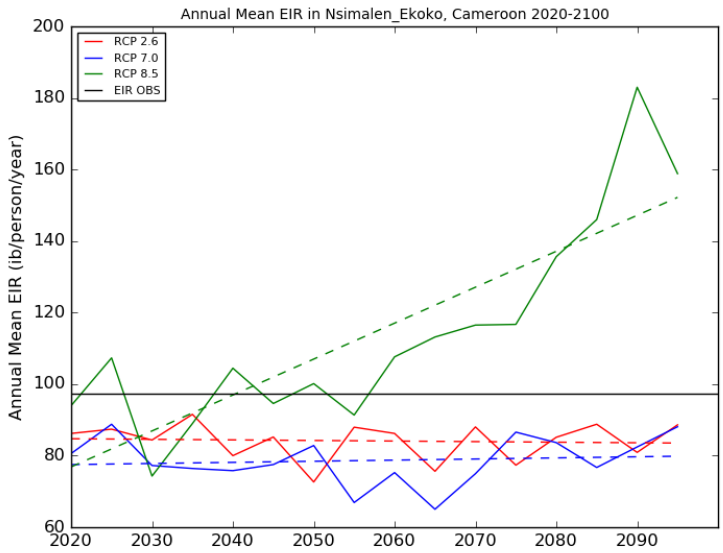

Fig 5.3.1(c) Annual Entomological Inoculation Rate (EIR) in Nsimalen Ekoko, Cameroon from 2020 – 2100 (red: RCP 2.6, green: RCP 7.0, blue: RCP 8.5, black: EIR observation in historical period)

EIR annual mean in Nsimalen Ekoko, Cameroon under RCP 2.6 and RCP 8.5 scenario underestimate EIR observation (black line, with EIR observation = 97.285) and overestimate under RCP 7.0 from year 2060s.

Fig 5.3.1 (a) – (c) describes EIR annual projection in Barkendji (Senegal), Mbansale (Democratic Republic of Congo) and Nsimalen Ekoko (Cameroon) under RCP 2.6, RCP 7.0 and RCP 8.5. We analyze which variable from climate forcing datasets (precipitation and temperature) give more impact to EIR in projection simulation in Barkendji (Senegal), Mbansale (Democratic Republic of Congo) and Nsimalen Ekoko (Cameroon).

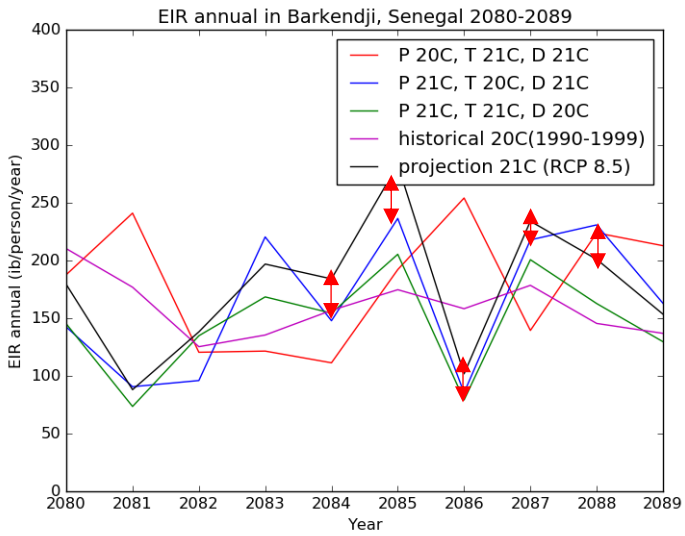

Fig. 5.3.1(d) Annual Entomological Inoculation Rate in Barkendji, Senegal under RCP 8.5 (P :

precipitation, T : temperature, D : population density)

Fig 5.3.1(d) describes EIR annual in Barkendji, Senegal under RCP 8.5 scenario from 2080 – 2089. Red line represent EIR annual using precipitation from historical period (using precipitation from corresponding historical period 20C (1990 – 1999)), blue line represent EIR annual using temperature from historical period (using temperature from corresponding historical period 20C (1990 – 1999)), green line represent EIR annual using population density from historical period (population density from corresponding historical period 20C (1990 – 1999)), magenta line represent EIR annual on historical period (1990 – 1999) and black line represent EIR annual on projection period (2080 – 2089). From this figure, trend of EIR annual on projection period (black line) is close with EIR annual using temperature from historical period (blue line) compare with EIR annual using precipitation from historical period (red line). It represents precipitation variability give more impact to EIR calculation in Barkendji, Senegal.

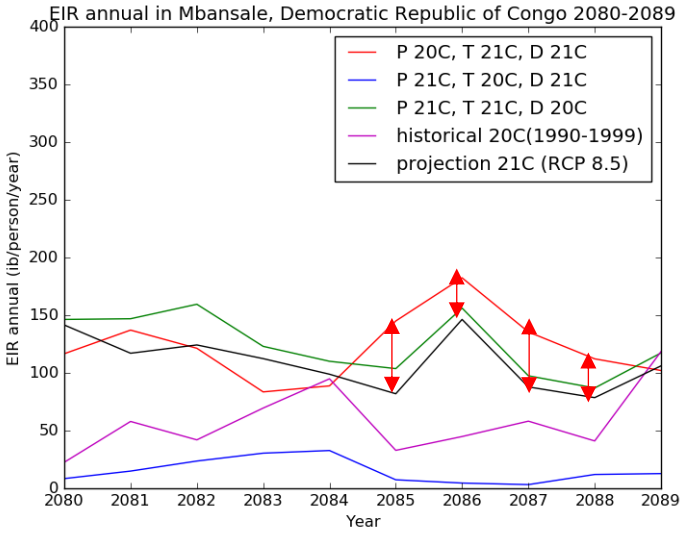

Fig. 5.3.1(e) Annual Entomological Inoculation Rate in Mbansale, Democratic Republic of Congo under RCP 8.5 (P : precipitation, T : temperature, D : population density)

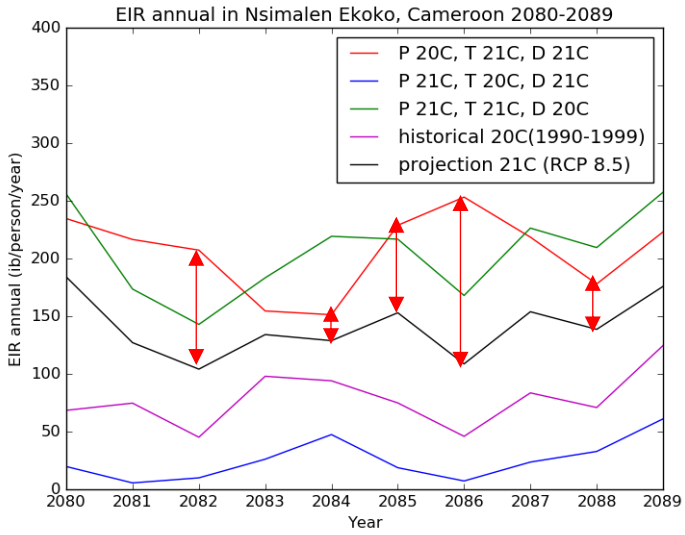

Fig. 5.3.1(f) Annual Entomological Inoculation Rate in Nsimalen Ekoko, Cameroon under RCP 8.5

(P : precipitation, T : temperature, D : population density)

From Fig 5.3.1 (e) and (f) represent EIR annual on projection period under RCP 8.5 (black line) has more similar trend simulation with EIR annual using precipitation from historical period (red line) compare to EIR annual using temperature from historical period (blue line) in Mbansale (Democratic Republic of Congo) and Nsimalen Ekoko (Cameroon). This represents temperature give more impact to EIR annual in Mbansale (Democratic Republic of Congo) and Nsimalen Ekoko (Cameroon).

5.3.2 Inter annual variability of EIR annual spatial average on projection simulation under RCP 2.6, RCP 7.0 and RCP 8.5

Inter annual variability of EIR annual average on projection period under three RCPs scenario is determined by calculating coefficient variation of EIR annual number. Coefficient variation is determined from standard deviation of EIR annual average divided by average of EIR annual. Coefficient variation average from EIR annual projection under RCP 2.6 is 0.079, under RCP 7.0 is 0.087 and under RCP 8.5 is 0.087. It represents that average of EIR annual on projection period under RCP 8.5 has higher variability compare to other two RCPs scenario.

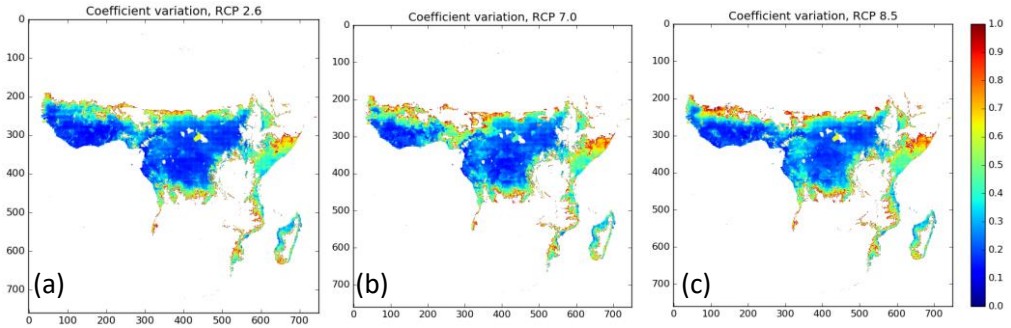

Fig 5.3.2 Coefficient variation distribution of EIR annual average on projection period under RCP 2.6 (a), RCP 7.0 (b) and RCP 8.5 (c).

5.4 Water fraction projection period with scenario RCP 2.6, RCP 7.0 and RCP 8.5

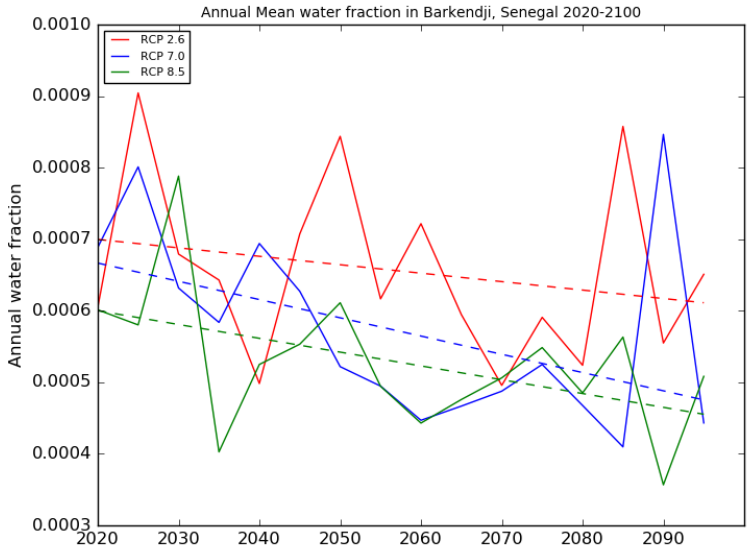

Fig 5.4(a) Water fraction annual mean in Barkendji, Senegal from 2020 – 2100 (red: RCP2.6, blue: RCP 7.0, green: RCP 8.5)

Annual mean of water fraction in Barkendji, Senegal tends to decrease in projection period under three RCP scenario. Water fraction annual mean under RCP 2.6 is higher than RCP 7.0 and RCP 8.5. This pattern of water fraction is following annual precipitation pattern.

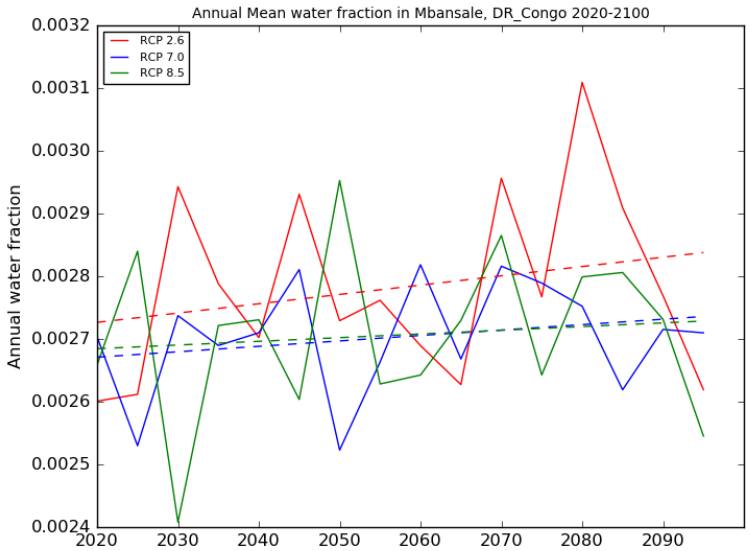

Fig 5.4(b) Water fraction annual mean in Mbansale, Democratic Republic of Congo from 2020 – 2100 (red: RCP2.6, blue: RCP 7.0, green: RCP 8.5)

Water fraction in Mbansale, Democratic Republic of Congo tends to increase under three RCP scenario. Water fraction annual mean under RCP 2.6 is higher than RCP 7.0 and RCP 8.5. Water fraction under RCP 7.0 is similar to RCP 8.5 which correspond to annual mean of precipitation pattern.

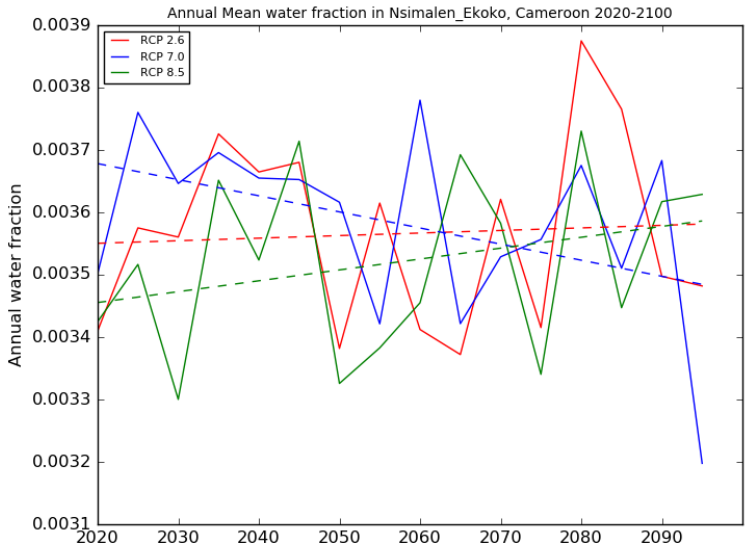

Fig 5.4(c) Water fraction annual mean in Nsimalen Ekoko, Cameroon from 2020 – 2100 (red: RCP2.6, blue: RCP 7.0, green: RCP 8.5)

Water fraction annual mean in Nsimalen Ekoko, Cameroon under RCP 2.6 and RCP 7.0 tends to increase in projection period. Meanwhile, annual mean of water fraction tends to decrease under RCP 8.5. This pattern following annual precipitation pattern in Nsimalen Ekoko, Cameroon.

5.5 Spatial distribution of malaria transmission with scenario RCP 2.6, RCP 7.0 and RCP 8.5

5.5.1 Monthly distribution of EIR projection period

Spatial distribution of malaria transmission monthly EIR under scenario RCP 2.6 is described in Fig. 5.5.1(a) – (l) as follow:

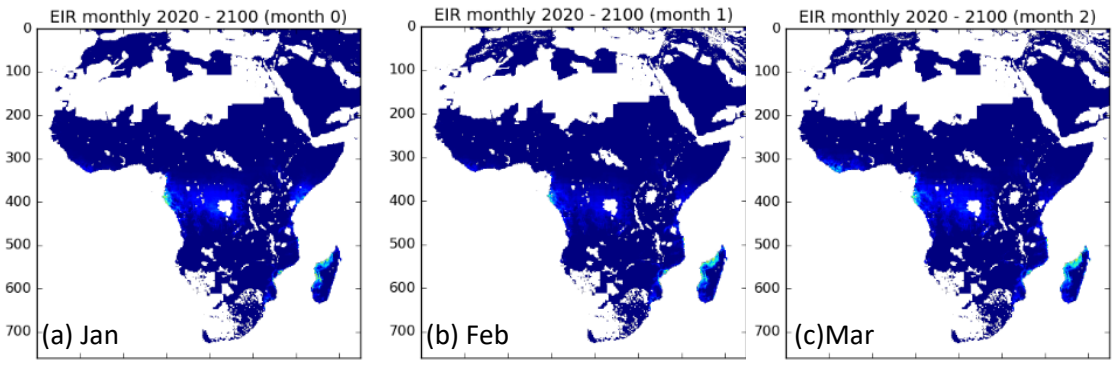

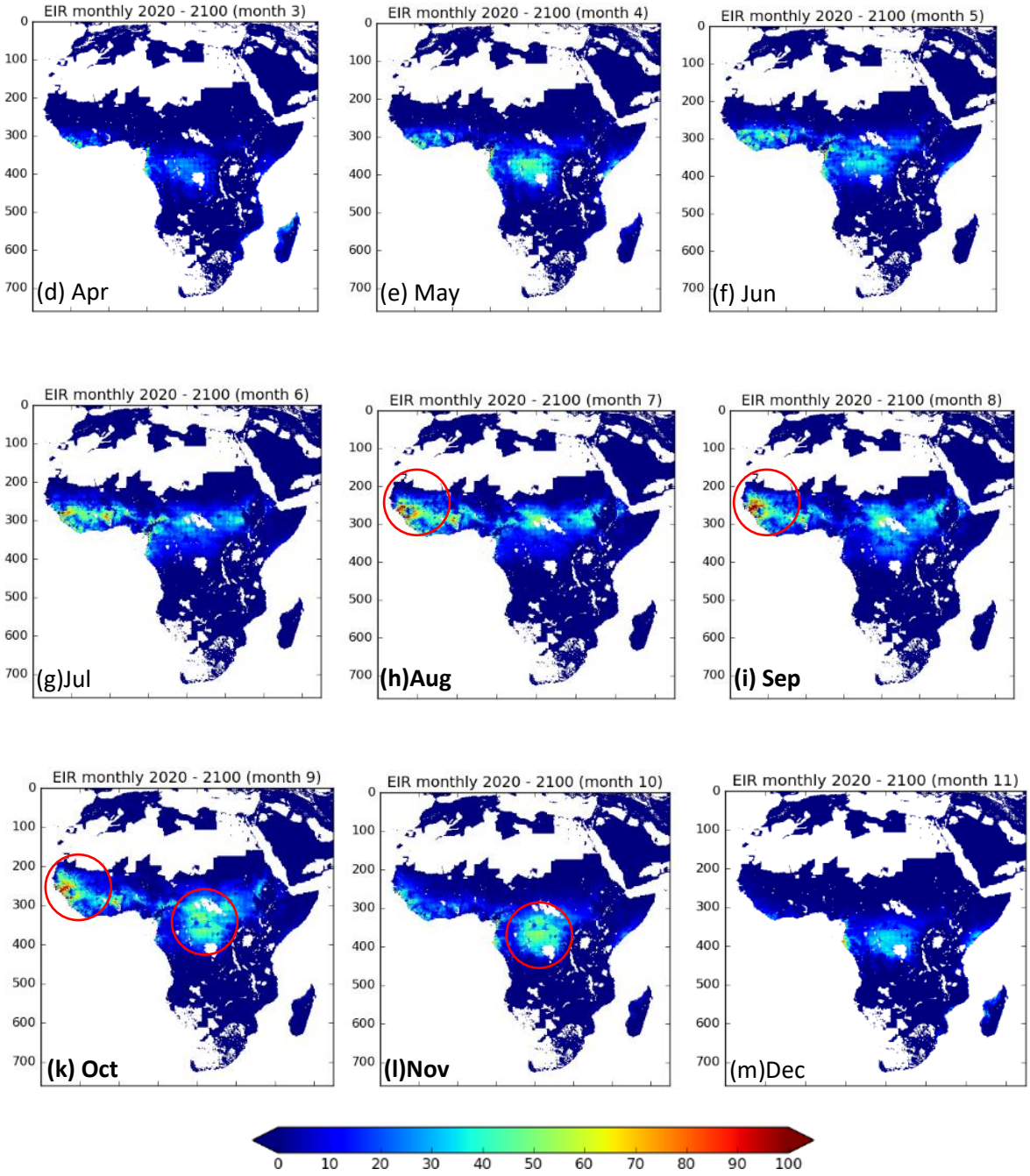

Fig. 5.5 (a) – (l) Spatial distribution of monthly EIR under RCP 2.6 scenario

Figure 5.5 (a) – (l) describes spatial distribution of monthly EIR under RCP 2.6 from 2020 – 2100. From this figure, it shows that in western part of Africa, EIR is high peak season from August – October. Meanwhile, for central part of Africa, EIR is peak season from October – November.

5.5.2 Spatial distribution of malaria risk in projection period

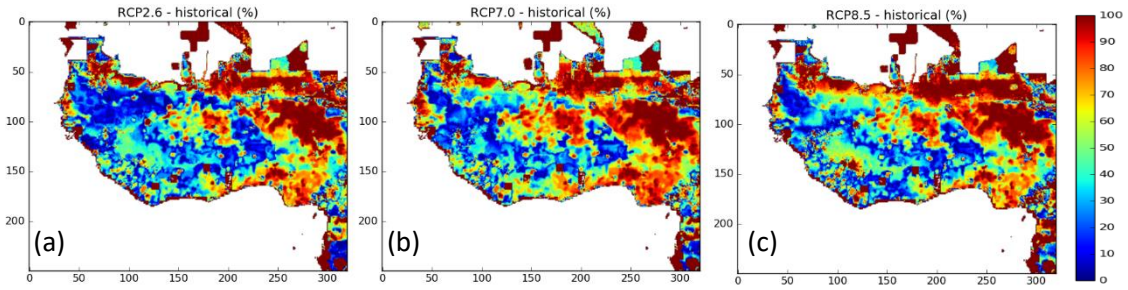

Fig 5.5.2 Malaria risk in west part of Africa on projection period compare to historical period (%) with (a) RCP 2.6, (b) RCP 7.0 and (c) RCP 8.5

Fig. 5.5.2 (a)-(c) represent percentage of malaria risk (the difference of EIR projection from EIR historical period) in west part of Africa. Spatial average of EIR difference under RCP 2.6 is -23.14%, under RCP 7.0 is -39.51% and under RCP 8.5 is -19.22%. In west part of Africa, the worst scenario in projection period is RCP 8.5. Meanwhile, the better scenario is RCP 7.0.

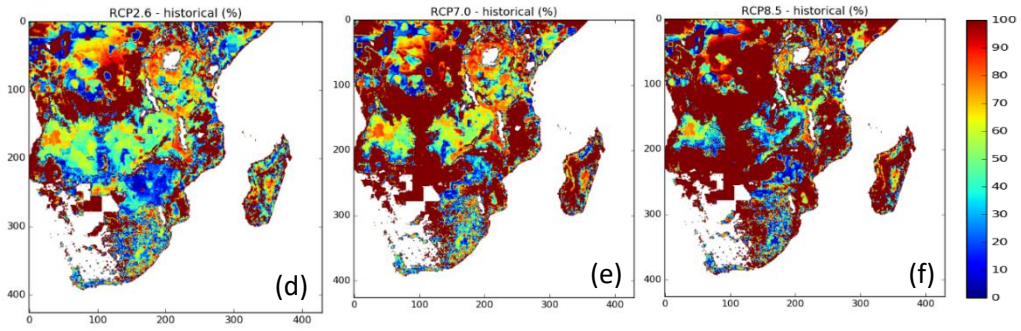

Fig 5.5.2 Malaria risk in central – south part of Africa on projection period compare to historical period (%) with (d) RCP 2.6, (e) RCP 7.0 and (f) RCP 8.5

Fig 5.2.2 (d)-(f) represent percentage of malaria risk (the difference of EIR projection from EIR historical period) in central – south part of Africa. Spatial average of EIR difference under RCP 2.6 is 40.48%, under RCP 7.0 is 45.23%, and under RCP 8.5 is 100.78%. In central – south part of Africa, the worst scenario in projection period is RCP 8.5, similar with west part of Africa. Meanwhile, the better scenario is RCP 2.6.

5.6 Impact of Precipitation and Temperature on Malaria Transmission Projection Period under RCP 2.6, RCP 7.0 and RCP 8.5

Climate impact on malaria transmission in the future simulation is highly uncertainties. Precipitation characteristic (monthly average of precipitation, monthly average of standard deviation of precipitation, and maximum monthly Consecutive Wet Days (CWD)) and temperature have impact on EIR. The relation of precipitation characteristic and temperature with EIR can be written as a function in equation (18):

$$\overline{EIR} = f(\bar{P}, \sigma_p, CWD, T) \quad (17)$$

Where:

$\overline{EIR}$: monthly average of Entomological Inoculation Rate

$\bar{P}$: monthly average of precipitation

σ_P : monthly average of standard deviation of precipitation

CWD : monthly maximum of Consecutive Wet Days

T : average of Temperature

From equation (17), we derive equation (18) as follow :

$$\widehat{\boldsymbol{EIR}} = \boldsymbol{a}\widehat{\bar{\boldsymbol{P}}} + \boldsymbol{b}\widehat{\boldsymbol{\sigma_P}} + \boldsymbol{c}\widehat{\boldsymbol{CWD}} + \boldsymbol{d}\widehat{\boldsymbol{T}} \quad (18)$$

After standardized all variables, we utilize multivariate regression to predict coefficient for each variable. To prevent multi collinearity between each coefficient, we consider from correlation coefficient between those variable and set a threshold 0.9. If correlation coefficient between two variables are higher than threshold value, we neglect one of them. We take into account variable which has higher correlation with EIR in the calculation. Then, we derive coefficient of each variable.

We divided analysis of impact of climate change on malaria transmission into two regions: west part of Africa (latitude: 0^0 – 25^0 N, longitude: -20^0W – 12^0 E) and central-south part of Africa (latitude: 25^0 – 38^0 S, longitude: 12^0E – 55^0 E) region under three RCPs scenario.

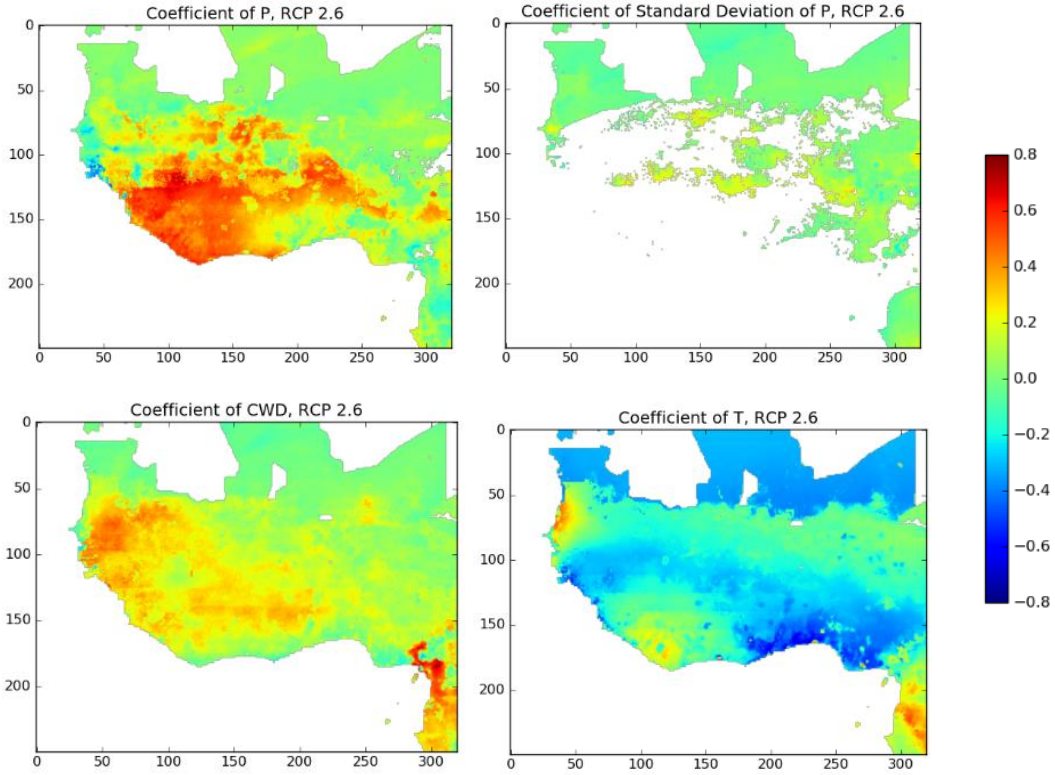

Fig 5.6 (a) Contribution map of monthly mean precipitation (P), standard deviation of precipitation (σ_P), consecutive wet days (CWD), and temperature (T) under RCP 2.6, in west part of Africa

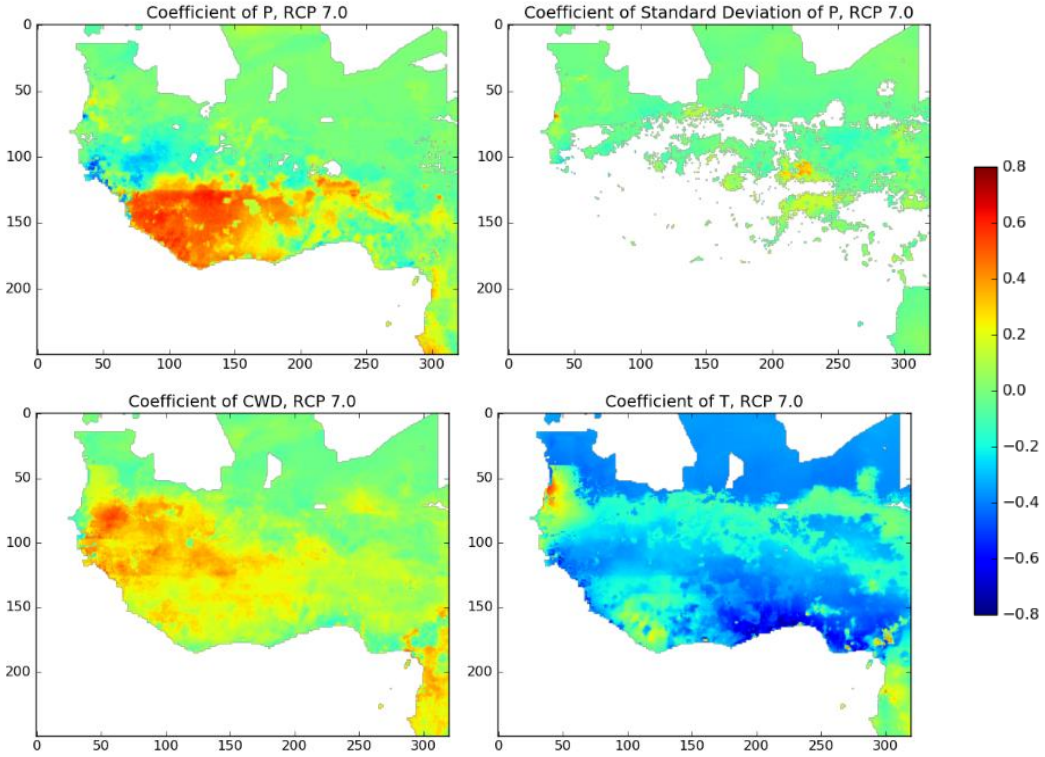

Fig 5.6 (b) Contribution map of monthly mean precipitation (P), standard deviation of precipitation (σ_P), consecutive wet days (CWD), and temperature (T) under RCP 7.0, in west part of Africa

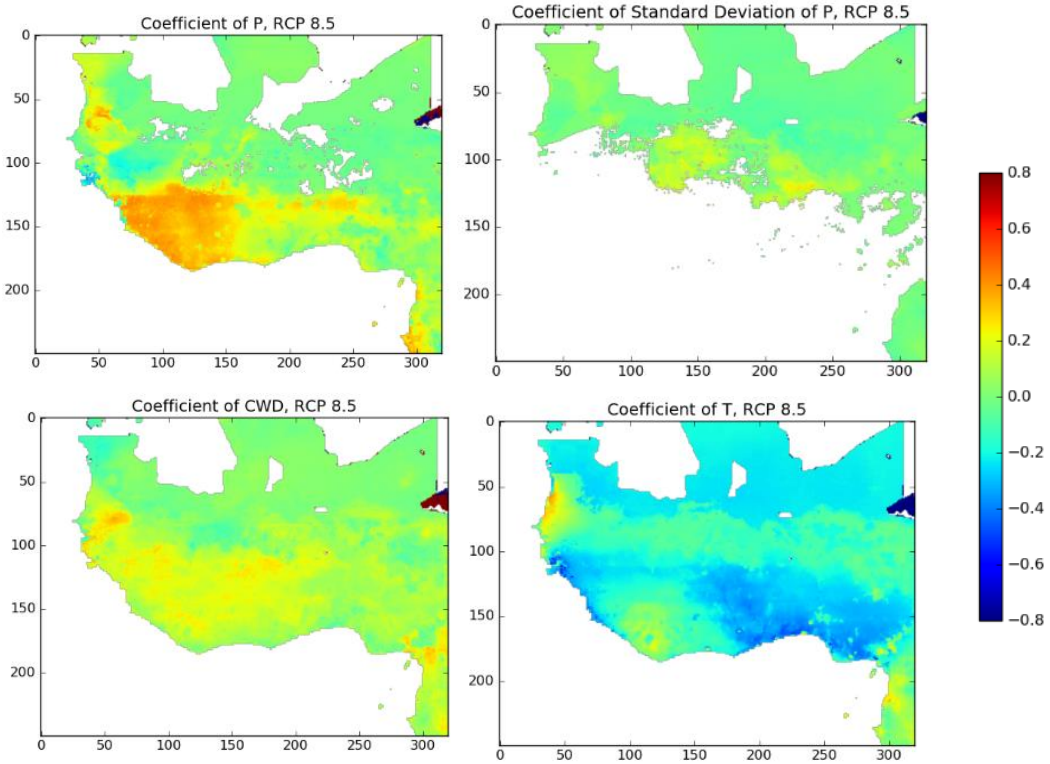

Fig 5.6 (c) Contribution map of monthly mean precipitation (P), standard deviation of precipitation (σ_P), consecutive wet days (CWD), and temperature (T) under RCP 8.5, in west part of Africa

Average of % contribution of each variable in west part of Africa are described in Table 5.6.1 as follow:

Table 5.6.1 Spatial average of contribution each variable (P, σ_P, CWD, and T) to EIR calculation in west part of Africa

Scenario	P	(σ_P)	CWD	T
RCP 2.6	61%	109%	-68%	-2%
RCP 7.0	55%	9%	44%	-9%
RCP 8.5	24%	70%	129%	-123%

From Table 5.6.1, in west part of Africa, under RCP 2.6, precipitation and standard standard deviation of precipitation has a positive contribution to EIR calculation with 61% and 109, respectively. Meanwhile, CWD and average of temperature has negative contribution which means inversely impact to EIR calculation. Under RCP 7.0, monthly average of precipitation, standard deviation of precipitation and CWD contribute to increasing EIR, with contribution 55%, 9% and 44%, respectively. Meanwhile, temperature decrease EIR value with -9%. Under RCP 8.5, monthly average of precipitation, standard deviation of precipitation, and CWD also increase EIR number, with 24%, 70% and 129%, respectively. Meanwhile, temperature decrease EIR number, with -123%. For these three scenario, monthly average of precipitation and standard deviation of precipitation gives a positive impact in increasing EIR number and temperature decrease EIR number. Meanwhile, CWD increase EIR value under RCP 7.0 and RCP 8.5, but decrease EIR number under RCP 2.6.

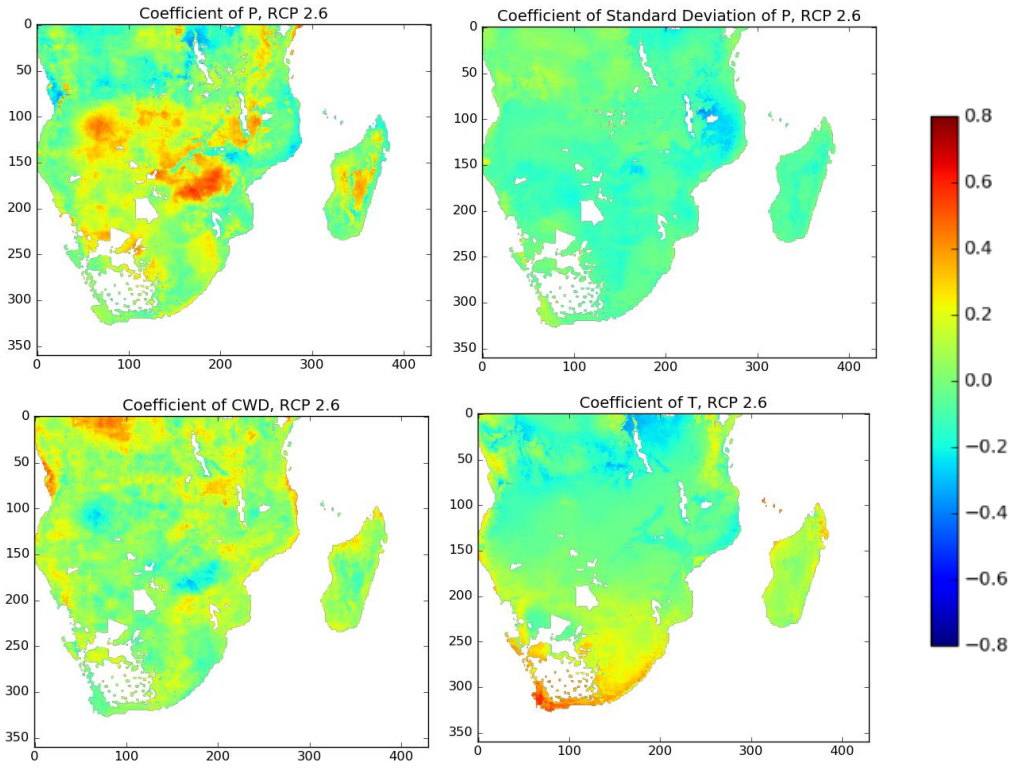

Fig 5.6 (d) Contribution map of monthly mean precipitation (P), standard deviation of precipitation (σ_P), consecutive wet days (CWD), and temperature (T) under RCP 2.6, in central-south part of Africa

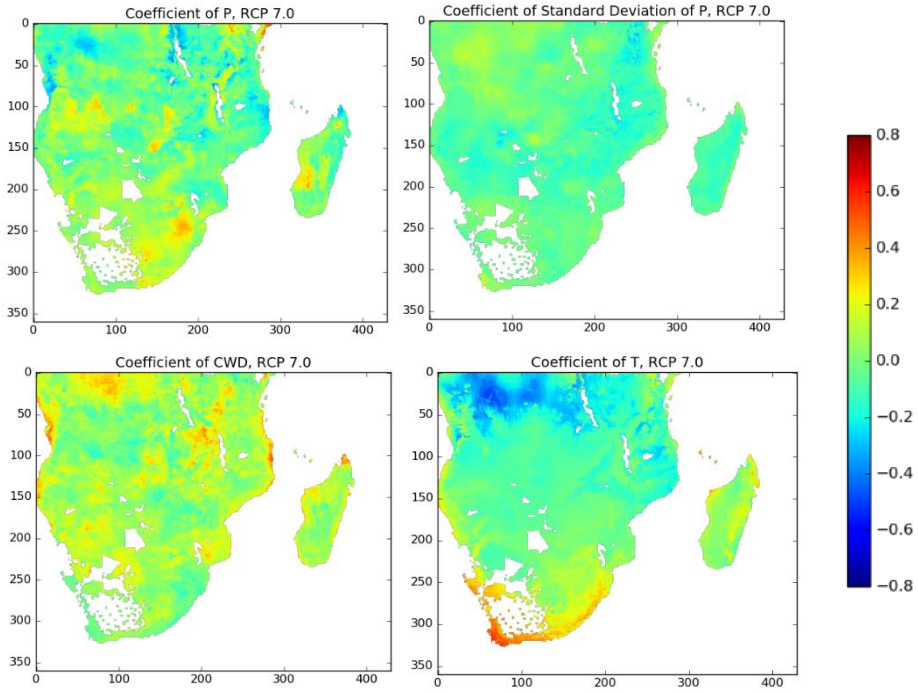

Fig 5.6 (e) Contribution map of monthly mean precipitation (P), standard deviation of precipitation (σ_P), consecutive wet days (CWD), and temperature (T) under RCP 7.0, in central-south part of Africa

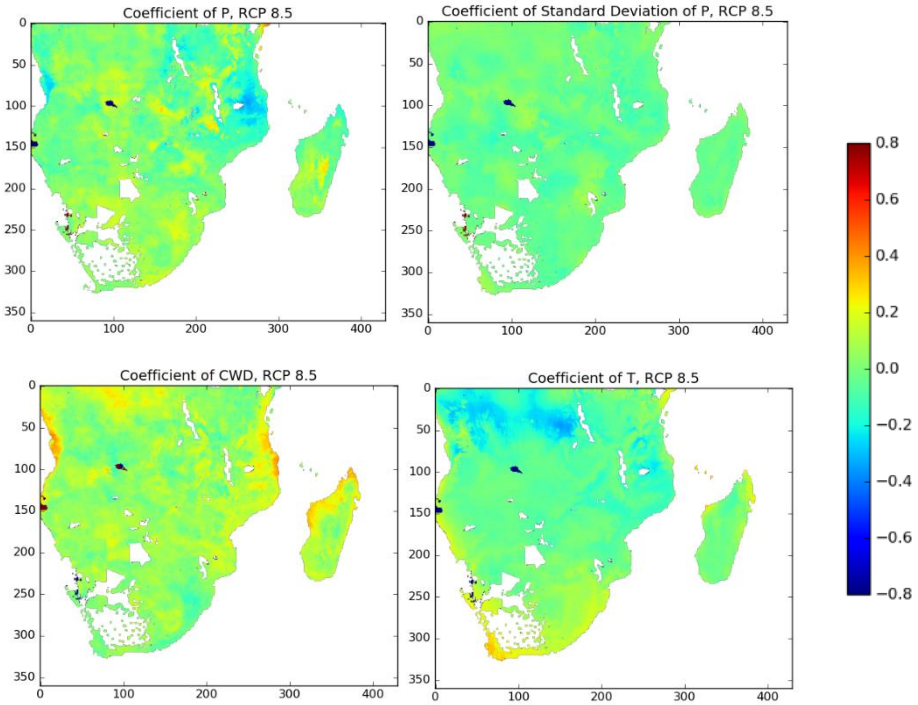

Fig 5.6 (f) Contribution map of monthly mean precipitation (P), standard deviation of precipitation (σ_P), consecutive wet days (CWD), and temperature (T) under RCP 8.5, in central-south part of Africa

Average of % contribution of each variable in west part of Africa are described in Table 5.6.2 as follow:

Table 5.6.2 Spatial average of contribution each variable (P, σ_P, CWD, and T) to EIR calculation in central – south part of Africa

Scenario	P	(σ_P)	CWD	T
RCP 2.6	162%	-160%	48%	50%
RCP 7.0	-4%	36%	6%	62%
RCP 8.5	41%	18%	-6%	48%

From Table 5.6.2, in central – south part of Africa, under RCP 2.6, monthly average of precipitation has the highest contribution in increasing EIR number with 162 %. Meanwhile standard deviation of precipitation decrease EIR number, with -160%. CWD and temperature also increase EIR, with 48% and 50%. Under RCP 7.0, precipitation decrease EIR number with -4%. Meanwhile, standard deviation of precipitation, CWD and temperature increase EIR number with 36%, 6% and 62%, respectively. Under RCP 8.5, monthly average of precipitation, precipitation, standard deviation of precipitation and temperature increase EIR number, with 41%, 18% and 48%, respectively. Meanwhile, CWD decrease EIR number with -6%. In central – south part of Africa, each scenario has different variable which increase or decrease EIR number.

5.7 Impact population density to EIR

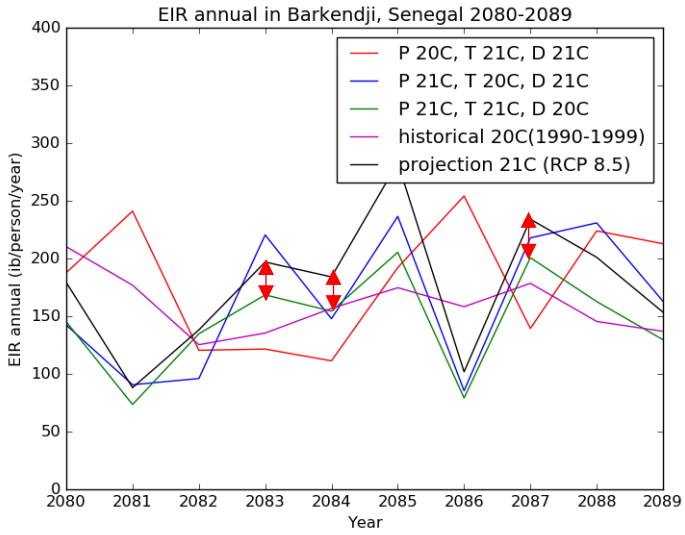

Fig. 5.7 Impact of population density on EIR in Barkendji, Senegal

Fig. 5.7 represents impact of population density on EIR calculation in Barkendji, Senegal under RCP 8.5. EIR using population density on projection data represents in black line, meanwhile EIR using historical population density data represents in green line. This figure shows, EIR using projection population density is higher than EIR using historical population density data. This means that changing of population density give proportional impact to increasing or decreasing EIR number.

5.8 Impact of water fraction on malaria transmission

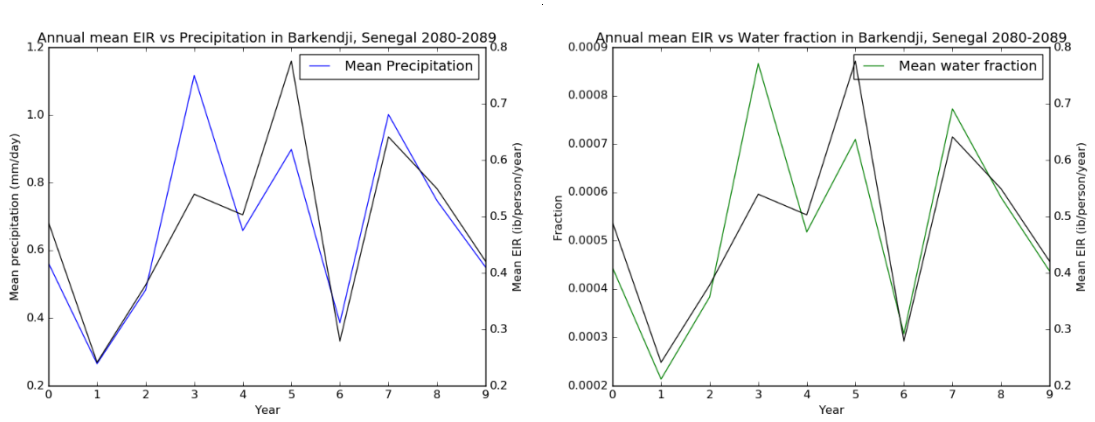

Fig. 5.8 Annual mean of EIR against precipitation (left) and EIR against water fraction (right) in Barkendji, Senegal 2080 – 2100 under RCP 8.5

Correlation coefficient between precipitation and EIR annual mean is 0.836. Meanwhile, correlation coefficient between water fraction and EIR annual mean is 0.843. precipitation affect to create water fraction as from equation (12). When there is no precipitation ($P = 0$) or $(w_{pond} = w_{max})$, amount of water fraction is determined by exponential function with rate $-K_w(E + I)$. Meanwhile, when there is no infiltration and evaporation ($E + I = 0$), amount of water fraction is determined by exponential function rate $-K_w P$. From this two explicit solution for water fraction, it gives a significant different to water fraction rate. Because of this, correlation coefficient between precipitation against EIR and water fraction against EIR is very close.

5.9 Correlation coefficient of EIR and variables (P, σ_p, CWD, and T) with three ensemble members of each RCPs scenario

Due to high uncertainties on projection period, we need to add ensemble members for each RCPs scenario to make our simulation result more robust. We add three ensemble member of each RCPs scenario. Then, to analyze malaria transmission in long-term period, of we calculate correlation coefficient between EIR changes (difference from EIR projection minus EIR historical period) and changes of each variable between projection and historical period which can be written as equation (19) as follow:

$$\delta\overline{EIR} = f\left(\delta\bar{P}, \delta\sigma_p, \delta CWD, \delta T\right) \quad (19)$$

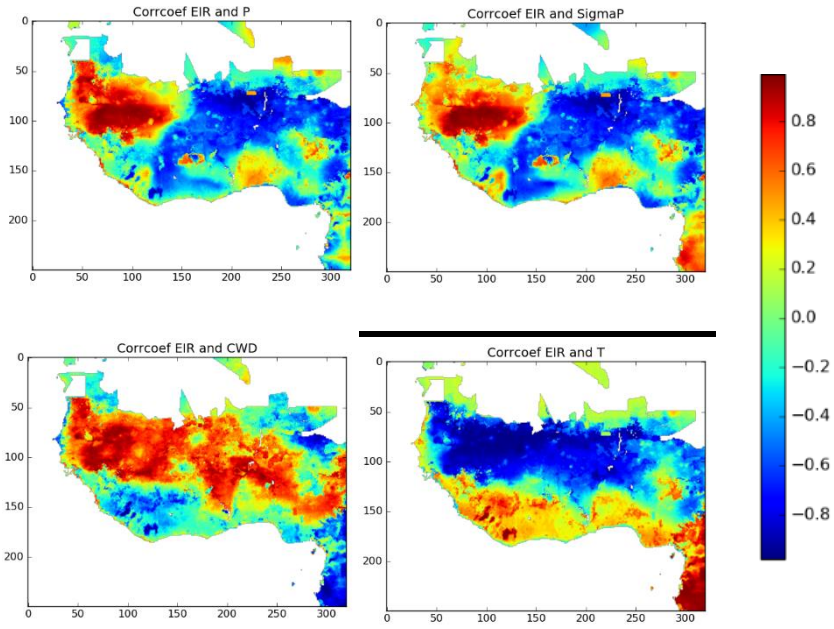

Fig. 5.9.1 Correlation coefficient map of delta of monthly average of precipitation and delta EIR in west part of Africa

In west part of Africa, spatial average of changes of monthly mean precipitation, standard deviation of precipitation and average of temperature give positive impact with 21.68%, 35.30%, and 49.72%, respectively. Meanwhile, changes of CWD inversely impact to changes of EIR with -6.71%.

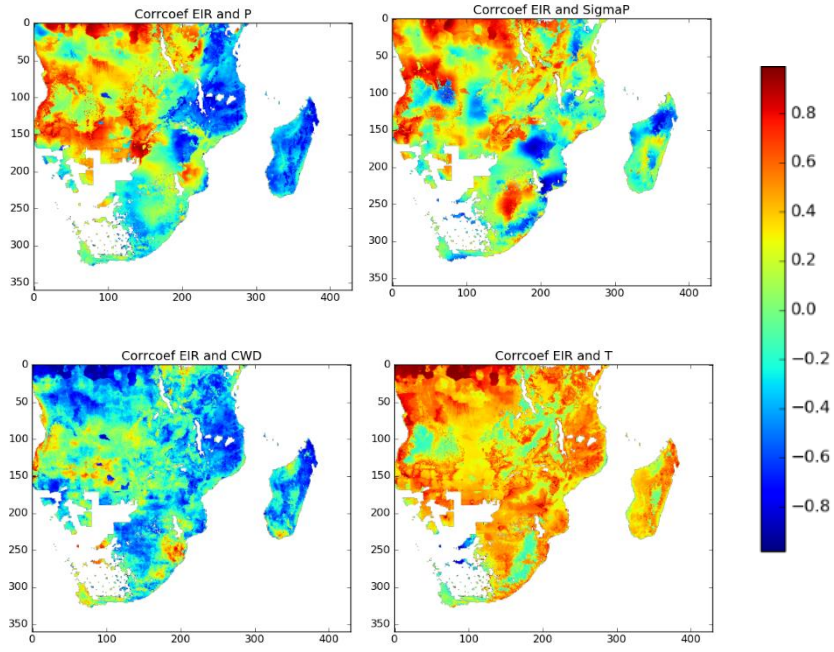

Fig. 5.9.2 Correlation coefficient map of delta of monthly average of precipitation and delta EIR in central – south part of Africa

In central – south part of Africa, spatial average of changes of monthly average of precipitation is lower than standard deviation of precipitation, with 0.85%. Meanwhile, temperature has the highest impact with 77.09% and CWD inversely impact to EIR calculation.

Table. 5.9 Correlation coefficient map of delta of monthly average of precipitation and delta EIR

Region	P	σ_P	CWD	T
West part of Africa	21.68%	35.30%	-6.71%	49.72%
Central – south part of Africa	0.85%	41.01%	-18.95%	77.09%

5.10 Finding of this study compare to previous studies about malaria transmission on projection period

This study corrects hydrological parameter of surface water formation which is a critical parameter for mosquito breeding places. This study also analyses the impact of precipitation characteristic on malaria transmission. Besides that, this study utilizes CMIP6 forcing data for precipitation and temperature which is recent product of climate projection simulation.

5.11 Conclusion

In Barkendji (Senegal) with precipitation range 0 – 1200 mm per month is drier compared to Mbansale (Democratic Republic of Congo) with precipitation range 0 – 4500 mm per month and Nsimalen Ekoko (Cameroon) with precipitation range 0 -3500 mm. Population density in Barkendji (Senegal), Mbansale (Democratic Republic of Congo), and Nsimalen Ekoko (Cameroon) is in range 0 – 35 people/km^2, 0 – 90 people/km^2, and 0 – 120 people/km^2. For malaria transmission number, under RCP2.6 projection, EIR annual range number in Barkendji (Senegal) is higher than in Mbansale (Democratic Republic of Congo) and Nsimalen Ekoko (Cameroon) with 100 – 350 infective bites/person/year, 50 – 100 infective bites/person/year, and 0 – 120 infective bites/person/year, respectively.

On projection period, precipitation will increase or decrease depends on the area in projection simulation. Meanwhile, temperature is increasing on projection period. West, central and southeast part of Africa are more favorable conditions for malaria transmission under three RCPs scenario. Inter annual variability of EIR annual mean is determined by coefficient variation. This number is derived by calculating standard deviation of EIR annual mean divided by EIR annual mean. Coefficient variation of spatial mean under RCP 2.6 is 0.079, under RCP 7.0 is 0.087 and under RCP 8.5 is 0.087. It represents EIR annual mean under RCP 8.5 has higher variability compare to other RCPs scenario.

Precipitation and temperature give impact to EIR number. In west part of Africa (latitude : 0^0 – 25^0 N, longitude: -20^0W – 12^0 E), the risk of malaria in projection period compare to historical period are -23.14% under RCP 2.6, -39.51% under RCP 7.0 and -19.22% under RCP 8.5. Therefore, the worst scenario is RCP 8.5 and the better scenario is RCP 7.0. In central – south part of Africa (latitude : 0^0 – 25^0 N, longitude: -20^0W – 12^0 E), the risk of malaria in projection period compare to historical period are 40.48% under RCP 2.6, 45.23% under RCP 7.0, and 100.78% under RCP 8.5. For central – south part of Africa, the worst scenario is RCP 8.5 and the better scenario is RCP 2.6.

Meanwhile, population density gives a proportional impact to increase or decreasing EIR number. Precipitation characteristics (monthly average of precipitation, standard deviation of precipitation, Consecutive Wet Days (CWD)) and temperature contribute to EIR calculation. Monthly average of precipitation and standard deviation of precipitation have relative contribution to EIR in west part of Africa, meanwhile CWD give more impact to EIR in central and southeast part of Africa. Correlation coefficient of precipitation and standard deviation is higher in western, central and eastern part of Africa, CWD's correlation coefficient is higher near equator line from west to eastern part of Africa and temperature's correlation coefficient from central part to southern part of Africa.

Highly uncertainties on projection simulation encourage us to add ensemble members for each RCPs scenario to make our simulation result more robust. By considering each value of correlation coefficient of each variable divided by value of total correlation coefficient of all variables, contribution of each variable related EIR changes from projection period compared to historical period for spatial mean of African region in west part of Africa is 21.68% for precipitation, 35.32% for standard deviation of precipitation, -6.71% for CWD and 49.72% for temperature. Meanwhile, in central – south part of Africa, the contribution of each variable is 0.85% for precipitation, 41.01% for standard deviation of precipitation, -18.95% for CWD and 77.09% for temperature.

CHAPTER 6

Conclusion and Recommendation

Abstract:

This chapter conclude and discuss recommendation to improve the studies in future. From this study, pond growth rate parameter is tuned against EIR and water fraction. A scaling factor, interpolation and topographical multiplication is need to derive a better pond growth rate parameter. The optimized pond growth rate is related to topographical parameter. The result shows that pond growth rate calibration is needed to improve malaria transmission model and make a better prediction of malaria transmission in the future. Malaria projection in the future is various in each different sites (the relationship between malaria transmission and precipitation, temperature and population density are non-linear). To improve and expand this study, more number of EIR observation and water fraction with high resolution datasets is needed.

6.1 Conclusion

From this study, we could conclude that:

- EIR observations data are collected in Senegal, Republic of Congo, Burundi, Gambia, Democratic Republic of Congo, Gabon, Cameroon, Eritrea, Uganda, Zambia, Tanzania, and Kenya.
- An adjusted pond growth rate parameter (K_w) could capture a better entomological inoculation rate simulation close to EIR observation in some sites in Senegal, Republic of Congo, Burundi, Gambia, Democratic Republic of Congo, Gabon, Cameroon, Eritrea, Uganda, Zambia, Tanzania, and Kenya
- There is not a clear relationship between pond growth rate and EIR observation number in all validation sites because pond growth rate is various in each EIR observation sites.
- A scaling factor, inverse distance interpolation method and topographical multiplication are needed to derive a better pond growth rate parameter
- Water fraction observation have a significant relation with precipitation in some sites from observation in some site. Meanwhile, in other sites, the correlation is not significant.

- Coefficient variation spatial average for EIR annual projection under RCP 2.6 is 0.079, under RCP 7.0 us 0.087 and under RCP 8.5 is 0.087. EIR annual projection under RCP 8.5 has higher variability compare to other two RCPs scenario.
- In west part of Africa (latitude : 0^0 – 25^0 N, longitude: -20^0W – 12^0 E), the risk of malaria in projection period compare to historical period are -23.14% under RCP 2.6, -39.51% under RCP 7.0 and -19.22% under RCP 8.5. The worst scenario is RCP 8.5 and the better scenario is RCP 7.0.
- In central – south part of Africa (latitude : 0^0 – 25^0 N, longitude: -20^0W – 12^0 E), the risk of malaria in projection period compare to historical period are 40.48% under RCP 2.6, 45.23% under RCP 7.0, and 100.78% under RCP 8.5. The worst scenario is RCP 8.5 and the better scenario is RCP 2.6.
- Precipitation characteristic (monthly average of precipitation, standard deviation of precipitation and consecutive Wet Days (CWD)) and temperature give impact to EIR calculation. Meanwhile, population density gives proportional impact to increase or decrease EIR number
- Due to highly uncertainties in projection period, after adding ensemble member of each RCPs scenario, contribution of each climate variable (monthly average of precipitation, standard deviation of precipitation, CWD and temperature) related to EIR changes from projection period compare to historical period, spatial mean of west part of Africa is 21.68% for monthly average of precipitation, 35.32% for standard deviation of precipitation, -6.71% for CWD, and 49.72% for temperature.
- In central – south part of Africa, the contribution of each climatic variable and EIR changes are 0.85% for precipitation, 41.01% for standard deviation of precipitation, -18.95 for CWD and 77.09% for temperature.

6.2 Recommendation

In this study, validation of the model result is limited to EIR observation. Meanwhile, the number of EIR observation is limited due to it takes risk, difficulties, time consuming and cost. The validation of the model would be better if this study can use other validation datasets, such as number of malaria cases number in each site in Africa.

Besides that, more highly resolution of water fraction can be used to improve the model. This study utilizes 0.1 degree (~11 km) water fraction datasets for calibration po growth rate. Higher resolution of

surface water with pond scale (<10 m) with daily datasets are need to take into account to improve the model performance and make the model result more reliable.

An economic growth for projection simulation period and other social factors (such as using some treatments, taking medicine, and other malaria control program need to be implemented in the future to make the simulation result improved and more realistic.

REFERENCES

Addawe, J., & Pajimola, A. K. (2016, October). Dynamics of climate-based malaria transmission model with age-structured human population. In *AIP Conference Proceedings* (Vol. 1782, No. 1, p. 040002). AIP Publishing.

Aron, J. L., & May, R. M. (1982). The population dynamics of malaria. Population Dynamics of Infectious Diseases. Theory and Applications.

Asare, E. O., Tompkins, A. M., & Bomblies, A. (2016). A regional model for malaria vector developmental habitats evaluated using explicit, pond-resolving surface hydrology simulations. *PloS one*, *11*(3), e0150626.

Baird, J. K., Jones, T. R., Danudirgo, E. W., Annis, B. A., Bangs, M. J., Basri, P. H., & Masbar, S. (1991). Age-dependent acquired protection against Plasmodium falciparum in people having two years exposure to hyperendemic malaria. *The American journal of tropical medicine and hygiene*, 45(1), 65-76.

Baird, J. K., Basri, H., Bangs, M. J., Andersen, E. M., Jones, T. R., Masbar, S., ... & Arbani, P. R. (1993). Age-specific prevalence of Plasmodium falciparum among six populations with limited histories of exposure to endemic malaria. *The American journal of tropical medicine and hygiene*, *49*(6), 707-719.

Baird, J. K. (1995). Host age as a determinant of naturally acquired immunity to Plasmodium falciparum. *Parasitology today*, *11*(3), 105-111.

Bayoh, M. N., & Lindsay, S. W. (2003). Effect of temperature on the development of the aquatic stages of Anopheles gambiae sensu stricto (Diptera: Culicidae). *Bulletin of entomological research*, *93*(5), 375-381.

Béguin, A., Hales, S., Rocklöv, J., Åström, C., Louis, V. R., & Sauerborn, R. (2011). The opposing effects of climate change and socio-economic development on the global distribution of malaria. *Global Environmental Change*, *21*(4), 1209-1214.

Bomblies, A., Duchemin, J. B., & Eltahir, E. A. (2008). Hydrology of malaria: Model development and application to a Sahelian village. *Water Resources Research*, *44*(12).

Caminade, C., Kovats, S., Rocklov, J., Tompkins, A. M., Morse, A. P., Colón-González, F. J., ... & Lloyd, S. J. (2014). Impact of climate change on global malaria distribution. *Proceedings of the National Academy of Sciences*, *111*(9), 3286-3291.

Craig, M. H., Snow, R. W., & le Sueur, D. (1999). A climate-based distribution model of malaria transmission in sub-Saharan Africa. *Parasitology today*, *15*(3), 105-111.

Depinay, J. M. O., Mbogo, C. M., Killeen, G., Knols, B., Beier, J., Carlson, J., ... & Toure, A. M. (2004). A simulation model of African Anopheles ecology and population dynamics for the analysis of malaria transmission. *Malaria journal*, *3*(1), 29.

Dirks, K. N., Hay, J. E., Stow, C. D., & Harris, D. (1998). High-resolution studies of rainfall on Norfolk Island: Part II: Interpolation of rainfall data. *Journal of Hydrology*, *208*(3-4), 187-193.

Elliott, R. (1972). The influence of vector behavior on malaria transmission. *The American Journal of Tropical Medicine and Hygiene*, *21*(5_Suppl), 755-763.

Ermert, V., Fink, A. H., Jones, A. E., & Morse, A. P. (2011). Development of a new version of the Liverpool Malaria Model. II. Calibration and validation for West Africa. *Malaria journal*, *10*(1), 62.

Ermert, V., Fink, A. H., Morse, A. P., & Paeth, H. (2011). The impact of regional climate change on malaria risk due to greenhouse forcing and land-use changes in tropical Africa. *Environmental Health Perspectives*, *120*(1), 77-84.

Fontenille, D., Lochouarn, L., Diatta, M., Sokhna, C., Dia, I., Diagne, N., ... & Trape, J. F. (1997). Four years' entomological study of the transmission of seasonal malaria in Senegal and the bionomics of Anopheles gambiae and A. arabiensis. *Transactions of the Royal Society of Tropical Medicine and Hygiene*, *91*(6), 647-652.

Filipe, J. A., Riley, E. M., Drakeley, C. J., Sutherland, C. J., & Ghani, A. C. (2007). Determination of the processes driving the acquisition of immunity to malaria using a mathematical transmission model. *PLoS computational biology*, *3*(12).

Garrett-Jones, C., Ferreira Neto, J. A., & World Health Organization. (1964a). *The prognosis for interruption of malaria transmission through assessment of the mosquito's vectorial capacity* (No. WHO/Mal/470.64). Geneva: World Health Organization.

Garrett-Jones, C. (1964b). The human blood index of malaria vectors in relation to epidemiological assessment. *Bulletin of the World Health Organization*, *30*(2), 241.

Garrett-Jones, C., & Shidrawi, G. R. (1969). Malaria vectorial capacity of a population of Anopheles gambiae: an exercise in epidemiological entomology. *Bulletin of the World Health Organization*, *40*(4), 531.

Gemperli, A., Vounatsou, P., Sogoba, N., & Smith, T. (2005). Malaria mapping using transmission models: application to survey data from Mali. *American Journal of Epidemiology*, *163*(3), 289-297.

Gupta S, Day KP. (1994). A theoretical framework for the immunoepidemiology of Plasmodium falciparum malaria. Parasite Immunol 16: 361–370.

Gupta, S., Snow, R. W., Donnelly, C., & Newbold, C. (1999). Acquired immunity and postnatal clinical protection in childhood cerebral malaria. *Proceedings of the Royal Society of London. Series B: Biological Sciences*, *266*(1414), 33-38.

Gupta, S., Snow, R. W., Donnelly, C. A., Marsh, K., & Newbold, C. (1999). Immunity to non-cerebral severe malaria is acquired after one or two infections. *Nature medicine*, *5*(3), 340.

Haines, A., Kovats, R. S., Campbell-Lendrum, D., & Corvalán, C. (2006). Climate change and human health: impacts, vulnerability and public health. *Public health*, *120*(7), 585-596.

Hamilton, M., Mahiane, G., Werst, E., Sanders, R., Briët, O., Smith, T., ... & Gething, P. W. (2017). Spectrum-malaria: A user-friendly projection tool for health impact assessment and strategic planning by malaria control programmes in sub-Saharan Africa. *Malaria journal*, 16(1), 68.

Hundessa, S., Williams, G., Li, S., Li Liu, D., Cao, W., Ren, H., ... & Guo, Y. (2018). Projecting potential spatial and temporal changes in the distribution of Plasmodium vivax and Plasmodium falciparum malaria in China with climate change. *Science of the Total Environment*, *627*, 1285-1293.

Hussien, H. H., Eissa, F. H., & Awadalla, K. E. (2017). Statistical methods for predicting malaria incidences using data from Sudan. *Malaria research and treatment*, *2017*.

Kibret, S., Lautze, J., McCartney, M., Nhamo, L., & Yan, G. (2019). Malaria around large dams in Africa: effect of environmental and transmission endemicity factors. *Malaria journal*, *18*(1), 303.

Lafon, T., Dadson, S., Buys, G., & Prudhomme, C. (2013). Bias correction of daily precipitation simulated by a regional climate model: a comparison of methods. *International Journal of Climatology*, *33*(6), 1367-1381.

Laneri, K., Bhadra, A., Ionides, E. L., Bouma, M., Dhiman, R. C., Yadav, R. S., & Pascual, M. (2010). Forcing versus feedback: epidemic malaria and monsoon rains in northwest India. *PLoS computational biology*, *6*(9), e1000898.

Lemasson, J. J., Fontenille, D., Lochouarn, L., Dia, I., Simard, F., Ba, K., ... & Molez, J. F. (1997). Comparison of behavior and vector efficiency of Anopheles gambiae and An. arabiensis (Diptera: Culicidae) in Barkedji, a Sahelian area of Senegal. *Journal of Medical Entomology*, *34*(4), 396-403.

Li, B., Wang, W., An, Z., & Zhao, H. (2018). Metanetwork Transmission Model for Predicting the Malaria Control Strategy. *Frontiers in genetics*, *9*, 446.

Lu, G. Y., & Wong, D. W. (2008). An adaptive inverse-distance weighting spatial interpolation technique. *Computers & geosciences*, *34*(9), 1044-1055.

Minakawa, N., Mutero, C. M., Githure, J. I., Beier, J. C., & Yan, G. (1999). Spatial distribution and habitat characterization of anopheline mosquito larvae in western Kenya. *The American journal of tropical medicine and hygiene*, 61(6), 1010-1016.

Minakawa, N., Sonye, G., Mogi, M., & Yan, G. (2004). Habitat characteristics of Anopheles gambiae ss larvae in a Kenyan highland. *Medical and veterinary entomology*, *18*(3), 301-305.

Muerth, M. J., St-Denis, B. G., Ricard, S., Velázquez, J. A., Schmid, J., Minville, M., ... & Turcotte, R. (2013). On the need for bias correction in regional climate scenarios to assess climate change impacts on river runoff. *Hydrology & Earth System Sciences*, *17*(3).

Muturi, E., Shililu, J., Jacob, B., Gu, W., Githure, J., and Novak, R. (2006). Mosquito species diversity and abundance in relation to land use in riceland agroecosystem in mwea, kenya. J Vector Biol, 31:129–137.

Nazarenko, L., Schmidt, G. A., Miller, R. L., Tausnev, N., Kelley, M., Ruedy, R., ... & Bleck, R. (2015). Future climate change under RCP emission scenarios with GISS M odelE2. Journal of Advances in Modeling Earth Systems, 7(1), 244-267.

Ngarakana-Gwasira, E. T., Bhunu, C. P., Masocha, M., & Mashonjowa, E. (2016). Assessing the role of climate change in malaria transmission in Africa. *Malaria research and treatment*, *2016*.

Nmor, J. C., Sunahara, T., Goto, K., Futami, K., Sonye, G., Akweywa, P., ... & Minakawa, N. (2013). Topographic models for predicting malaria vector breeding habitats: potential tools for vector control managers. *Parasites & vectors*, *6*(1), 14.

Orwa, T. O., Mbogo, R. W., & Luboobi, L. S. (2018). Mathematical model for hepatocytic-erythrocytic dynamics of malaria. *International Journal of Mathematics and Mathematical Sciences*, *2018*.

Paaijmans, K. P., Jacobs, A. F. G., Takken, W., Heusinkveld, B. G., Githeko, A. K., Dicke, M., & Holtslag, A. A. M. (2008). Observations and model estimates of diurnal water temperature dynamics in mosquito breeding sites in western Kenya. *Hydrological Processes: An International Journal*, *22*(24), 4789-4801.

Patz, J. A., Campbell-Lendrum, D., Holloway, T., & Foley, J. A. (2005). Impact of regional climate change on human health. *Nature*, *438*(7066), 310.

Riahi, K., Van Vuuren, D. P., Kriegler, E., Edmonds, J., O'neill, B. C., Fujimori, S., ... & Lutz, W. (2017). The shared socioeconomic pathways and their energy, land use, and greenhouse gas emissions implications: an overview. *Global Environmental Change*, *42*, 153-168.

Robinson, T. P., & Metternicht, G. (2006). Testing the performance of spatial interpolation techniques for mapping soil properties. *Computers and electronics in agriculture*, *50*(2), 97-108.

Ryan, S. J., McNally, A., Johnson, L. R., Mordecai, E. A., Ben-Horin, T., Paaijmans, K., & Lafferty, K. D. (2015). Mapping physiological suitability limits for malaria in Africa under climate change. *Vector-Borne and Zoonotic Diseases*, *15*(12), 718-725.

Sattler, M. A., Mtasiwa, D., Kiama, M., Premji, Z., Tanner, M., Killeen, G. F., & Lengeler, C. (2005). Habitat characterization and spatial distribution of Anopheles sp. mosquito larvae in Dar es Salaam (Tanzania) during an extended dry period. *Malaria journal*, *4*(1), 4.

Semakula, H. M., Song, G., Achuu, S. P., Shen, M., Chen, J., Mukwaya, P. I., ... & Zhang, S. (2017). Prediction of future malaria hotspots under climate change in sub-Saharan Africa. *Climatic Change*, *143*(3-4), 415-428.

Shapiro, L. L., Whitehead, S. A., & Thomas, M. B. (2017). Quantifying the effects of temperature on mosquito and parasite traits that determine the transmission potential of human malaria. *PLoS biology*, *15*(10), e2003489.

Smith, T., Charlwood, J. D., Kihonda, J., Mwankusye, S., Billingsley, P., Meuwissen, J., ... & Tanner, M. (1993). Absence of seasonal variation in malaria parasitaemia in an area of intense seasonal transmission. *Acta tropica*, *54*(1), 55-72.

Smith, D. L., Guerra, C. A., Snow, R. W., & Hay, S. I. (2007). Standardizing estimates of the Plasmodium falciparum parasite rate. *Malaria journal*, *6*(1), 131.

Tanser, F. C., Sharp, B., & Le Sueur, D. (2003). Potential effect of climate change on malaria transmission in Africa. *The Lancet*, *362*(9398), 1792-1798.

Tompkins, A. M., & Ermert, V. (2013). A regional-scale, high resolution dynamical malaria model that accounts for population density, climate and surface hydrology. *Malaria journal*, *12*(1), 65.

Trape JF, Rogier C, Konate L, Diagne N, Bouganali H, Canque B, Legros F, Badji A, Ndiaye G, Ndiaye P, et al.: The Dielmo project: a longitudinal study of natural malaria infection and the mechanisms of protective immunity in a community living in a holoendemic area of Senegal. The American Journal of Tropical Medicine and Hygiene 1994, 51:123-137.

Van Lieshout, M., Kovats, R. S., Livermore, M. T. J., & Martens, P. (2004). Climate change and malaria: analysis of the SRES climate and socio-economic scenarios. *Global Environmental Change*, *14*(1), 87-99.

White, M. T., Walker, P., Karl, S., Hetzel, M. W., Freeman, T., Waltmann, A., ... & Mueller, I. (2018). Mathematical modelling of the impact of expanding levels of malaria control interventions on Plasmodium vivax. *Nature communications*, *9*(1), 3300.

Witteveen, J., & Bijl, H. (2009). Explicit mesh deformation using inverse distance weighting interpolation. In *19th AIAA Computational Fluid Dynamics* (p. 3996).

Xie, Y., Chen, T. B., Lei, M., Yang, J., Guo, Q. J., Song, B., & Zhou, X. Y. (2011). Spatial distribution of soil heavy metal pollution estimated by different interpolation methods: Accuracy and uncertainty analysis. *Chemosphere*, *82*(3), 468-476.

Yamana, T. K., & Eltahir, E. A. (2010). Early warnings of the potential for malaria transmission in rural Africa using the hydrology, entomology and malaria transmission simulator (HYDREMATS). *Malaria journal*, *9*(1), 323.

Yamana, T. K., & Eltahir, E. A. (2013). Incorporating the effects of humidity in a mechanistic model of Anopheles gambiae mosquito population dynamics in the Sahel region of Africa. *Parasites & vectors*, *6*(1), 235.

Yamana, T. K., & Eltahir, E. A. (2013). Projected impacts of climate change on environmental suitability for malaria transmission in West Africa. *Environmental health perspectives*, *121*(10), 1179-1186.

Acknowledgements

Bismillah, the following words express my gratitude to Allah SWT and prophet Muhammad SAW for all the things to achieve my PhD degree.

First and foremost, I would like to express my deepest appreciation to my supervisor Professor Kei Yoshimura for his kindness, warmness, patience, and guidance until this step. I am very grateful become one of your student. Your leadership, guidance, hard work, and valuable things help me to improve my research and personal life.

From the deepest of my heart, I also would like to thank to Professor Taikan Oki, Professor Takashi Mino, Professor Akiyuki Kawasaki and Assoc. Prof. Hyungjun Kim who kindly give valuable advice, suggestions and comments to improve my research.

I like to specially thank to Nitta-san who always support, help and give valuable advice and comments. I also thank to Hibino-san, Onuma-san, and Toride-san for a help and valuable discussion of my research.

I would like to acknowledge the funding received from Indonesian Ministry of Research, Technology and Higher Education (MRTHE) to conduct my doctoral research.

I'd like to thanks to Salem, Hatono-san, Panduka, Puy, Ishitsuka-san, and Arnida for helping, discussion, and support during my research and personal life.

I 'd like to thanks to the secretaries: Noguchi-san, Miyagi-san, and Mawatari-san for helping all the documents required and for kindly supports, thank you very much!

I also would like to thanks to Aoyama-san and Foreign Student Office in Civil Engineering Tonegawa-san and Matsumoto-san for helping me with the documents in civil engineering.

I also thanks to Xiaojun, Ma-san, Xiaoxing, Haimao, Kino-san, Alex. Thanks for the advice, talks, suggestion, support and wonderful lab life! All ylab members: Miura-san, Moriyama-san, Subha, Takeshima-san, Harada-san, Hanazaki-san, Arai-san and Koike-san for the kindness during my life and interaction in ylab.

I also would like to thanks to Sobhan, Matsumoto-san, Ali, Sithija, Isabel, Xiaoya, Tidar, Rahul, Yoshida-san, Ikeuchi-san, Taguchi-san, for your kindness, help, and support during my research in Oki-Lab.

I'd like to thanks to Indonesian Student Association for the warmness and help. Moreover, all Indonesian students in Kashiwa campus who always support and helping me to enjoy my life in Japan!

I also thanks to Suzuki-san and Akaike-san to hold host family program and introduce me to my host family: Otousan, Okaasan and Mizuki (Ochi-san's family) who always give me support and sharing the good moments! I also thanks to my host family in Gifu: Kaede, Mama and Papa (Kohno's family) to give the warmness and help during my homestay.

I want to express my deep gratitude for my Mother and Older Brother for your supports, unconditional love and everything and always makes me motivated to finish my study.

Finally, I would like to dedicate this achievement, to my late Father and Younger Brother. I express my deepest gratitude and this thesis is dedicated to them.

Last but not least, I would like to thanks to all support for everyone who help me for life and research in Japan whom I haven't mention.

Kashiwa, February 20th, 2020

Inna Syafarina

So which of the favors of your Lord would you deny?

[Ar Rahman : 13]

APPENDIX A

EIR observation site location

No	Reference	Country	Site	Lon	Lat	start month	start year	end month	end year	EIR obs
1	Le Masson et al. 1997	Senegal	Barkendji	-14.87	15.28	7	1994	3	1996	111.1
2	Trape et al. 1987	Republic of Congo	Linzolo	-4.41	15.11	10	1983	9	1984	234.6
3	Van Bortel et al. 1996	Burundi	Gasange	29.6	-4.32	11	1992	10	1993	267
4	Van Bortel et al. 1996	Burundi	Kazirabageni	29.63	-4.23	11	1992	5	1994	35.4
5	Van Bortel et al. 1996	Burundi	Gisenga	29.67	-4.44	11	1992	5	1994	251.7
6	Thomson et al. 1994	Gambia	Dasilami	-14.27	13.41	1	1991	12	1991	1.2
7	Lindsay et al. 1993	Gambia	Dongoro Ba	-15.28	13.38	1	1988	12	1988	80
8	Thomson et al. 1995	Gambia	Jahally	-14.97	13.55	1	1991	12	1991	4.2
9	Lindsay et al. 1993	Gambia	Jalangbereh	-15.4	13.38	1	1988	12	1988	70
10	Lindsay et al. 1993	Gambia	Jessadi	-15.3	13.63	1	1988	12	1988	64
11	Thomson et al. 1995	Gambia	Kulari	-14.08	13.4	1	1991	12	1991	7.8
12	Lindsay et al. 1993	Gambia	Madina	-15.25	13.52	1	1988	12	1988	177
13	Lindsay et al. 1993	Gambia	Katamina	-15.28	13.55	1	1988	12	1988	4
14	Thomson et al. 1995	Gambia	Sare Alpha	-13.98	13.37	1	1991	12	1991	11.2
15	Lindsay et al. 1991	Gambia	Saruja	-14.9	13.55	3	1987	6	1988	3
16	Karch et al. 1993	Democratic Republic of Congo	Kinkolé	15.51	-4.36	2	1990	12	1991	40.2
17	Coene 1993	Democratic Republic of Congo	Kinshasa, Kimbangu 3 district	15.31	-4.35	9	1988	12	1989	29.2
18	Karch et al. 1992	Democratic Republic of Congo	Kinshasa, semi-rural area	15.35	-4.36	4	1989	10	1990	198.7
19	Karch et al. 1992	Democratic Republic of Congo	Kinshasa, urban area	15.31	-4.31	4	1989	10	1990	2.8

20	Karch et al. 1993	Democratic Republic of Congo	Mbansalé	15.64	-4.26	2	1990	11	1990	175.2
21	Elissa et al. (2003)	Gabon	Benguia	13.515	-1.625	5	2003	4	2004	239.07
22	Elissa et al. (2003)	Gabon	Dienga	12.68	-1.87	5	2003	4	2004	97.83
23	Fondjo et al. (1992)	Cameroon	Bikok	11.482	3.867	3	1989	2	1990	14.212
24	Fondjo et al. (1992)	Cameroon	Bisson	11.44	3.865	4	1989	3	1990	30.28145
25	Njan Nloga et al. (1993)	Cameroon	Ebogo	11.469	3.397	4	1991	3	1992	7.763514
26	Cohuet	Cameroon	Nkoteng	12.05	4.5	2	1999	1	2000	44.9
27	Antonio-Nkondjio et al. (2012)	Cameroon	Nsimalen_Ekoko	12.12	3.82	4	1991	3	1992	97.285
28	Antonio-Nkondjio et al. (2012)	Cameroon	Nsimalen_Nkol_Mefou	11.58	3.626	4	1991	3	1992	59.116
29	Antonio-Nkondjio et al. (2012)	Cameroon	Simbock-Block6	11.3	3.5	1	1999	12	1999	94.343
30	Coene (1993)	Democratic Republic of Congo	Kimbangu	15.31	-4.36	9	1988	8	1989	24.32204
31	Coene (1993)	Democratic Republic of Congo	Kwamutu	15.28	-4.47	9	1988	8	1989	3.98957
32	Karch et al. (1993)	Democratic Republic of Congo	Mbansale	16.8	-4.19	5	1990	4	1991	175.2
33	Shililu et al. (2003)	Eritrea	Adibosqual	38.38956	15.41725	1	1999	12	1999	5.041667
34	Shililu et al. (2003)	Eritrea	Anseba_Hagaz	38.16784	15.41902	10	1999	9	2000	0.357798
36	Shililu et al. (2003)	Eritrea	Debub_Mai-Aini	39.05765	14.4851	10	1999	9	2000	5.4405
37	Shililu et al. (2003)	Eritrea	Gash_Barka_Hiletsidi	36.39091	15.0705	10	1999	9	2000	33.56322
38	Shililu et al. (2003)	Eritrea	Hiletsidi	36.39091	15.0705	1	1999	12	1999	77.12644
39	Okello et al. (2006)	Uganda	Kyenjojo_Kasiina	30.62	0.62	6	2001	5	2002	78.8925
40	Kent 2007	Zambia	Chidakwa	26.79061	-16.3929	11	2005	10	2006	1.608
41	Bodker et al. (2003)	Tanzania	Bagamoyo	38.264	-5.04	10	1995	9	1996	1.831369
42	Bodker et al. (2003)	Tanzania	Balangai	38.277	-4.556	10	1995	9	1996	0.000432
43	Shiff et al. (1995)	Tanzania	Chasimba	38.82	-6.58	1	1992	12	1992	28.6
44	Shiff et al. (1995)	Tanzania	Kongo	38.83	-6.53	1	1992	12	1992	110.7
45	Bodker et al. (2003)	Tanzania	Kwameta	38.291	-5.066	10	1995	9	1996	7.337828

46	Bodker et al. (2003)	Tanzania	Kwamhanya	38.276	-5.035	10	1995	9	1996	0.292441
47	Bodker et al. (2003)	Tanzania	Magundi	38.283	-5.053	10	1995	9	1996	0.606179
48	Shiff et al. (1995)	Tanzania	Matimbwa	38.87	-6.5	1	1992	12	1992	73.3
49	Bodker et al. (2003)	Tanzania	Milungui	38.233	-4.453	10	1995	9	1996	0.022361
50	Smith et al. (1993)	Tanzania	Yombo	38.844	-6.585	1	1992	12	1992	45.3
51	Muturi et al. (2008)	Kenya	Mbuinjeru	37.622	-0.818	4	2004	3	2005	0.00197
52	Muturi et al. (2008)	Kenya	Murinduko	37.45	-0.57	4	2004	3	2005	0.031139
53	Mbogo et al. (1993)	Kenya	Sokoke	39.877	-3.332	12	1990	11	1991	7.711005